EVALUATION OF A CENOZOIC LACUSTRINE BASIN – HANÇILI FORMATION
(KALECİK-ANKARA) AND ITS PALEOENVIRONMENT AND PALEOCLIMATE ANALYSIS
BASED ON MINERAL FACIES

A THESIS SUBMITTED TO
THE GRADUATE SCHOOL OF NATURAL AND APPLIED SCIENCES
OF
THE MIDDLE EAST TECHNICAL UNIVERSITY

BY

SERDAR AKER

IN PARTIAL FULFILLMENT FOR THE REQUIREMENTS
FOR
THE DEGREE OF DOCTOR OF PHILOSOPHY
IN
DEPARTMENT OF GEOLOGICAL ENGINEERING

JANUARY 2013

Approval of the Thesis

EVALUATION OF A CENOZOIC LACUSTRINE BASIN – HANÇILI FORMATION (KALECİK-ANKARA) AND ITS PALEOENVIRONMENT AND PALEOCLIMATE MODELLING BASED ON MINERAL FACIES

submitted by **SERDAR AKER** in partial fulfillment of the requirements for the degree of **Doctor of Philosophy in Geological Engineering Department, Middele East Technical University** by,

Prof. Dr. Canan ÖZGEN   _____
Dean, Graduate School of **Natural and Applied Sciences**

Prof. Dr. Erdin BOZKURT   _____
Head of Department, **Geological Engineering**

Prof. Dr. Asuman GÜNAL TÜRKMENOĞLU   _____
Supervisor, **Geological Engineering, METU**

Examining Committee Members:

Prof. Dr. Kadir DİRİK   _____
Geological Engineering, Hacettepe University

Prof. Dr. Asuman GÜNAL TÜRKMENOĞLU   _____
Geological Engineering, METU

Assoc. Prof. Dr. İ. Ömer YILMAZ   _____
Geological Engineering, METU

Asst. Prof. Dr. Zehra KARAKAŞ   _____
Geological Engineering, Ankara University

Asst. Prof. Dr. Fatma Toksoy KÖKSAL   _____
Geological Engineering, METU

Date : 29.Jan.2013

I hereby declare that all information in this document has been obtained and presented in accordance with academic rules and ethical conduct. I also declare that, as required by these rules and conduct, I have fully cited and referenced all material and results that are not original to this work.

Name, Last Name: Serdar Aker

Signature:

ABSTRACT

EVALUATION OF A CENOZOIC LACUSTRINE BASIN – HANÇILI FORMATION (KALECİK-ANKARA) AND ITS PALEOENVIRONMENT AND PALEOCLIMATE ANALYSIS BASED ON MINERAL FACIES

Aker, Serdar
Ph.D., Department of Geological Engineering
Supervisor: Prof. Dr. Asuman Günal Türkmenoğlu
January 2013, 95 pages

The major purpose of this study is to evaluate the paleoenvironmental and paleoclimatological conditions during the Middle Miocene-Early Pliocene in Kalecik-Ankara by using mineralogical and geochemical proxies from Hançılı Formation.

To achieve a high-resolution paleoclimate data, 2 stratigraphic sectioning and 1 continous core drilling were examined. Field studies were followed by analytical techniques on the selected representative samples. The mineralogical compositions of the bulk samples and the minerals of the clay fractions were determined by X-ray diffractometer. Scanning electron microscopic analyses were also carried on the specific samples which have the potential to define the important microstructural units. The major and trace elemental compositions were determined by X-ray fluoresence spectrometer. Additionally, the stable isotope compositions of the samples selected from the continous core drilling on Hançılı formation were among the major proxies to gather a paleoenvironmental and paleoclimatrological approach.

All the proxies employed for this study clearly indicate that mineralogical and geochemical signatures are consistent with each other and can be used for paleoclimatic interpretations. The stable isotope values point that C4 plants were dominant during the deposition of Hançılı Formation, while evaporation caused the development of alkaline environment which is seasonally dry with depositional temperature approximately between 25-30°C. During deposition, lava flowand tuff were deposited due to the volcanic activity in the vicinity of the lake. Based on this volcanism, economical bentonite deposits were originated. The lake at which the Hançılı formation was deposited, completed its development in a time to time silicate rich and salty-alkaline anvironment.

Key Words:

Kalecik-Hasayaz basin, paleo-climate, paleo-environment, lake, clay minerals, Pliocene, Hançılı formation, lake sediments drilling sections.

ÖZ

SENOZOYİK YAŞLI GÖLSEL HAVZANIN DEĞERLENDİRİLMESİ – HANÇILI FORMASYONU (KALECİK-ANKARA) VE MİNERAL FASİYESİNE BAĞLI OLARAK FORMASYONUN PALEOÇEVRE VE PALEOİKLİM ANALİZİ

Aker, Serdar
Doktora, Jeoloji Mühendisliği Bölümü
Danışman: Prof. Dr. Asuman Günal Türkmenoğlu
Ocak 2013, 95 pages

Bu çalışma ile Kalecik – Hasayaz havzasının Orta Miyosen –Erken Pliyosen evresinde gölsel Hançılı Formasyonunun mineralojik ve jeokimyasal yöntemler kullanılarak paleoiklimsel ve paleo-ortamsal özelliklerinin belirlenmesi amaçlanmıştır.

Yüksek çözünürlüklü veri elde etmek için 2 stratigrafik kesit ve 1 adet 60 m derinliğinde devamlı karotlu sondaj çalışması yapılmıştır. Arazi çalışmalarını, sahayı temsil eden örnekler üzerinde yapılan analitik teknikler takip etmiştir.

Tüm kayaç örneklerinin mineralojik kompozisyonları ve kil mineralleri X-ışınları toz difraksiyon metodu ile tayin edilmiştir. Olası mikro-yapısal birimleri tesbit edebilmek için seçilmiş örnekler taramalı electron mikroskobu ile incelenmiştir. Majör ve iz element kompozisyonları X-ışını floresans spektrometresi ile incelenmiştir. Bütün bunlara ek olarak, paleo-ortam ve paleo-iklim yaklaşımı elde edebilmel için Hançılı Formasyonunda açılan karotlu sondajdan alınan örnekler üzerinde duraylı izotop kompozisyonları tayin edilmiştir.

Mineralojik ve jeokimyasal yaklaşımlardan elde edilen bütün veriler birbiri ile uyumlu ve paleo-ortam paleo-iklim yorumları için kullanılabilir niteliktedir. Duraylı izotop değerleri ispatlamıştır ki C4 bitkileri Hançılı Formasyonunun çökelimi sırasında oldukça yoğundur. Buna mukabil buharlaşma, mevsimsel olarak kuru ve yaklaşık olarak 25-30°C sıcaklıkta olan alkalin çevrenin gelişmesi sonucu oluşmuştur. Çökelme esnasında volkanik hareketlilik gölün gelişmesinde ortama lav akıntısı ve tüf katmanlanması ile katkı sağlamıştır. Bu sayede birim içinde ekonomik değere sahip olduğu düşünülen bentonitik kiltaşı istiflenmiştir. Hançılı Formasyonunun geliştiği göl oluşumu yine zaman zaman silikatça zengin tuzlu-alkali ve nemli ortamda tamamlanmıştır.

Anahtar Kelimeler:

Kalecik-Hasayaz havzası, paleo-iklim, paleo-çevre, göl, kil mineralleri, Pliyosen, Hançılı formasyonu, göl sedimanı sondaj kesiti.

To my family

ACKNOWLEDGEMENTS

TABLE OF CONTENTS

LIST OF FIGURES

LIST OF TABLES

CHAPTER 1

INTRODUCTION

1.1. Purpose

Due to the visible negative feedbacks of the modern climate change, paleoenvironment and paleoclimate studies have been recently much more popular in all over the world. As the name implies, paleoclimatology is the study of the past climates. To reconstruct the paleoclimates of a region, first of all the climate-dependent parameters (proxy data) should be evaluated. Bradley (1999) listed the most important proxies for the past climate reconstructions. Among them, lake sediments with their faunal and floral abundances, oxygen and carbon isotope compositions, clay mineralogies and pedological features are very important and can provide considerable data for determining processes of previous climatic changes and geological evolution of a region (Chamley, 1989).

With this perspective, the purpose of this study is to evaluate the mineralogical and geochemical compositions of the Hançılı Formation to constrain a paleoclimate history for the Mio-Pliocene in Central Anatolia. Although there have been many studies regarding the Miocene climate of the western and southwestern Turkey, unfortunately very few contibutions have been made to the paleoclimate of Central Anatolia. For this reason, this thesis study will provide compareable proxies for the region to reconstruct the Mio-Pliocene climates.

The scope of this work is to evaluate and discuss the worldwide literature regarding mineralogical and geochemical proxies of the lake deposits, to describe the mineralogical phases and geochemical characteristics of the Mio-Pliocene sedimentary units in the region and to construct both Mio-Pliocene paleoenvironmental and paleoclimatic model for the region.

1.2. Location Of The Study Area

The study area is at Kalecik-Hasayaz basin which is nearly 100 km north-east of the Ankara, Central Anatolia (Figure 1.1). Sampling studies were carried around Hançılı Village, specifically at Koyunbaba and Höyüklü Hills as stratigraphic sectioning and at Tepetarla location as borehole coring (Figure 1.1).
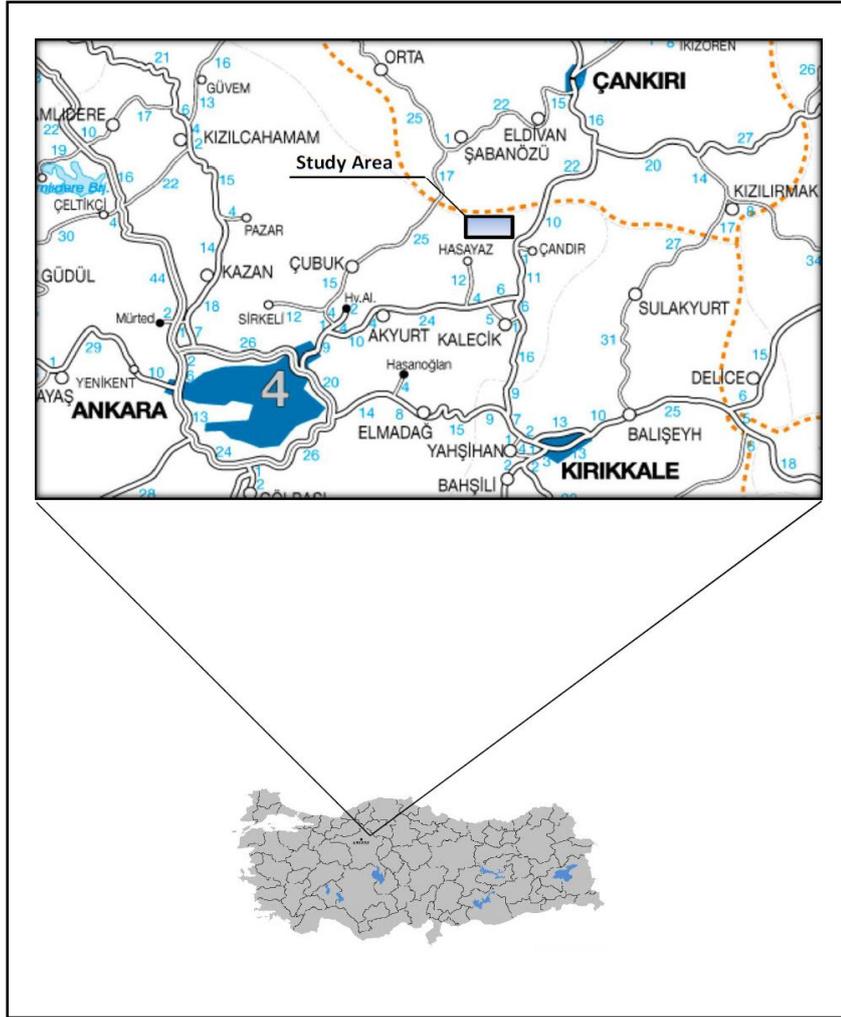
Figure 1.1. Location of the study area.

1.3. Importance Of Lake Deposits On Paleoenvironmental And Paleoclimatological Studies

As Bradley (1999) described, paleoclimatology is known as a study of the climate prior to the period of instrumental measurements. In this respect, the proxy data, which is the best for the geological point of view, is climate-dependent parameters used to understand the past climates. Bradley (1999) also listed the major proxies used in such studies and pointed the importance of the lake deposits with their mineralogical, geochemical, faunal and floral compositions and with specific clay minerals, erosional features, pedological structures, pollen concentrations, diatoms, ostracods and other biota assemblages. In this list, other than geological proxies, additionally glaciological, biological and histrocial ones are also described.

Bradley (1999) defined the importance of lake sediments in climate studies and stated that since lakes accumulate sediments from their surrounding region, they provide a record of the environmental change. Moreover it is mentioned that due to high accumulation rate in lakes, they may provide high-resultion records of the past climates. Continental deposits, especially lacustrine deposits are also sensitive to astronomically induced climate change in the continental realm (Aziz et al. 2003).

It is known that there are two types of sediments composing the lake deposits. Allochthonous material is transported to lakes by rivers and streams. The other one is autochthonous sediments are either biogenic in origin or it may result from inorganic precipitation within the water column (Bradley, 1999). Both of them can be used for paleoclimatic reconstructions. Pollens are also very common proxy providers in paleoclimate studies and usually studied in lake deposits.

Inorganic precipitation within carbonate-rich lakes can provide an isotopic record that may reflect the varying composition of the meteoric waters entering the drainage basin over time (Bradley, 1999).

The mineralogical and chemical compositions of the clay minerals are controlled by the chemical activity of the soil solution, which is definitely influenced by the amount of the seasonality of the rainfall (Buol et al., 1997; Tabor, 2002). This relation shows that the clay minerals are sensitive to the climatic changes. Therefore, they are used as good proxies to estimate the long-term climatic fluctuations. However, there are some limitations to use the clay minerals in such studies. First of all, the origin of the clay minerals should be known before proceeding. If it is authigenic in origin, then it is definitely correct to use for the climatic reconstruction. However, if it is not, the climatic signals may be deformed or even obliterated (Chamley, 1989). Diagenetic changes also can cause such effects and alter the climatic signals.

The geochemical signatures of the lake deposits are also very important in such studies. Especially the stable isotope compostions of the carbonates and pyhllosilicates are used widely to estimate the local meteoric conditions.

1.4. A Review On Miocene-Early Pliocene Climate Of Mediterrannean

As Yao et al. (2011) emphasized, the Neogene climate system is a transitional stage from the greenhouse climate of the Palaeogene to the icehouse climate of the Quaternary, since very dramatic climatic, tectonic and biotic key events occurred on the globe during this phase. Therefore, it is very important to understand the long-term climatic changes in Eurasia, and globally (e.g., Mosbrugger et al., 2005).

Ivanov et al. (2011) documented that the Miocene was the last warm episode prior to the establishment of the large Northern Hemisphere ice sheets. Harzhauser et al. (2011) pointed the major two climatic events as Miocene Climate Optimum (MCO; Zachos et al., 1994; Böhme, 2003; Sun and Zhang, 2008) and the Middle Miocene Climate Transition (MCT; Shevenell et al., 2004; Lewis et al., 2007). In the same study, it was also mentioned that in Eurasia, this climate change is accompanied by an increase of seasonality and aridity (Eronen et al., 2009; Bruch et al., 2010) and a replacement of Early to Middle Miocene broad-leaved evergreen forests by deciduous forests during the late Middle and Late Miocene (Eder-Kovar et al., 2008).

The studies regarding the Miocene climates show that this period was characterized by tremendous geological events like large scale transgressions and pronounced regressions, e.g. opening and closure of marine corridors, appearance and disappearance of lakes and swamps in Europe (Kojumdgieva and Popov, 1989; Meulenkamp et al., 1996; Rögl, 1998, 1999, 2001; Meulenkamp and Sissingh, 2003; Ilyina et al., 2004a,b; Harzhauser and Piller, 2007; Harzhauser et al., 2007; Harzhauser and Mandic, 2008).

As a very important event, Messinian salinity crisis happened during the Miocene. The sea level sharply fell and this affected the physiography of the Mediterranean Region. In Zachos et al. (2001), the compilation data from more than 40 DSDP (Deep Sea Drilling Project) and ODP (Ocean Drilling Project) sites were compared their global deep-sea oxygen and carbon isotope compositions. That study pointed that the warming starting from Mid-Miocene Climatic Optimum caused the C4 grasses to expand, aridity became seasonally dominant.

1.5. Methodology

After proposing the study area, five field studies were performed to select the best places to sample. The studies on field sampling were carried as stratigraphic sectioning and borehole coring. Along two stratigraphic sections belonging to Hançılı formation, the sampling study was performed in Koyunbaba village and Höyüklü hill. To have a high resolution proxy data on continous lake sediments, 60m deep borehole was opened by Petra Eng. Con. and Const. Ltd. Company at the Tepetarla location, western part of the Hançılı village and named as SSK-1. On SSK-1, continuous core samples were taken to analyse (Figure 1.2).

Figure 1.2. SSK-1 borehole drilling in the field.

After field studies, the analytical techniques were performed on the selected samples. The laboratory works were composed of mineralogical, petrographical, geochemical studies. Thin sections of the selected samples were prepared at the Middle East Technical University, Department of Geological Engineering, in Thin Section Preparation Laboratory. Mineralogical compositions and the textural relations of the minerals were analysed by the optical microscope. X-Ray Diffraction analyses were performed at the General Directorate of Mineral Research and Exploration (MTA), Department of Mineral Analysis and Technology in XRD Laboratory. For the determination of non-clay minerals, beside the thin section analyses, X-Ray Diffraction was also used as a complemantary method and it is called as "bulk analysis". The sample preparation procedure for the XRD analyses was done at the Middle East Technical University, Department of Geological Engineering. After grinding the rock samples, they were sieved with the 170 mesh sieve. For the determination of clay minerals, oriented samples are prepared at the Middle East Technical University, Department of Geological Engineering, Clay Mineralogy Laboratory. After grinding the samples by an agat mortar, size fraction less than 2 μm was separated by sedimentation method according to "Stoke's Law". XRD spectrums were gathered as air dried, ethylen glycolized, heated at 300°C and 550°C.

The micromorphological properties of zeolit and clay minerals which were selected at the end of the thin section analyses were determined by SEM analyses at the METU Department of Metalurgical and Material Engineering SEM Laboratory. EDX analyses were also performed to determine chemical compositions of the minerals.

The major and trace element compositions of the some of the selected samples were analysed at Leeds University, London by X-Ray floresence spectrometer. SiO_2, TiO_2, Al_2O_3, Fe_2O_3, MnO, MgO, CaO, Na_2O, K_2O, P_2O_5, loss on ignition (LOI) were measured as % weight ; Sc, V, Cr, Co, Ni, Cu, Zn, Rb, Sr, Y, Zr, Nb, Ba, Pb, Th and U were measured as ppm. The geochemical analyses of the rest were determined at LABDAN Laboratory Tests Consulting Ltd. Company (Ankara) by implementing spectrophotometric titration method which obeys new Europe Standarts (TS EN) accepted by Turkish Standarts Instutitute (TSE). SiO_2, Al_2O_3, Fe_2O_3, MgO, CaO, Na_2O, K_2O, SO_3 and LOI ratios were measured as weight percentages (%).

To provide an independent check on the interpretations, the $\delta^{18}O$ compositions of 11 samples that were selected from the continous borehole samples were determined at METU Central Laboratory by Thermofinnagan DELTA PlusXP Stable Isotope Ratio Mass Spectrometer. To prepare the samples for the isotope analysis, rock surfaces were smoothened firstly and then polished powder samples were prepared by using auger. The organic matter was removed from the samples by washing the samples with Sodium HypoChlorite (NaOCl) and by distilled water three times.

Because of the budget limitations, the geochronological determinations were once tried on the pollen data, however unfortunately the samples from the borehole SSK-1 were all steryl.

CHAPTER 2

LITERATURE REVIEW

2.1. Previous Works On The Study Area

Tekkaya et al. (1975) carried a biostratigraphic research about terrestrial Neogene deposits at Kalecik region. According to vertebrate fossils that found in red colored terrestrial sedimentary unit (Çandır formation) which is located at North of the Çandır town, the age of formation is determined as Middle Miocene. Over that formation, Lower Pliocene lacustrine deposits are located.

Özoğul (1976) stated that generally terrestrial and lacustrine regimes were dominated during the Neogene in the region. In this study it was also stated that at the west of the study area, in and around Gündoğmuş location, the Pliocene sediments lie over the andesite and basalt which are the productions of the increasing volcanic activity of the region after the Miocene. The bentonites that belongs to Early Pliocene units, also contains andesitic tuff levels.

Akyürek et al. (1980) studied on geological properties of Şabanözü-Hasayaz-Çandır-Kalecik region and determined units that forms both base and fills of the basin.

Eroğlu and Farsakoğlu (1982) examined the geological structure of the region that is located between Hançılı and Demirtaşlı villages (Çankırı H30b2, b3 plates) which are in border of Ankara - Kalecik town and they specified the genesis of the Hançılı bentonite deposits (region between Tepetarla- Bağlarbaşı hill- Türbebaşı hill), usage fields and reserve of bentonite. The region which was the Neogene lake, joins to Çankırı basin by thresholds. The lithological units of the region are the Lower Crateceous ophiolitic series (serpentinite, spilite and limestone), Tertiary (Upper Miocene) deposits (bentonite, tuff, green-blue-grey colored claystone, marl, sandy and pebbly series and limestone) and Quaternary deposits (alluvium, colluvium, breccia series).

Akyürek et al. (1984) studied fundamental geologic characteristics of Ankara-Elmadağ-Kalecik region. Under the light of the field data they suggested a tectonic evolution model for Central Anatolia. During the Oligocene, the region was transformed into an intermountain basin. Alluvial fans, the evaporatic lake and the meandering river deposits (Kavaklı formation) were formed parallel to aridity. The lake was broad and prolonged finally whole basin gained lacustrine characteristics.

The study area which is exposed to compression tectonics after the Oligocene, the trust faulting which the most intensive one is at Upper Miocene were formed from the North to the South. During the deposition of Kavaklı formation at the west part of the region volcanism (Tekke volcanics) was activated and the lakes were filled with aglomerate extensively. Upper Miocene-Pliocene aged Kavaklı formation which is composed of clayey limestone, marl, claystone, conglomerate, sandstone and tuffite alternation is correlated with Hançılı formation (Akyürek et.al., 1980). In that formation andesite sills are also observed.

Türkmenoğlu et.al. (1987) examined mineralogy, petrography and formation of Hançılı (Kalecik), Küçükhacıbey and Büyükhacıbey villiages's bentonites. Bentonites include detrital-originated feldspar, montmorillonite, volcanic and metamorphic rock fragments, and authigenic clay minerals which have pyrite and mixed layer illite-smectite. On the basis of bentonite mineralogy, they reached to that the lake environment had alkaline characteristics.

Özalp et al. (1991) showed existence of analcime-calcite/dolomite-feldspar and quartz minerals in the claystones of Hançılı formation which is exposed at Hançılı village, Killik location. Common presence of analcime and dolomite indicates that salty-alkaline

characteristics of Miocene aged "Hançılı Lake". They also stated that bentonite is formed during sedimentary processes and smectite minerals have detrital origin.

Türkmenoğlu et al. (1991), studied on clay mineralogy and chemical characteristics of Hançılı bentonites. Dioctahedral smectite is in composition of montmorillonite. Researchers emphasized that montmorillonite were formed due to decaying of pyroclastic rocks at atmospsheric conditions and this result indicates the sedimentary origin of Hançılı bentonite.

Türkmenoğlu et al. (1994) worked on geological evolution and economic potential of Southwest Çankırı basin by field studies, mineralogical-petrographic analysis and method of remote sensing. They selected 8 main types of study areas. Kalecik-Hasayaz basin had been transformed to a molass depression at Oligocene by separating from the other parts of Çankırı basin by a threshold which was NW-SE oriented. Upper Miocene aged Aslantaş formation and Early Pliocene aged Hançılı formation includes fluvial and lacustrine facies. To that deposition, the products of Galatya volcanism also contributed. At the end of the Early Pliocene it was divided into 4 limited depressions (Çandır-Hançılı-Hasayaz-Kalecik) by Kalecik-Hasayaz basin thrust faults. The results of mineralogical examination indicated that detrital illite and chlorites which were transported to basin during the deposition reflects active tectonics and also smectite, calcite-dolomite-analcime formations symbolized the dry/semi-dry climatic conditions.

Koçyiğit et al. (1995) mentioned about end of collision tectonic regime of study area which is located Eskişehir-Ankara-Çankırı part of İAESZ and gathered data about that a regime by examining Upper Miocene-Lower Pliocene aged fluvial-lacustrine units (molas depression sedimentary deposit). For the research 3 type locations (Hançılı-Yurtyenice, Büyükhacıbey ve Yeşilöz) were selected and the stratigraphic properties- deposition environments of the units were determined. At the stratigraphic section of type location that is located 1.2 km NNW of Yurtyenice village Early Pliocene aged and nearly 700 m in thickness Hançılı formatin lies over the Late Laghian-Tortonian aged Aslantaş formation (Kumartaş Fm.). The Hançılı formation which includes yellow colored porous limestone levels and grey-green marl, yellow-brown-black colored marl which includes coal seams, yellow lacustrine limestone levels and green mudstone interlayers, cherty limestone interlayers and green-blue-grey colored mudstone from bottom to top, deposited at mud plain-swampy-back swampy-lacustrine environments at the paleotectonic period. That formation overlay Late Cretaceous aged ophiolitic mélange with a tectonic boundry or underlay unconformably by Küçükhacıbey formation which advanced as alluvium fan at neotectonic period. At the North limb of Ekinbayırı syncline, the lower levels of Hançılı formation are observed and it is mentioned that the regressive-transgressive changes took place at lake level due to climatic changes.

 At the west of study area, around the Kınık and Ödek villages, Hançılı formation contains andesitic tuffite and bentonitic interlayers.

Türkmenoğlu et al. (1995) worked on geology and clay mineralogy of Tertiary lake sediments at Kalecik-Hasayaz basin. At the west of the Demirtaş village, at the sedimentary deposits that presents the deep part of the lake, sandstone lenses and laminated-thin bedded limestone alternation and biotite, plagioclase, quartz, volcanic-metamorphic rock fragments and calcite-analcime-dolomite group are characteristic. Smectite has detritalorigin. Chlorite and ilite indicates active tectonism. The available data shows salty-alkali lake water and dry/semi-dry climatic conditions.

Şen et al. (1998) made biochronological and lithostratigraphic correlations of mammalian fossil groups at 17 locations which include Kılçak, Şemsettin, Tüney, Çandır, Karaçay, Çorak Yerler, Akkaşdağı, Yarmatepe, Süleymanlı and Kavurca at Çankırı-Çorum basin. It is

determined that Kumartaş (=Aslantaş) formation which is located under the Hançılı formation is Early-Middle Miocene in age and Kılçak stratigraphic unit should be Early Miocene in age due to its location under the Kumartaş formation. Şemsettin fossil group is matched with lower levels of Kumartaş formation.

Karadenizli (2011) studied the same region. In his study, Oligocene to Pliocene palaeogeographic evolution of the Çankırı-Çorum Basin (ÇÇB), central Anatolia, Turkey was the subject. To achieve the palaeogeographic analysis of the ÇÇB, a geological map of a large area was prepared using revisions of previous works. The upper half of the basin-fill, ca. 4000 m, was analyzed measuring sixteen stratigraphic sections. This study suggests that during Late Miocene, there were different types of lacustrine environments in the northern and southern parts of the basin: a hypersaline lake characterized by evaporitic deposits in the north and carbonate-rich shallow lakes and swamps in the south. A younger evaporitic lake formed in Early Pliocene in the northern part of the basin and covered vast areas. Its deposits are as thick as 400 m. From Late Pliocene, the thick sedimentary sequences deposited during the Oligocene–Early Pliocene interval become fragmented and deformed by a tectonic wedge bounded by a normal fault in the west and a thrust in the east.

2.2. Previous Works About The Subject Of The Thesis Study

Lewis and Weibezahn (1981) performed chemical and mineralogical characterization of 7.5 m (latest 13,000 years) core sample which belongs to Valencia Lake (Venezuela). The basins started to its evolution under dry climatic conditions and then it transformed to very salty lake environment. That environment was continued until 9000 B.P. and that period was determined by high Mg:Ca ratio at aragonites and carbonates. At later periods the lake evolution was continued by fluctuations at salt ratio. At that study also the total mineral ingredients and main element ratios of samples were used as valuable data source.

Cosby and Brigham-Grette (2001) studied on Late Cenozoic paleoclimatological records of 300 metered sedimentary deposits of El'gygytgyn Lake (Russia). In that research grain size analyses and clay mineralogy determinatation were performed. Along the core samples it is determined that illite, mixed layered illite-smectite (I-S) and chlorite ratios and degree of crystallization show variability along the stratigraphic sequence. As a result, 1) at warm climatic conditions ratio of mixed layered illite-smectite (I-S) is raised and on the contrary percentage of illite is decreased inversely, 2) chlorite crystallization degree and chlorite ratio are increased with cold climatic conditions.

Deocampo (2002) stated that chemical properties of clay minerals of lake sediments which are sampled along the stratigraphic sections and by boreholes, are very important in terms of defining paleochemical changes especially cases that absence of microfossils in silica and carbonate composition. The octahedric layer compositions of illite and smectite which are < 0.1 micrometre in grain size in the sediments of East Africa lakes (Olorgesailie, Amboseli, Natron, Ngorongoro, Olduvai and Eyasi lakes) were determined as (Mg/(Al+Fe) ratio and by microprobe analysis method. The water level changes of lake are determined as using that ratio as paleo-saltness/alkalinity index. It is also stated that changes can be controlled by Milankovich cycle, by tectonism, volcanic activity, diagenesis and paleo-hydrogeological factors.

Gierlowski-Kordesch (2002) summarized the development of "Lake Basin Models" over the time. During 20. Century limnogeological studies were started and further years paleo-environmental analysis which were based on geochemical indicators and stable isotope analyses performed and by combining sedimentological, lithological and tectonic data 3-D modeling of lake basins were formed. Today magnetic measurements, radiometric age determination and geochemical analyses come into prominence in order to examining lacustrine sedimentary sequences in a detailed way.

Morrill et. al. (2002) used the radiocarbon ages and oxygen isotope values at the study which is on Ahung Co Lake (Tibet). At older sediments presence of higher percentage of detrital material, lower $\delta^{18}O$ values, biological data show deep and dispersal lake water level, at younger sediments, higher $\delta^{18}O$ and $\delta^{13}C$ values mark dry climatic conditions to lake water.

Yuretic (2002) examined 35 metered borehole samples of Thomson Lake sediments which is at Majove Desert (USA) and searched about paleo-environment evolutions of the lake. At top, sandy sediments show Pleistocene coast and Holocene sand dune and playa environments. Under that unit silty clay and laminated clays which were deposited at deep lake environment are located with an unconformity. Smectite and illite are major minerals. $CaCO_3$ amount is determined as inversely proportional to clay mineral percentages. Analcime is abundant and it was formed due to alteration of smectite under effects of alkaline liquids.

Dean et.al. (2002) examined Holocene sedimentary sequence last 26,000 year) of Bear Lake (USA). Sediments that were deposited at last glacial period contain carbonates, poor in organic material and are red colored silty clay. Those glacial sediments probably were transported by Bear River which was active in that period. At Holocene as a result of disconnection of the river with lake, carbonate deposition was started and increasing in salt percentage of water causes firstly calcite then aragonite formation. Borehole samples (120 m section) that represent sedimentary sequence which deposited during last 250,000 years, include carbonated, grey-black colored silty clay in which calcite is major mineral. They explained that abundance of silisiclastic material shows river was connected to lake however red colored sediments were not deposited or sediments that were rich in organic material turns to grey-black color from the red. Before the Holocene aragonite formation, at two different period aragonite formations which were occured interglacial and warm climate, were discovered.

Kidder and Gierlowski-Kordesch (2002) indicated that improvement of two different well developed grasslands at Miocene increased lacustrine diatomite deposition. They stated that alhough volcanic silica was active in formation of diatomite; grassland distribution was more effective mechanism as a resource of silicate for lake. For "Opaline phytolith" mobilization of soil silicates by herbal assimilation is much more effective than other biochemical processes.

Fagel (2003) searched about Late Qartenary paleoclimatic changes by help of climatological archive of hemipelagic continuous sediment sequence of Baikal Lake. The alternated layers which were rich in diatom and clay were studied by using biological factors (diatom, pollen, spor etc.) in previous studies. In that study detrital clay minerals were used as a tool for climatic reconstruction. In the borehole samples it is observed in the diatoms rich sediments, smectite ratio increases systematically and this is a climatic footprint. These findings match with warm climatic conditions in which active hydraulic activity was dominant at drainage basin and melted glaciers.

Aziz et al. (2003) studied the middle Miocene sedimentary fill of the Calatayud Basin in north-eastern Spain. This paper presents the results of detailed sedimentological analysis of the various sedimentary facies deposited in the study area. The geometrical relationships between cyclically bedded deposits and lake margin and alluvial fan sediments provide the basis for a palaeoenvironmental reconstruction of the area during the middle Miocene. The basic mudstone – carbonate units of the small-scale cycles in the central parts of the lake basin are interpreted in terms of depositional environment, lake level and climate changes.

Spain Deocampo (2004) examined chemical properties of < 0.1 micrometer grain size of East African sediments. He defined Mg/(Al+Fe) ratio as octahedric cation index (OCI). That ratio has a range between OCI<0.1 at detrital dioctahedric clay minerals and OCI>4 at salty-alkaline lacustrine originated trioctahedric clay minerals. Octahedric layer composition of mid-basin clay minerals of paloe-lake Olduvai shows that lake was widen twice previously. Those expansion periods correlated with rainy periods which were stated as marine depositions of Africa. Chemical properties of clay minerals have an important role on

gathering paleoclimatic data in the case that absence of pollen and microfossils which contain carbonates-silicates.

Ivanov et al. (2011) presented the Miocene vegetation and climate dynamics in Eastern and Central Paratethys (Southeastern Europe). This study suggests that the Middle Miocene was the warmest period with mean annual tempretaure (MAT) of 17 °C to 19 °C and winter temperatures from 7 °C to 12.5 °C. It is also mentioned that climatic changes after the Miocene climatic optimum caused changes in floristic composition and vegetation structure. The vegetation shows a decreasing trend in abundance of palaeotropic and thermophilous elements, reduction of macrothermic elements, and disappearance of evergreen laurel forests. The available data indicate that major vegetation changes occur in the late Miocene. This period is characterized by more diverse climatic conditions, which were directed by global climatic changes and probably complicated by regional palaeogeographic reorganizations and tectonic processes.

CHAPTER 3

DESCRIPTION OF THE STUDY AREA

3.1. Geology Of The Region

Two major references, Akyürek et al. (1988) and Dönmez and Akçay, (2010), are referenced in this chapter. The following stratigraphical summary is generalized from them. The geological map of the study area (Figure 3.1) is from Dönmez and Akçay (2010). The generalized stratigraphical section is from Kaymakçı (2000) (Figure 3.2).

The oldest unit in the study area is Eldivan Ophiolite Complex (Ke) belonging to the İzmir-Ankara-Erzincan Suture Zone. It was defined as a complex of ultramafics, serpentinized ultramafics, gabbro-diabase, splite, radiolarian mudstone, chert limestone slices and plagiogranites by Akyürek et al. (1979, 1980, and 1981). Due to the tectono-stratigraphic relation between the Eldivan Ophiolite Complex and Karadağ Formation (Kk), the age of the complex was accepted as Senomanian-Campanian in these two major references. Serpentinite, peridotite and pyroxenite (Kesp) form the the bottom unit of the ophiolite in the region. Towards the upper units in the ophiolite, splite and spilitic basalt (Kes) are found. The upper most part is composed of radiolarite-mudstone (Ker) and cherty limestone (Keç).

The other major unit in the region is Dereköy Ophiolitic Melánge (Kd) (Akyürek et al., 1997). It consists of basic, ultrabasic, volcanic, ophiolitic and sedimentary rocks. Hisarköy formation is one of the units found in the ophiolitic melange. It is composed of olistoliths and olistostroms derived from the ophiolite. Limestone blocks (K) observed in the mélange is also found in the study area.

Karadağ formation (Kk) is observed in the study area. It is an alternation of volcanoclastic conglomerate, sandstone, mudstone and pelagic clayey limestone (Akyürek et al., 1982, 1984). This formation was dated by its fossil contents and so the age was reported as Senomanian-Campanian by Akyürek et al. (1997). Kurşunludüz Unit (Kkk) belongs to Karadağ formation and is formed from clayey limestones.

The study are also comprises of the cover units of Tertiary and Quaternary age which unconformably overlie the older units. One of them is Kumartaş Formation (Tmku) which consists of the alternation of red-gray colored conglomerates, sandstones, siltsontes, marl, tuff and clayey limestone (Akyürek et al., 1997). This formation is transitional vertically and horizontally with Hançılı Formation.

The age of Kumartaş Formation is accepted as Early-Late Miocene with its mammalian fossil content by Karadenizli et al. (2004). On the other hand, Dönmez et al. (2009a) gave Early Miocene age for Kumartaş Formation due to the coeval Aydos volcanics the age of which was assigned as Early Miocene.

Kumartaş Formation (Tmku) is vertically transitional to Hançılı Formation (Tmh). Hançılı Formation is composed of fluvio-lacustrine units of conglomerates, sandtones, siltstones, marl, clayey limestones, tuffs, gypsum and bituminous shales (Akyürek et al., 1980). It is mostly seen around Gündoğmuş, Ödek, Hançılı, Beykavağı, Satılarköy, Çankaya, Hacılar, Keklicek and Kalecik. Mostly it is overlain by Gölbaşı Formation (Tg).

The age of this unit is considered as Early Miocene since it is vertically and horizontally transitional with the Kumartaş Formation and Aydos volcanics. Türkecan et al. (1991) gave an age of Early Miocene due to some micro-mammallian fossil content, on the other hand, Akyürek et al. (1997) found some other fossils and gave an age range of Serravalian-Tortonian. Dönmez and Akçay (2010) accepts the age of Hançılı Formation as Early-Middle Miocene. Differently, the age of the Hançılı Formation is determined as Early Pliocene by Türkmenoğlu et.al. (1994).

Karakoçaş Formation (Tmka) is mostly seen on the road of Şabanözü-Eldivan. It is formed from red-gray colored conglomerates and mudstones (Akyürek et al., 1988). Due to intercalation with Aydos volcanics, the age of this unit is accepted as Early-Middle Miocene (Dönmez and Akçay, 2010).

Stratigraphically the younger unit than Karakoçaş Formation is Bozkır Formation (Tplb) which is comprised of gypsum, mudstones, sandstones and tuffs. The literature regarding the study area, unfortunately, do not put any age for this unit by fossil content, however, Karadenizli et al. (2004) accepted Pliocene age for Bozkır Formation.

The youngest unit in the region is the alluvium (Qeal, Qal). It consists of both the oldest and the youngest Quaternary fluvial sediments which are unconsolidated sand, clay and gravles (Dönmez and Akçay, 2010).
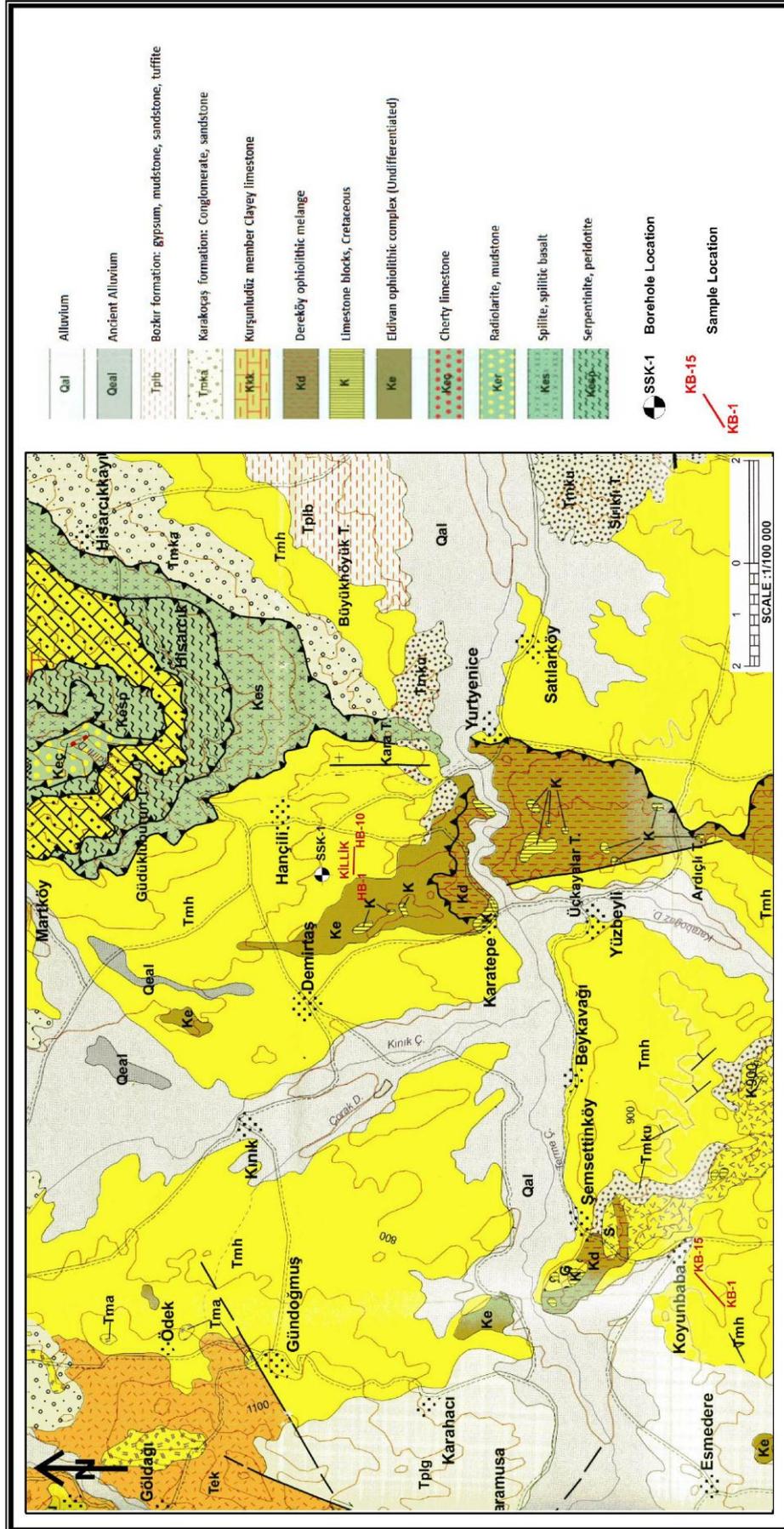
Figure 3.1. Geological map of the study area (from Dönmez and Akçay, 2010).

AGE	UNIT	THICK. (m)	LITHOLOGY	DESCRIPTION	FOSSILS	FACIES
GELASIAN MN-17	DEYİM.	20		1. Poorly to unsorted, polygenetic loosely packed conglomerates		FLUVIAL
BURDIGALIAN TO LANGHIAN (MN-4 to MN-5)	HANCILI FORMATION	190		2. Gray, Greenish blue shale with bentonite occurrences 3. Mudstone/shale RODENT FAUNA 4. Thin bedded clayey limestone with chert nodules 5. Dark gray mudstone with bentonitic and organic rich levels 6. Alternation of yellow to buff clayey lacustrine limestone shale and marl. 7. Thin coal seams	*Megacricetodon* cf. *collongensis*, *Democricetodon* sp. *Cricetodon* sp. *Anomalomys* sp. (minor group) *Eumyarion* sp. *Spalacid indet.* (two species) *Peridyromys* sp.	LACUSTRINE
BURDIGALIAN (MN-3 to MN-4)	ALTINTAS FORMATION	150		8. Red sandstone and siltstone RODENT FAUNA 9. Fining and thinnig upwards sequence of poorly sorted, loosly packed polygenetic red conglomerate UNCONFORMITY	*age of the unit is based on Şen et al. (1998)*	FLUVIAL
UPPER CRET.	NAOM			10. Ophiolitic melange		

Figure 3.2. Generalised stratigraphical section of the study area (Kaymakçı, 2000).

3.2. Description Of The Sampling Locations

3.2.1. Koyunbaba (Kalkan Tepe) Section

The first sampling site was Koyunbaba Villiage where the Hançılı Formation is well-exposed. It was a 75 m deep section from which 15 samples were taken along (Figure 3.3). The section generally composed of fine to medium grained clastic sedimentary rocks. The explanation of lithological facies is given from bottom to top of the section. The bottom-most part of the unit is occupied by massive, gray-blue colored mudstone of 5.5. m thickness. The sample taken from this level is named as KB-1. Above KB-1, light-brown colored sily sandtone was found. It is a 0.5m thick unit of the sample KB-2. Fissile-shale with sandy bottom part was found up to the section. It has a 4 m thickness. KB-3 sample were taken from this unit.

Above KB-3 sample level, conglomeratic sandstone unit was found. It is a 9.5m thick unit and the sample from this unit is called as KB-4. KB-5 sample was taken from almost the middle part of the section where 0.5m thick sandstone unit was occupied. The following unit is a marl with 2m thickness and the sample from this unit is named as KB-6. At the middle of the section, there was an alternation of marl and sandtone. This unit is the thickest one (17 m thickness). The sample taken from the middle part of this alternation was called as KB-7.

A very thin shale level was found above KB-7 unit. This unit was 0.5m thick and the sample taken form there was named as KB-8. 9.5 m thick sandstone unit following the KB-7 sample level was not sampled but measured through the section. Above this, 1.5m thick marl unit was sampled and the sample was called as KB-9. A very thin unit of fissile shale (0.5m thick) followed the KB-9 level. It was named as KB-10. 9m thick alternation of sandstone and shale is observed through the upper parts of the section. KB-11 sample was taken from this unit. It is followed by 6m thick shale unit from which KB-12 sample was taken. The upper units which have 3 m total thickness show alternations of mudstone (KB-13), shale (KB-14) and sandstone (KB-15). The uppermost unit was rippelled sandstone with 6 m thickness. This unit was only measured but not sampled.

Section Depth (m)	Thickness (m)	Lithology Profile	Description	Sample
			Rippled Limestone	
	6.0			
	3.0		Alternation of Shale, Sandstone and Mudstone	KB 15 / KB 14
	6.0		Shale	KB 13
	9.0		Alternation of Sandstone and Shale	KB 12 / KB 11
	0.5		Fissile Shale	KB 10
	1.5		Marl	KB 9
	9.5		Sandstone	
	0.5		Shale	KB 8
	17.0		Alternation of Marl and Sandstone	KB 7
	2.0		Marl	KB 6
	0.5		Sandstone	KB 5
	9.5		Conglomeratic Sanstone	KB 4
	4.0		Fissile Shale	KB 3
	0.5		Silty Sandstone	KB 2
	5.5		Mudstone	KB 1

Figure 3.3. Columnar section of the Koyunbaba Section.

3.2.2. Hançili (Killik Location) Section

Hançılı section (Figure 3.4) which is exposed at Hançılı village, Killik location, measured as 16.5 m stratigraphic section through Hançılı Formation (Figure 3.5). Lithological units were explained in this section from bottom to top.

The brownish bottom unit of the section which is almot 2.8 m deep was sandy-clayey mudstone. HB10 sample was taken from this unit. It is follwed by 3.7 m deep clayey mudstone with brownish color. HB9 sample was taken from this unit. It is overlain by 1.5 m deep bentonitic claystone with grayish color. HB8 sample was gathered from this level. A bentonite level with 1 m depth follows the bentonitic clayestone. It has a white – cream color with massive structure. HB6 sample was taken from this unit. On top of it, bentonitic mudstone layer with 3.5 m depth was found. HB4 sample belongs to this unit. Up to the section, red mudstone unit with 2.5 m depth was found and the sample HB2 was taken. At the top, 1.5 m deep tuff layer exists. HB1 sample was form this unit.

Figure 3.4. The Field view of Hançılı Formation at Killik Location

Thickness (m)		Lithology	Sample no.
1.5		Tuff	HB-1
2.5		Red Mudstone	HB-2
3.5		Bentonitic Mudstone	HB-4
1.0		Bentonite	HB-6
1.5		Bentonitic claystone	HB-8
3.7		Clayey Mudstone	HB-9
2.8		Sandy Mudstone	HB-10
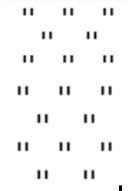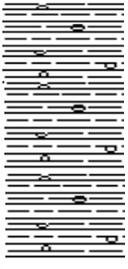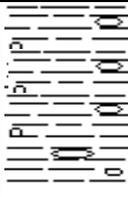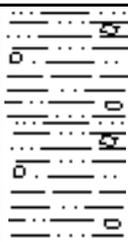
Figure 3.5. Measured stratigraphic section of Hançılı Village Killik Location (non-scaled).

3.2.3. Borehole SSK-1 Section

The borehole opened at Tepetarla location (Figure 3.6 and 3.7), Hançılı, Ankara was named as SSK-1 borehole. The drilling was started on January 11th, 2006 by gathering 1.5 m core first. Unfortunately, due to the bad weather conditions, the borehole machine was broken down, the operation was withdrawn to February, 2006. Under proper climatic conditions, the borehole machine was again operated. On March 15th, 2006, by taking 60 m continous core samples which crossed the lake sequence, one of the most important part of drilling with core, was completed. It was very important to take such a continous core from this region to reconstruct continous climatic history. This location was the best to drill because, it is placed at the centre of the syncline so provides the thickest point of the lake sequence (Figure 3.8).

Figure 3.6. The far view of Tepetarla location where the borehole studies are performed.

Figure 3.7. The close view of the borehole study.
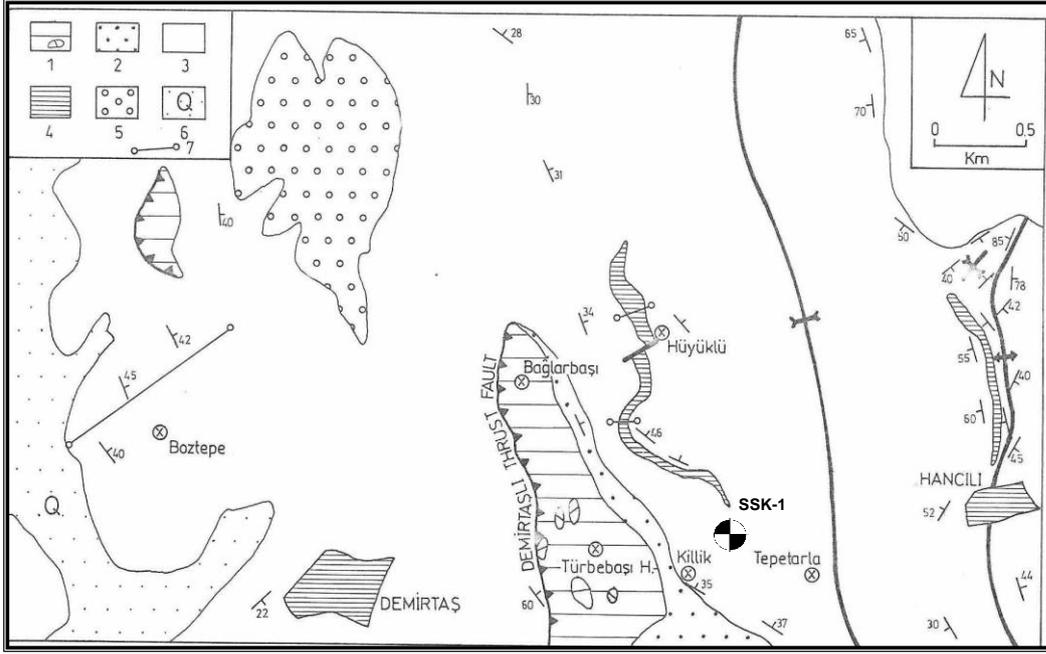
Figure 3.8. Geological map of Demirtaş-Hançılı region (Türkmenoğlu et.al.,1994).

1-Upper Cretaceous Ophiolithic Melange (Anatolian Complex), 2-Aslantaş Fm., 3-Hançılı Fm., 4-Bentonite and pluvial cherty limestone, 5-Büyükhacıbey Fm., 6-Quaternary deposits, 7-Measured startification location, SSK-1 – Borehole location

Borehole studies finally completed on May, 2006. The core samples which were taken during the borehole studies are boxed (Figure 3.9) and sent to METU Geological Engineering, Clay Mineralogy Laboratory for experimental studies and protection purposes.

Figure 3.9. A sample picture for the SSK-1 borehole cores.

Figure 3.9 cont'd.

Figure 3.9 cont'd.

BOREHOLE NO: SSK-1

DEPTH: 18.00 m - 22.00 m

Figure 3.9 cont'd.

BOREHOLE NO: SSK-1

DEPTH: 22.00 m - 26.50 m

Figure 3.9 cont'd.

BOREHOLE NO: SSK-1

DEPTH: 26.50 m - 31.50 m

Figure 3.9 cont'd.

BOREHOLE NO: SSK-1

DEPTH: 31.50 m - 36.00 m

Figure 3.9 cont'd.

Figure 3.9 cont'd.

Figure 3.9 cont'd.

Figure 3.9 cont'd.

Figure 3.9 cont'd.

Core samples were examined in terms of their lithologies and the borehole stratigraphic section was gathered. Appendix-1 shows the changes on the lithology, lake level and the analysis done on Hançılı and Aslantaş Formation.

Totally 60m deep core was drilled. At the bottom of the section SSK-1, Aslantaş Formation with mudstone of gray – red colored was found. On the continous section, it has a 7.3m depth. The literature given on the geology chapter shows that Aslantaş Formation is of Late Langhian-Tortoian and represents alluvial-fluvial environment (Türkmenoğlu et.al., 1994).

Hançılı Formation overlies Aslantaş Formation. The total depth of the Hançılı Formation on the continous SSK-1 section is 52.7m (Appendix-1). Hançılı Formation started with reddish to brown colored, fine - coarse grained sandstone unit of 2.2m depth. On top of the bottom sandstone unit, while Lacustrine environment was dominant, limestones with grayish green color, reddish brown-grayish colored marl and dark gray colored mudstone units were deposited. Their total thickness is 20.5 m. Then, the deposition of the lake sediments stopped with the mudflow most probably triggered by the volcanism (Appendix-1).

The product of this volcanism was a thin andesite band followed by a thin conglomerate layer. The following 16.5m deep layer was a clastic Lacustrine products which were stopped by 3 times with a 3 different tuff deposition. It points the active volcanism around Hançılı Formation. White-crème colored, clayey-, micritic limestone and marl sequence including mudstone and siltstone units were found at the middle to the top of the section. The last 15.5 m sequence at the top ended with dirty white-crème colored, fine grained, hard, clayey limestone (Appendix-1). This section was sampled from HAN1 to HAN60 from top to bottom. Samples were arranged for the XRD, isotope, geochemistry and thin sections.

CHAPTER 4

MINERALOGY

This chapter includes the determination of mineral compositions in bulk and clay fractions of the samples by X-ray diffraction analysis, the qualitative evaluation of the minerals and the their interpretations in thin section of the selected samples. Also, scanning electron microscope (SEM) studies were employed to define the crystal shapes, morphologies and textural relations between some minerals.

Clay minerals are very important in paleoclimate studies, since their formations are mostly climate dependent. Therefore, the presence of any authigenic clay mineral in a sequence may provide long-term climatic interpretation of the region studied. To have a good clay data, firstly clay fraction should be separated from the bulk. It was explained in the Methodology chapter. (Chapter 1.5) The clay fraction, then were X-rayed to have qualitative and semi-qantitative data of the section studied. Qualitative determination of the clay minerals were conducted according to Brindley (1980), Thorez (1976) and Chen (1977).

Three sections from the study area were mineralogically evaluated according to their bulk and clay fractions. The first two sections were from outcrops but the last one which is SSK-1 was a drillhole, therefore it provides core data.

4.1. Koyunbaba (Kalkan Tepe) Section

The first sampling site was Koyunbaba Villiage where the Hançılı Formation is well-exposed. Through this section, 15 samples were taken. Samples were analysed by XRD. The section generally composed of fine to medium grained clastic sedimentary rocks.

The bottom-most part of the unit is a mudstone. The sample taken from this level is named as KB-1 consisting of dolomite, analcime, feldspar, quartz and cristobalite (Figure 4.1). Illite and smectite, on the other hand was determined as clay minerals of this unit (Figure 4.2).

Above KB-1, light-brown colored silty sandtone named as KB-2 includes feldspar, quartz, and clinoptilolite/heulandite as non-clay minerals (Figure 4.3). The clay minerals of this unit are illite and little amount of smectite (Figure 4.4). The sample gathered from this unit was named as KB-2.

Fissile-shale with sandy bottom part (KB-3) was found in the section. It has non-clay minerals of dolomite, analcime, feldspar, quartz and cristobalite. As clay mineral illite, smectite and chlorite were determined.

Above KB-3 sample, the sample unit called as KB-4 has non-clay components, feldspar, quartz, clinoptilolite / heulandite were determined. As clay minerals illite and very small amount smectite were found.

KB-5 sample is composed of clay and non-clay mineral contents which are exactly the same as the unit KB-4 taken out. The following unit is marl and the sample from this unit is named as KB-6. Here, dolomite and feldspar exists as non-clay minerals. But the clay minerals are same with the units of KB-4 and KB-5.

At the middle of the section, there was a thick alternation of marl and sandtone consisting of non-clay minerals of dolomite, analcime, feldspar, quartz and and clay minerals of illite with little amount of smectite (KB-7).
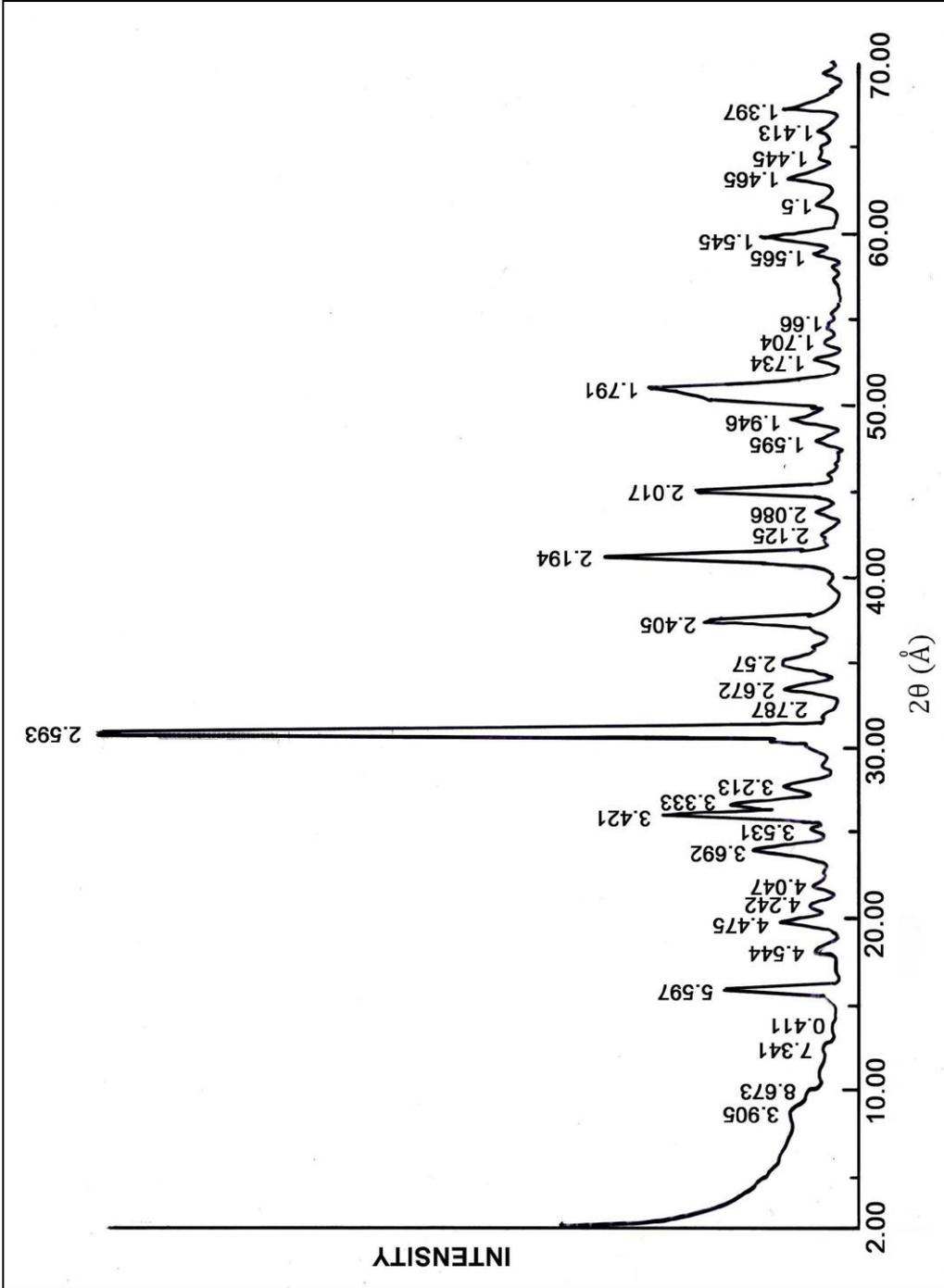
Figure 4.1. Bulk mineral content of KB-1 sample determined by XRD

A shale level as KB-8 was evaluated mineralogically and so quartz, calcite, analcime, feldspar are found as non-clay components, whereas illite-smectite (mixed layered clay mineral) and very small amount chlorite are determined as clay minerals. Scanning electron microscope (SEM) image of KB-8 also shows the presence of I/S mixed-layer (Figure 4.5)

.
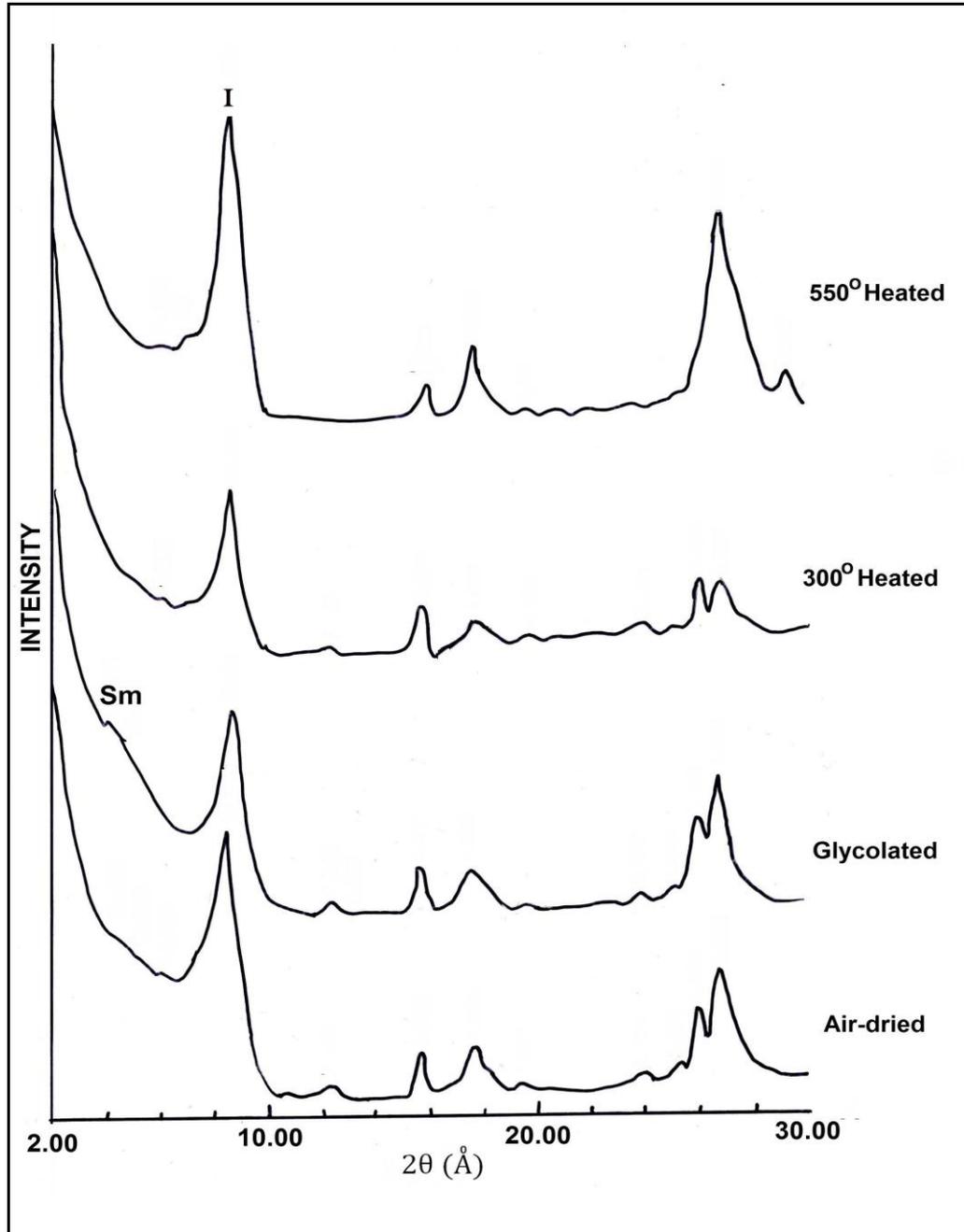
Figure 4.2. XRD analyses on the clay fraction of KB-1 sample.
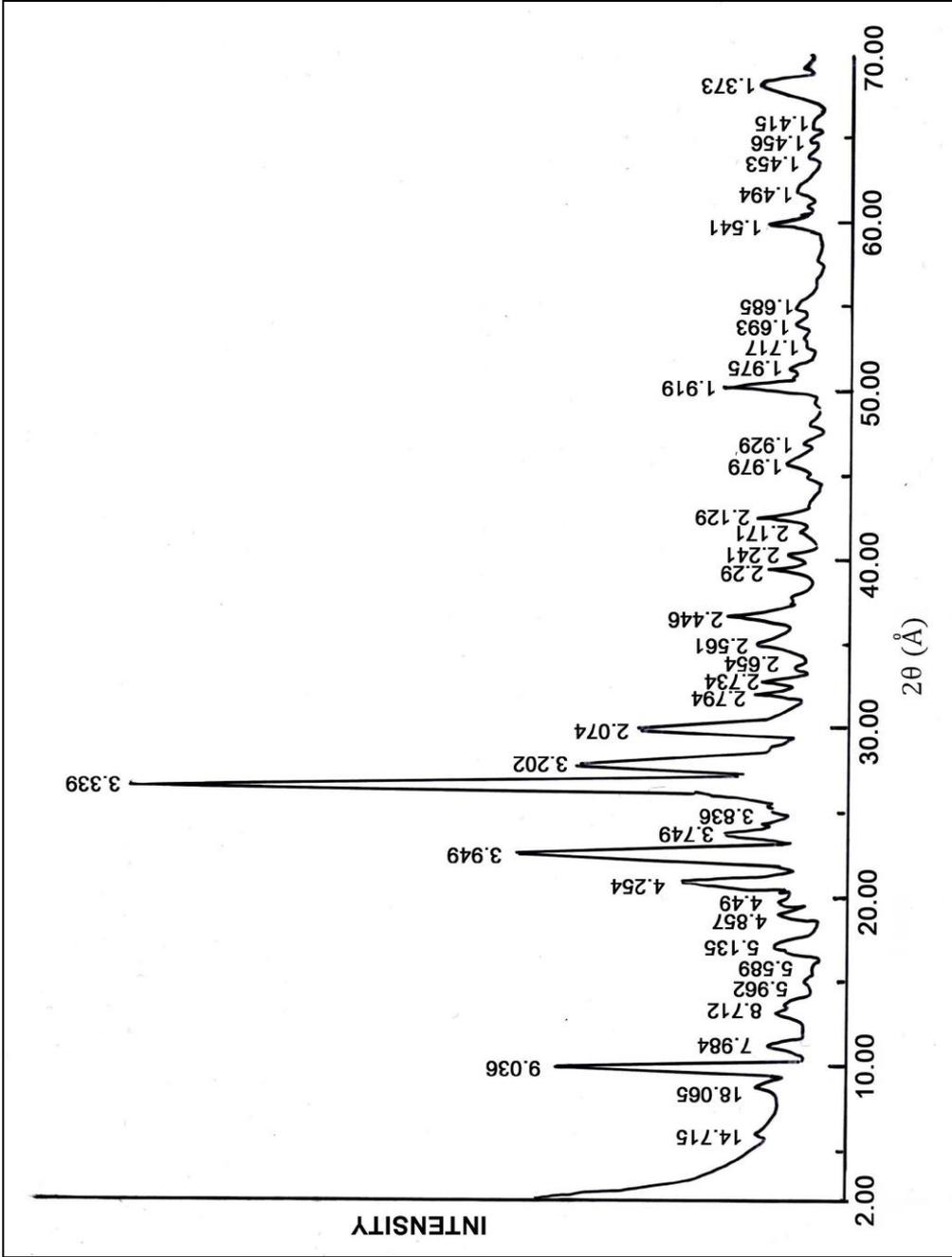
Figure 4.3. Bulk mineral content of KB-2 sample determined by XRD
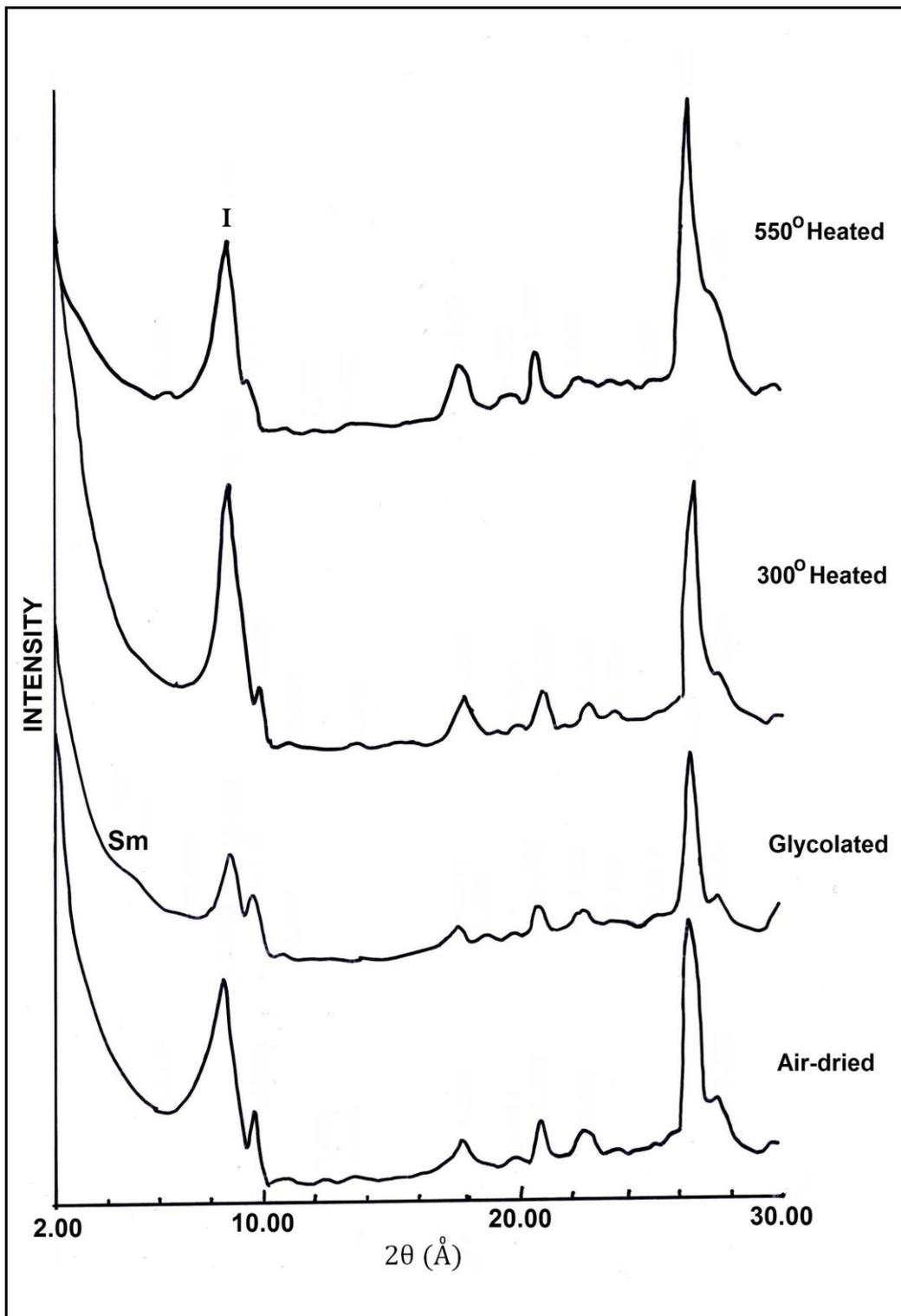
Figure 4.4 XRD analyses on the clay fraction of KB-2 sample.
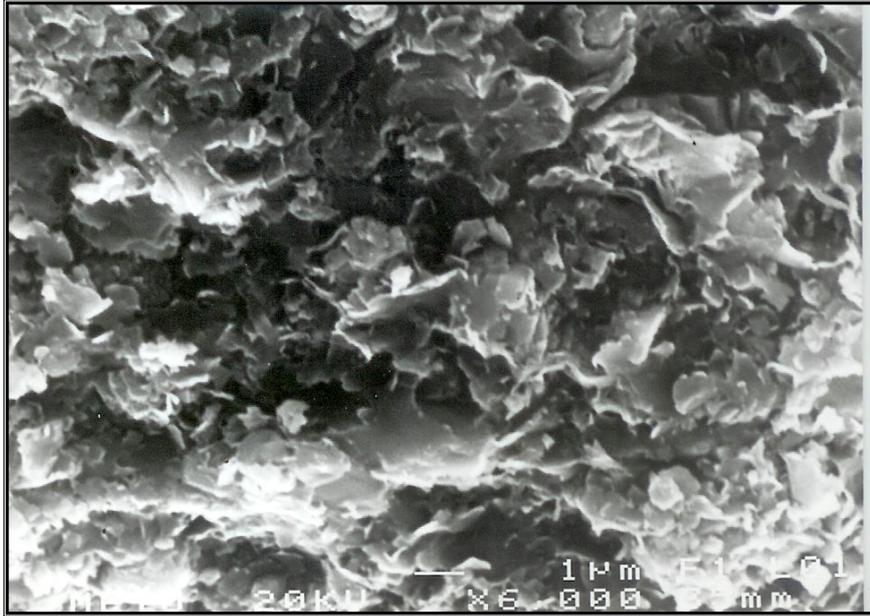
Figure 4.5. The SEM image of KB-8 sample showing illite-smectite mixed layered.

KB–9 sample is composed of dolomite, feldspar, quartz and analcime as non-clay minerals. As clay minerals, very small amount llite was found. The non-clay components of the following KB-10 sample are the same with KB-9 but illite-smectite mixed layered clay mineral was found as clay minerals

From the thick alternation of sandstone and shale, KB-11 sample was taken which includes dolomite, analcime, quartz and feldspar as non-clay components. As clay minerals, illite-smectite mixed layered and very small amount of illite were determined. To the top of the section, KB-12 sample has quartz, calcite, feldspar, analcime and clinoptilolite/heulandite. Also, illite-smectite mixed layer was observed in this unit as clay mineral component.

The upper units which have 3 m total thickness show alternations of mudstone (KB-13), shale (KB-14) and sandstone (KB-15). Dolomite, feldspar, quartz, analcime (Figure 4.6) and clinoptilolite/heulandite were observed. On the XRD diffractograms, illite-chlorite-smectite mixed layers, illite and small amount of smectite were determined. The uppermost unit was rippelled sandstone with 12 m thickness. This unit was only measured but not sampled.
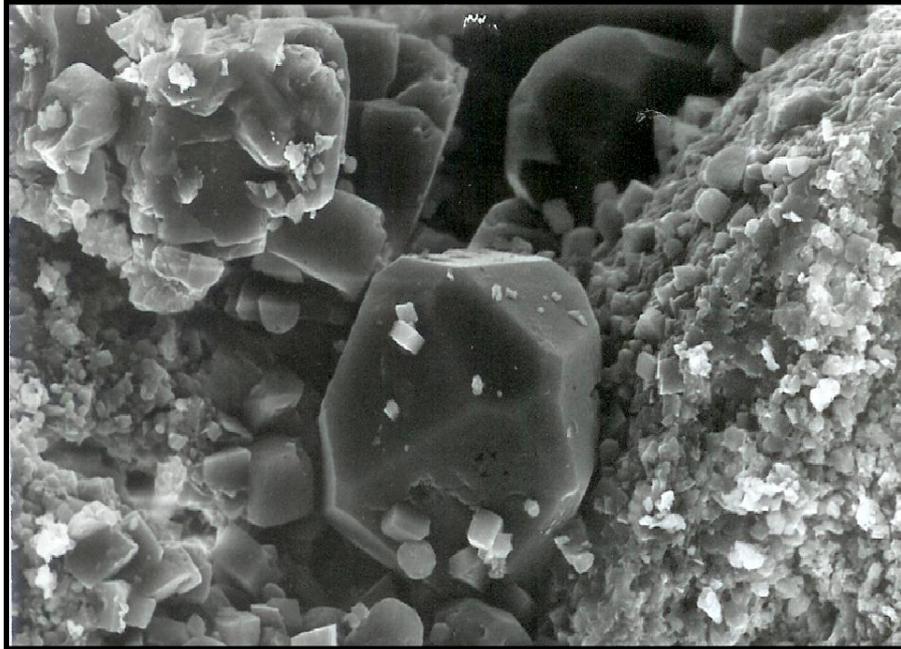
Figure 4.6. The SEM image of KB-11 sample showing analcime crystal.

4.2. Hançili (Killik Location) Section

Hançılı section like Koyunbaba Section was studied mineralogically by XRD and SEM studies. From bottom to top, the mineralogical compositions were explained here. The brownish bottom unit of the section was sampled as HB10 which is composed of quartz, plagioclase, cristobalite as non-clay minerals and smectite as clay-components. The following HB9 sample includes smectite as a clay mineral and quartz, plagioclase, biotite and cristobalite as non-clay minerals and also volcanic rock fragments are determined by optical microscope. HB8 sample consists of smectite and a very small amount of illite-smectite mixed layer. Also, quartz, plagioclase, biotite and cristobalite exist in HB-8. Th overlying unit is composed of Na-smectite as clay mineral and quartz, plagioclase, biotite, muscovite, cristobalite and volcanic rock fragments as non-clays. Then, HB4 sample consists of smectite, analcime, quartz and feldspar minerals. To the top, HB2 sample includes smectite and very small amount illite-smectite mixed layer, together with analcime, quartz and feldspar in the bulk fraction. The top most unit was sampled as HB1 and mineralogically analysed. Analcime, micritic calcite, quartz, feldspar, biotite and volcanic rock fragments are determined in HB-1 unit.

4.3. SSK-1 Section

The lowermost unit is Aslantaş Formation and samples of HAN-59, HAN-60, HAN-61, HAN-62, HAN-63, HAN-64, HAN-65 were examined under optical microscope. The presence of heulandite mineral which is a mineral of zeolite group was determined under microscope on HAN-60 sample (Figure 4.7). By X-ray diffraction analysis on samples of HAN-59, HAN-61, HAN-63 and HAN-65, illite-smectite mixed layer was determined (Figure 4.8).

Figure 4.7. Photomicrograph of heulandite crystal HAN–60 sample (4x10, XPL)
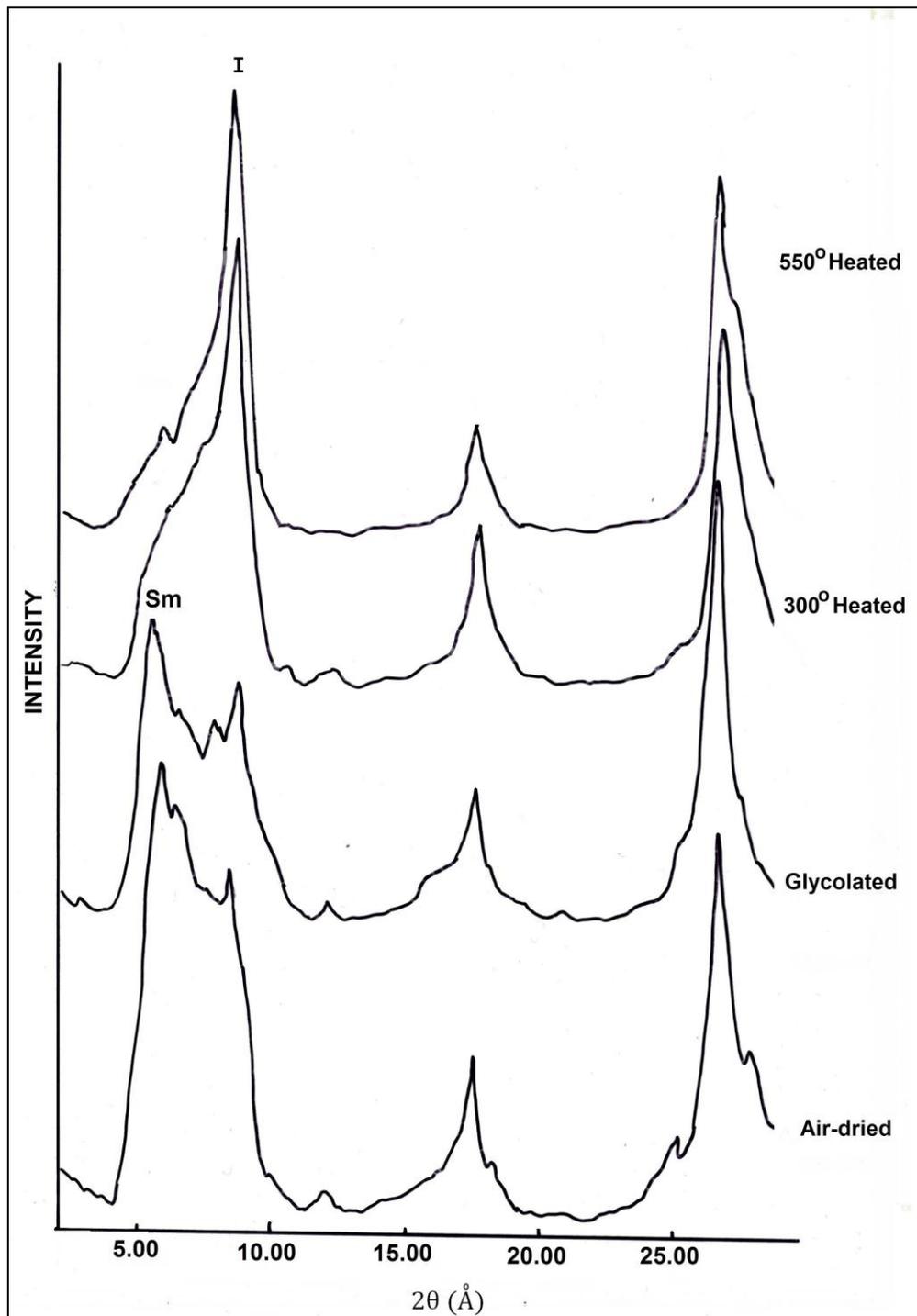
Figure 4.8. XRD analyses on the clay fraction of SSK-1 section, HAN63 sample.

Over Aslantaş Formation, the sequence of Hançılı Formation starts. The optical mineralogy study on the thin section of the sandstone unit at the bottom of the formation clearly shows its arkosic characteristics (Figure 4.9).
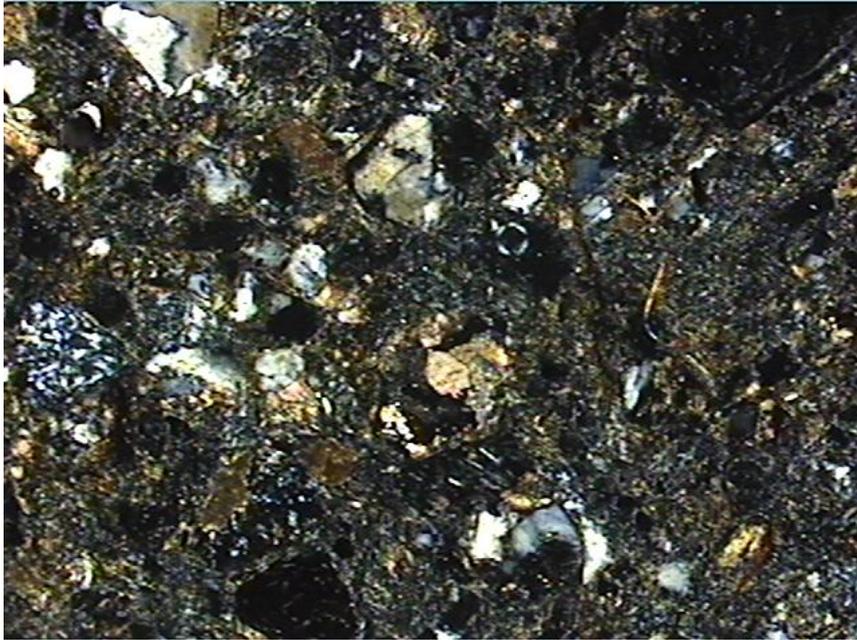
Figure 4.9. Photomicrograph of silt grains which formed by metamorphic rock fragments and surrounding clayey matrix and cement in the sandstone(HAN–58, XPL, 4x10).

The overlying limestone unit was also sampled. Thin section of HAN-57 sample shows diagenetic texture developed. It contains dissolution cavities and pores which were filled with secondary sparry carbonates. It is also observed that clay illuviations are found as brown colored laminated infillings (Figure 4.10). X-Ray Diffraction study on the clay fraction of HAN-57 reports the presence of illite-smectite mixed layer.

Figure 4.10. Photomicrograph of limestone that shows diagenetic texture (HAN–57, 4x 10, XPL).

Up to the section, reddish brown, grayish green colored silty clayey marl lies over the limestone. Fe-oxide linings and rarely framboidal micritic calcite occurrunces are determined. As clay mineral components of this level, illite-smectite mixed layer and few chlorites were observed by XRD. Over this unit, reddish brown colored mudstone is found. On the thin sections, fine sand and coarse silt grains are determined. Following unitwhich is reddish brown - grayish green, silty, clayey marl sampled as HAN-49. It shows peloidal/ooidal fragments, thin bioturbations and subangular paleosol (Figure 4.11).
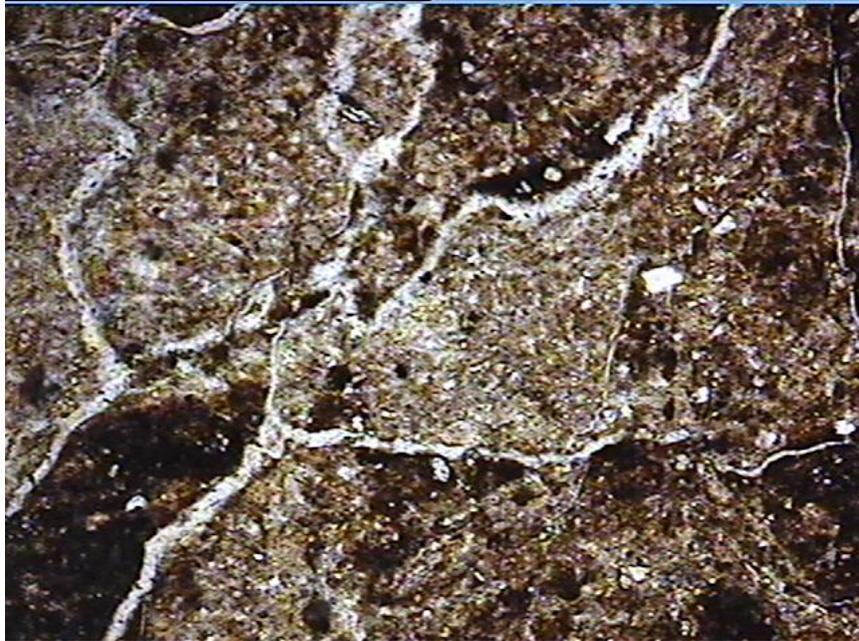
Figure 4.11. Photomicrograph of subangular soil structure in the marl (HAN–49, 4 x10, XPL).

Then, the overlying unit which is micritic limestone shows the presence of small amount fresh quartz microcrystals and very small amount microcrystalline feldsparsl. No fossil was recorded in this level. The clay fraction of this limestone is composed of illite-smectite (smectite dominant) mixed layer.

Overlying unit, dark gray locally reddish brown colored mudstone, has Fe-oxide linings together with fresh quartz crystals, plagioclase, biotite and volcanic glass fragments (HAN-43). Illite-smectite (smectite dominant) mixed layer is observed in clay fraction by XRD. At a depth of 29.50m, andesite was observed at the middle of the core. Under optical microscope, plagioclase phenocrysts surrounded by micrite presenting flow texture were observed (Figure 4.12).
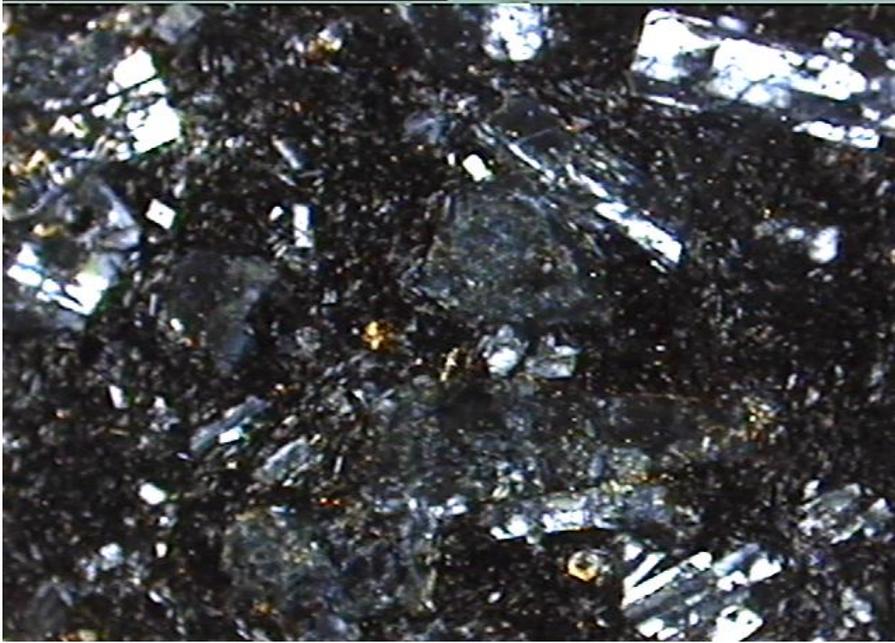
Figure 4.12. Photomicrograph of andesite showing plagioclase phenocrysts (HAN–41, 4x10, XPL).

Just above the andesite unit, there is a thin conglomerate level. Under microscope, rock fragments of quartzite and volcanic rocks are observed (Figure 4.13).
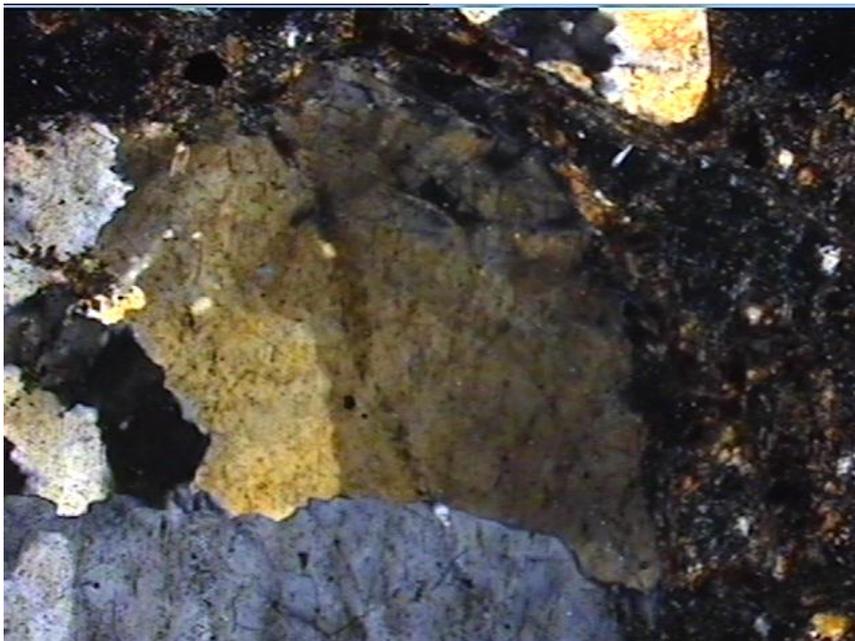
Figure 4.13. Photomicrograph of rock fragments of conglomerate (HAN–40,XPL, 4x10).

The overlying bentonitic claystone unit was sampled and evaluated mineralogically. In the thin sections, quartz and feldspar crystals surrounded by Fe-oxide linings are determined. In the section there is also radial zeolite that accompanying with opacity (Figure 4.14). The clay fraction of this unit has well crystallized smectite and a very small amount chlorite.
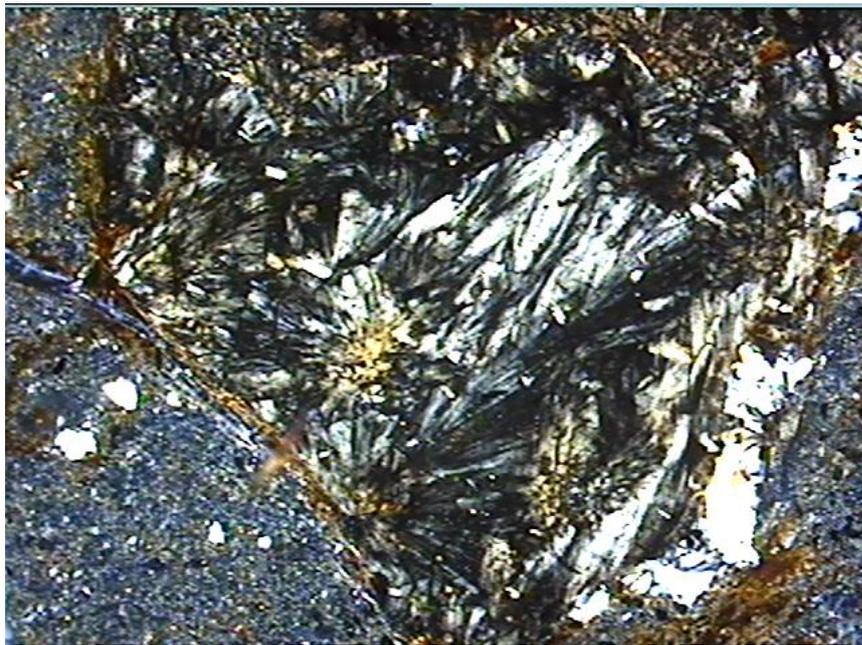
Figure 4.14. Photomicrograph of zeolite mineral (HAN–36,XPL, 4x10).

Over the bentonite, the claystone is observed with metamorphic rock fragments, quartz, plagioclase microcrystals, biotite, argillaceous pumice relict texture, few micritic calcitization and zeolitization (heulandite) under optical microscope. The clay fraction of HAN-31, HAN-32, HAN-33, HAN-34 and HAN-35 samples from the claystone have very well crystallized smectite mineral together with chlorite (Figure 4.15).
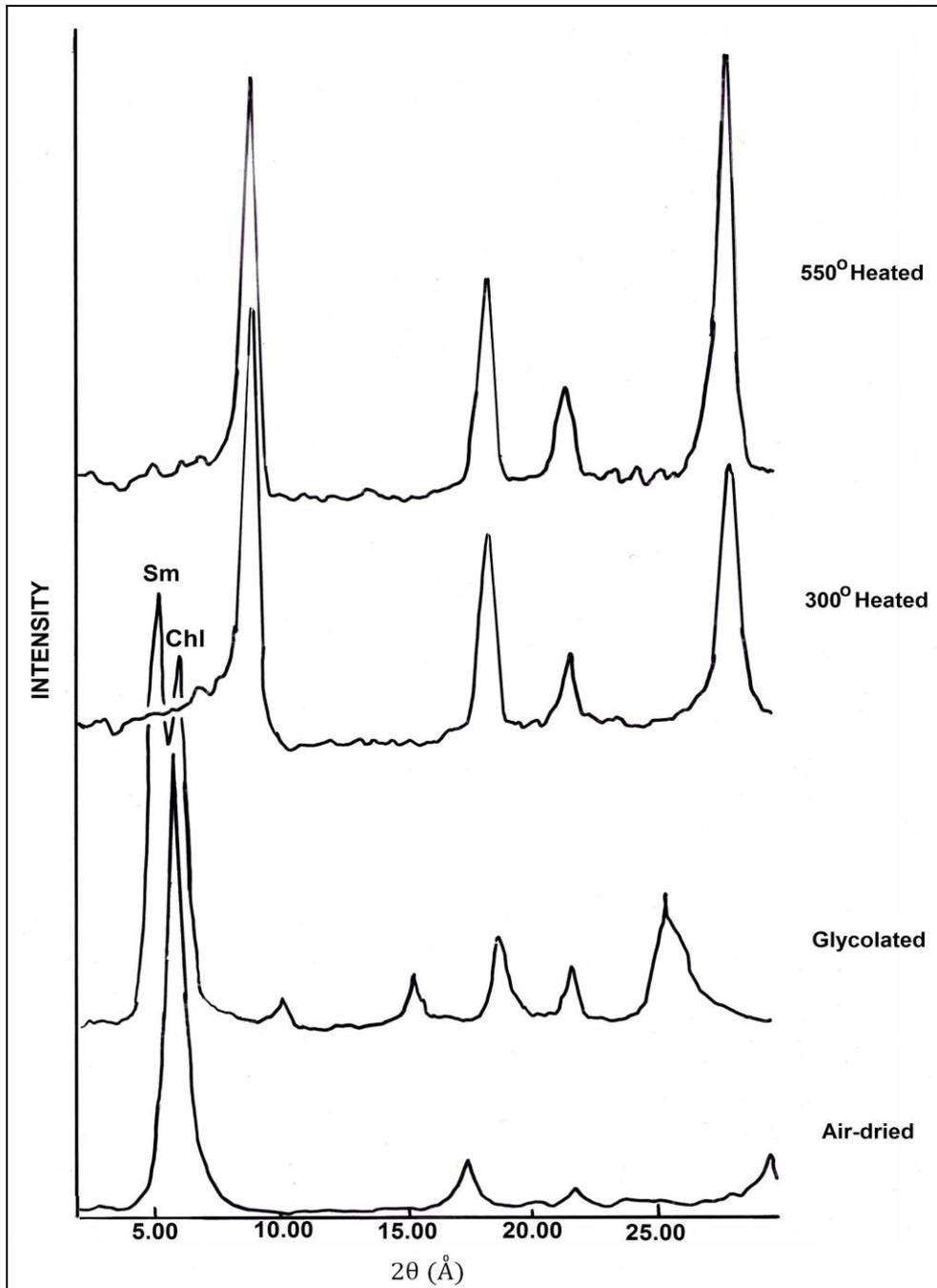
Figure 4.15. XRD analyses on the clay fraction of HAN-35 sample from SSK-1 section.

Overlying mudstone unit has dolomite and small amount quartz. Additionally, on the thin section of HAN-30 sample, heulandite mineral developed inside the braciapoda is observed (Figure 4.16). The clay fraction shows the presence of smectite-illite (smectite dominant) mixed layered and very small amuount of chlorite.
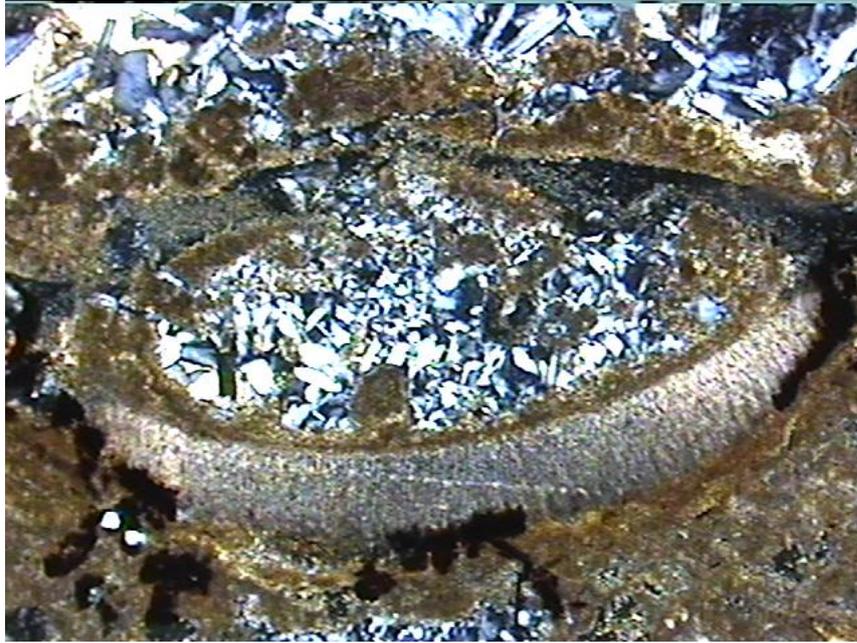
Figure 4.16. Photomicrograph of heulandite crystal inside the braciapoda (HAN-30, XPL, 4x10).

Up to the section, the overlying gray-grayish green colored, fine grained tuff has chalcedone (Figure 4.17). XRD analyses show abundant quartz and small amount dolomite and HAN-19 sample shows the presence of small amount illite-smectite mixed layered and chlorite in the clay fraction.
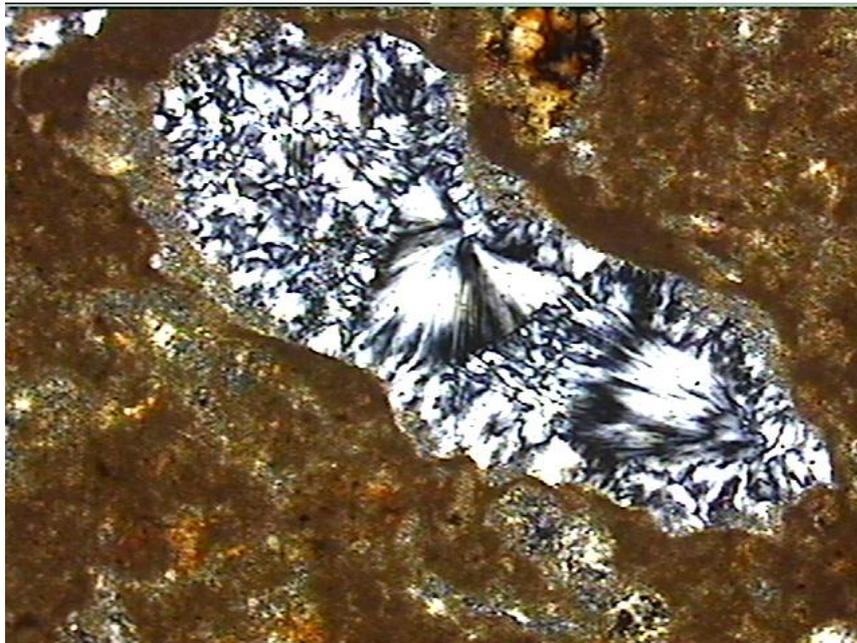
Figure 4.17. Photomicrograph of chalcedone mineral as infilling (HAN-19, XPL, 4x 10).

Up to the section HAN-17 sample from mudstone unit has mixed layered illite-smectite in the clay fraction. Then, clayey limestone - limestone which shows micritic texture and joints surrounded by Fe-oxide linings are found. Also as detritic materials small amount chert, metamorphic rock fragments, plagioclase and opaque minerals are found (Figure 4.18).
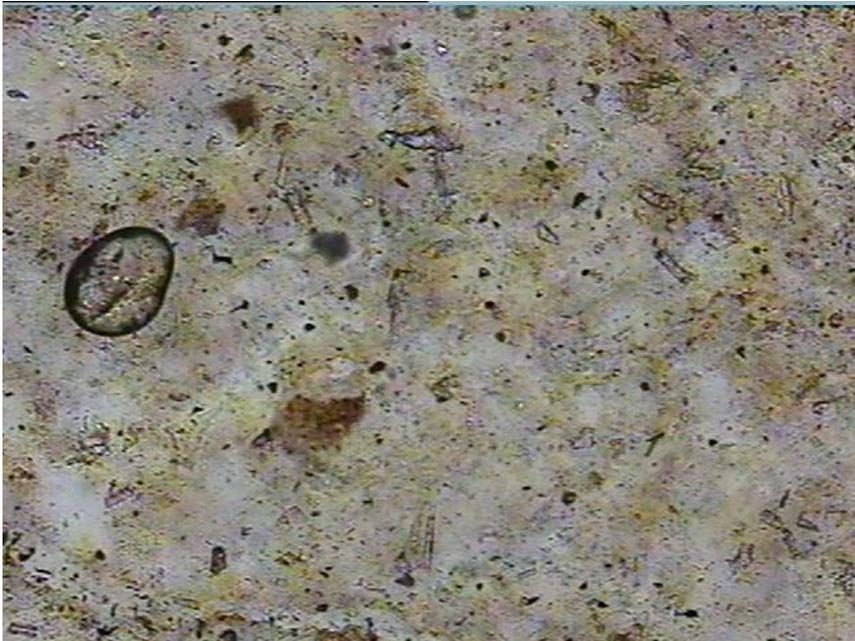
Figure 4.18. Photomicrograph of micritic clayey limestone (HAN-15, PPL, 4x10).

HAN-15 sample, illite-smectite (illite dominant) mixed layer and chlorite are observed in the clay fraction. HAN-14 sample from 14 m at depth, has volcanic and metamorphic rock fragments and feldspar grains in the tuff unit under microscope (Figure 4.19). Also abundant and fresh plagioclase crystals and quartz are determined (Figure 4.20) In the clay fraction, glass is observed as amorphous material and zeolite is possibly found.
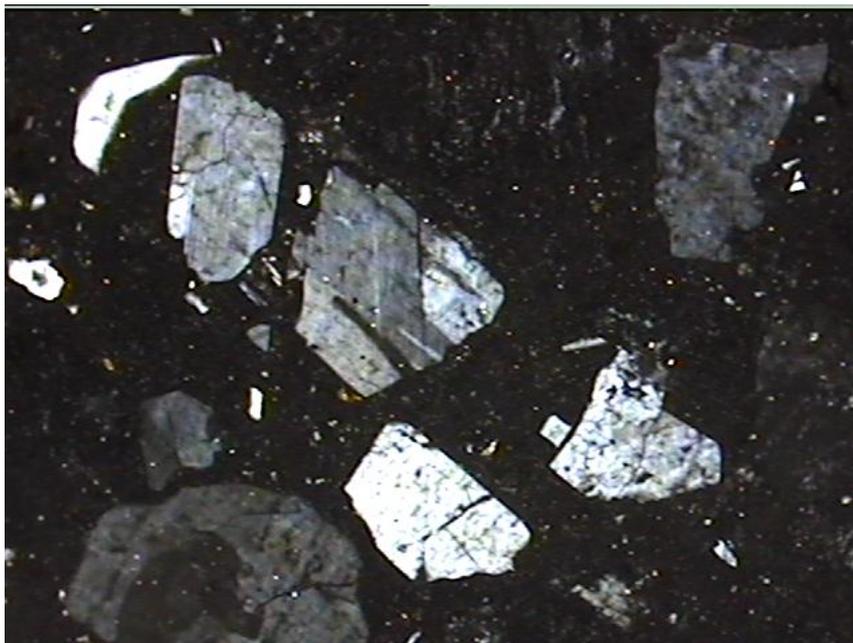
Figure 4.19. Photomicrograph of vitrified tuff, HAN-14 (XPL, 4x10).
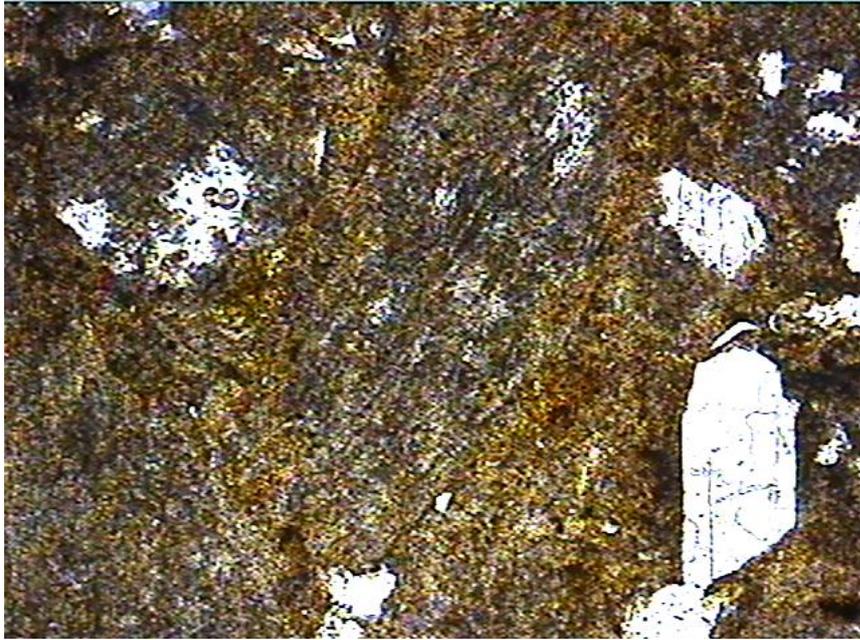
Figure 4. 20. Photomicrograph of pumice and volcanic crystals in the tuff (HAN-14,PPL,4x 10)

HAN-12 and HAN-13 samples have almost the same mineral components as ilite-smectite mixed layer, plagioclase and quartz. HAN-11, on the other hand, includes only chlorite as clay mineral. HAN-9 sample's clay fraction shows the presence of illite-smectite mixed layer, analcime and plagioclase. The bulk composition of the HAN-8 sample from mudstone unit shows abundant dolomite and ilite-smectite (50% illite and 50% smectite) mixed layer. It has also heulandite determined microscopically (Figure 4.21). In clay fraction of HAN-7 sample, illite-smectite (smectite dominant) mixed layered, small amount chlorite and analcime are observed.
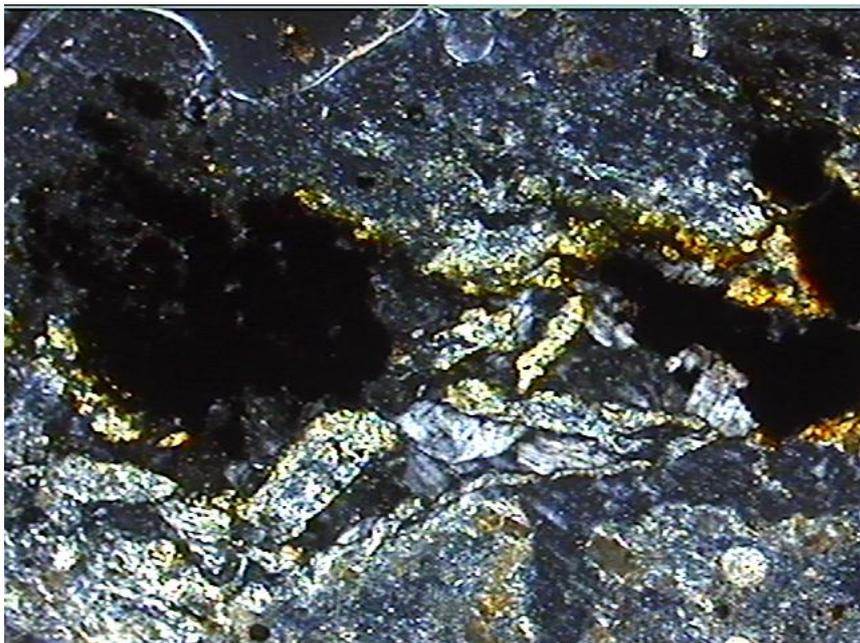
Figure 4. 21. Photomicrograph of heulandite crystal (HAN-9, XPL, 4x10).

Up to the section, siltstone unit of HAN-4, HAN-5, HAN-6 were sampled. In the clay fraction of these samples, illite-smectite (smectite dominant) mixed layer, very small amount chlorite and analcime are determined (Figure 4.22).
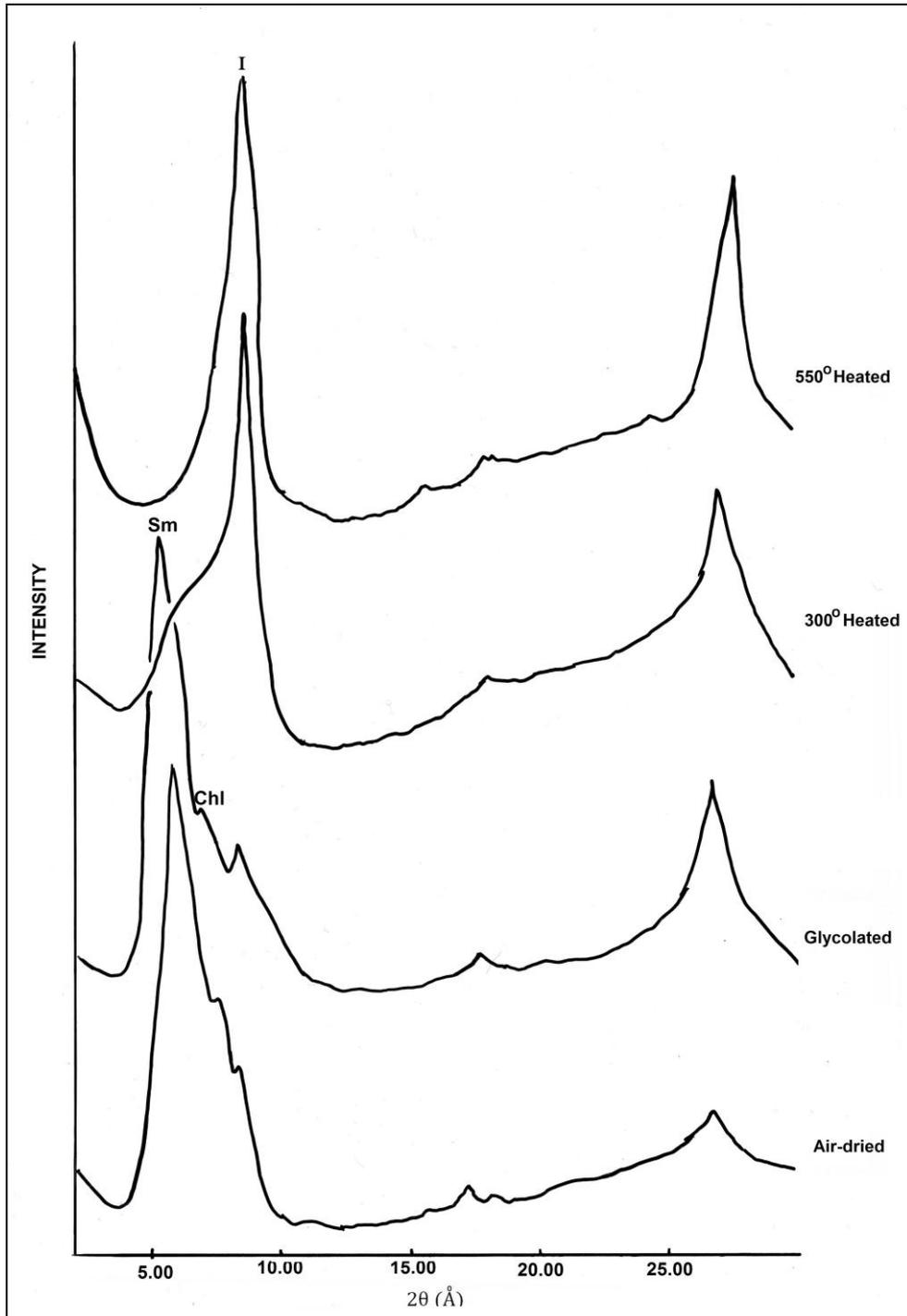
Figure 4.22. XRD analyses on the clay fraction of HAN 4 sample from SSK-1 section.

At the top most unit of SSK-1 borehole, there is microscopically dirty white-crème colored, hard, fine grained micritic clayey limestone (Figure 4.23)
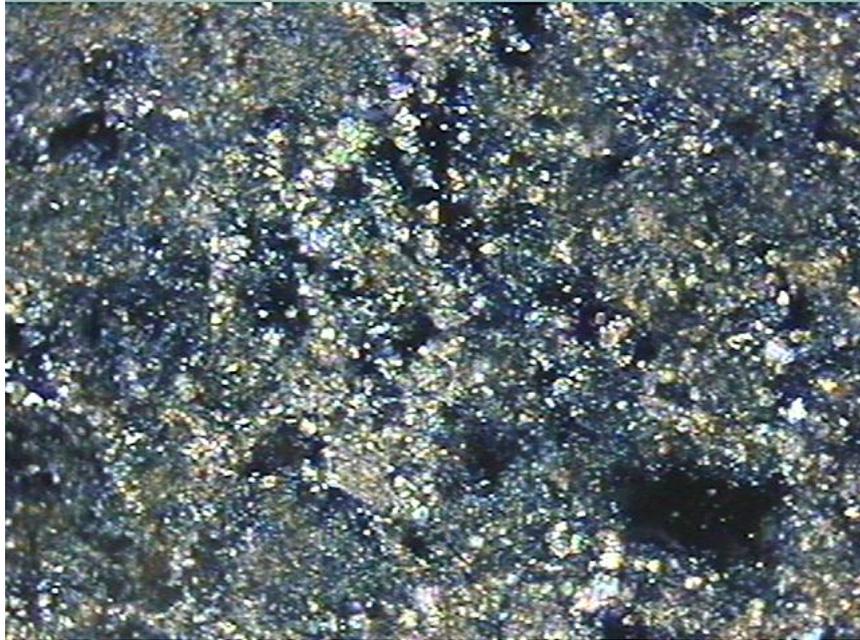
Figure 4.23. Photomicrograph of clayey limestone (HAN-1, XPL, 4x10)

In the limestone there are very large dissolution pores developed through the samples. The internal walls of the pores are covered with sparry calcite crystals. The inner parts of pores are also filled with analcime minerals (Figure 4.24). In the bulk composition of the clayey limestone, small amount quartz and abundant dolomite are observed. At a point heulandite mineral that is covered by analcime at the pore (Figure 4.25).
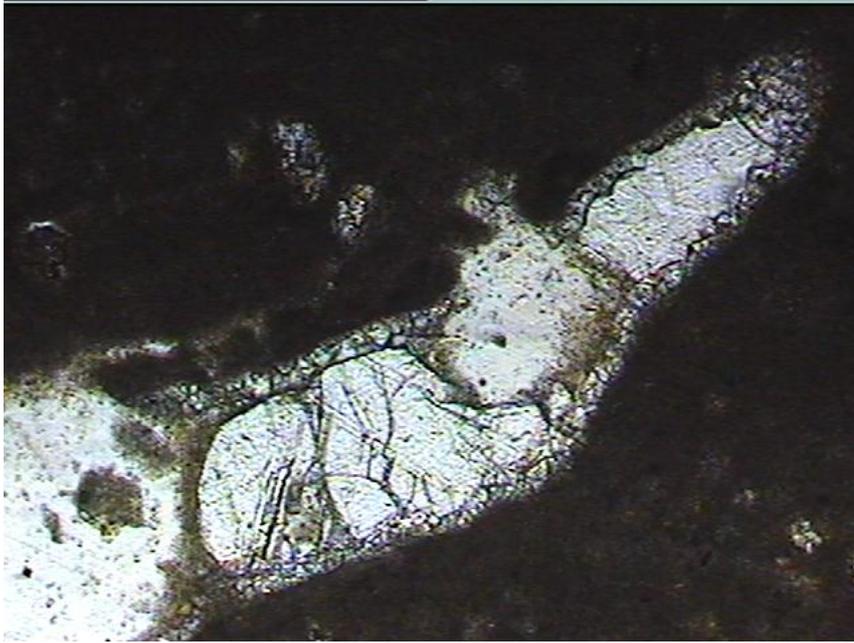
Figure 4. 24. Photomicrograph of analcime crystal (HAN–3, XPL,10x10)
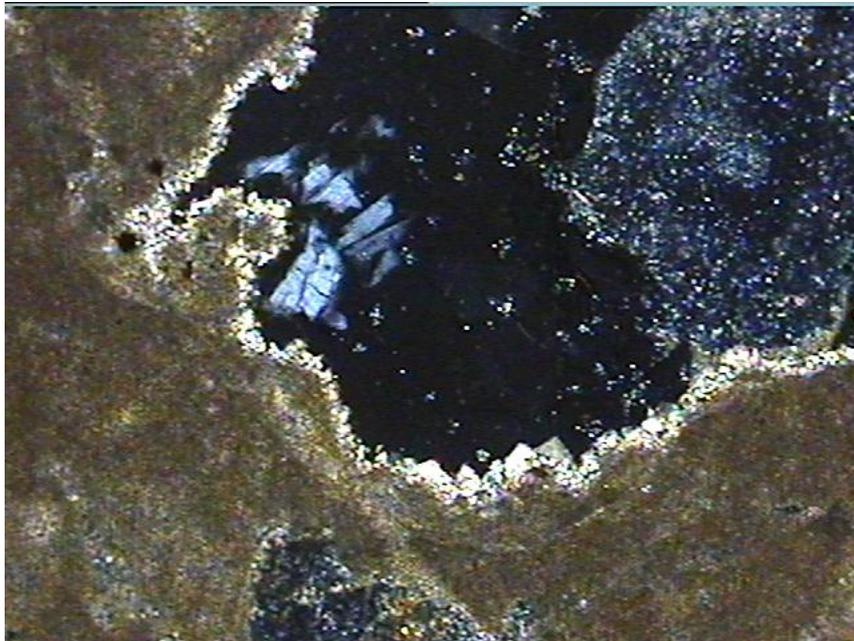
Figure 4.25. Photomicrograph of heulandite (HAN-3, XPL, 10x10)

CHAPTER 5

GEOCHEMISTRY

5.1. Introduction

Bradley (1999) stated that lakes accumulate sediments from their surrounding environment and therefore the sediment cores recovered from lakes can provide a record of environmental change. The mineralogical and geochemical compositions of the lacustrine deposits are important proxy providers. Due to high accumulation rates in lakes, they offer the potential for high-resolution records of past climate (Bradley, 1999). Moreover, Sheldon and Tabor (2009) and Retallack (2001) provided summary tables in which different proxies based on geochemical analyses revealing the intensity of the chemical weathering (Table 5.1.).

Major oxide concentrations are given as weight percentages (wt %) of the whole rock, on the other hand trace element abundances are reported as parts per million (ppm). Therefore in this thesis study, variations of these elements as well as weathering and alteration intensities for each section as a function of a depth were drawn and evaluated.

Other than the major and trace element variations through the section, some other parameters were used to evaluate the weathering and alteration intensities.

Rollinson (1993) explained the most commonly used geochemical criteria of sediment maturity are the SiO2 content and the SiO2 / Al2O3 ratio (Potter, 1978), reflecting the abundance of quartz, clay and feldspar content. Chemical maturity can be calculated from the ratio of Na2O/K2O (Rollinson, 1993).

Table 5.1. Molecular weathering and pedogenesis ratios (modified from Sheldon and Tabor, 2009; and Retallack, 2001).

Ratio	Formula	Pedogenic Process
Al/ ΣBases	$Al_2O_3/(CaO+MgO+K_2O+Na_2O)$	Hydrolysis
Clayeyness	Al_2O_3/SiO_2	Hydrolysis
Base Loss	Ba/Sr	Leaching_Hydrolysis
Gleization	FeO/Fe_2O_3	Oxidation
Gleization	ΣFe/Al	Oxidation
Gleization	ΣFe+Mn/Al	Oxidation
Silica/Sesquioxides	$SiO_2/ (Fe_2O_3+Al_2O_3)$	Hydration
Base Loss	Base/Ti	Leaching
Provenance	Ti/Al	Acidification(~pH)
Alkalis to Alumina	$(K_2O+Na_2O)/Al_2O_3$	Salinization
Soda to Potash	Na_2O/K_2O	Salinization
Parent Material	La/Ce, Sm/Nd, U/Th	Acidification (~pH)

The Pedogenic processes can be inferred from the elemental ratios shown in Table 5.1. Hydrolysis, one of the most important pedogenic process, can be assessed by molecular weathering ratios of alumina/bases, alumina/silica and barium/strontium (Retallack, 2001).

Clayeyness, a result of hdrolysis is defined as aluminum divided to silica. Leaching can be quantified by the ratio of Ba to Sr. High ratio of Ba/Sr implies more leaching conditions (Sheldon and Tabor, 2009). As Retallack (2001) stated hydration or dehydration reactions are revealed by the ratio of silica to iron and alumina. Molecular weathering ratio of soda to potash, alkalis to alumina and soda to alumina are used to assess the degree of salinization. Calcification, important parameter revealing subhumid and semi-arid climates, can be quantified with the ratio of calcium and magnesium to alumina. A reaction in which an element suffers electron loss when forming a compound is named oxidation, reversely, electron gain is due to reduction process (Retallack, 2001).

Degree of chemical weathering can be obtained from the chemical index of alteration (CIA) (Nesbitt and Young, 1982). The CIA is a measurement of the weathering of feldspar minerals and their hydration to form clay minerals. As clay content increases Al should also increase, whereas Ca, K, and Na contents should decrease, leading to higher CIA values (Sheldon and Tabor, 2009). Additionally, $(Na_2O+CaO) - Al_2O_3 - K_2O$ diagram of Nesbitt and Young (1984, 1989) shows the weathering trends. Magnesium index is also a measure for the chemical alteration and calculated by using MgO and Al_2O_3 values.

$$CIA = Al_2O_3 / (Al_2O_3+CaO+K_2O+Na_2O)$$
$$Mg\text{-}I = Al_2O_3 \times 100 / (Al_2O_3+MgO)$$

Ratios of La/Ce, Sm/Nd and U/Th can be used to infer the acidification of the parent material. Sheldon and Tabor (2009) explained that U, Th, V, Ti, Zr, Nb are all relatively immobile during weathering. U is leached away during pedogenesis and Th remains. This indicates very intense weathering and strong redox gradient. Oppositely, if pedogenesis is not effective and if there is no strong redox gradient then the U/Th ratio is expected to be constant all through the profile. The ratios of Sm/Nd and La/Ce are used to refer the provenance of the sediments.

5.2. Koyunbaba Section

Whole rock geochemical analysis of the lake deposits in Koyunbaba Section is listed in Table 5.2. Major element concentrations are given in weight percentages. The molecular weathering ratios and chemical index of alteration values are calculated according to the given formulas in Table 5.1. Due to the resistancy for mobilization, Ti is accepted as a normalizing element for major and trace element concentrations of Koyunbaba section. The values are then plotted against depth to reveal the changes.

Table 5.2. Main and trace element analyses results of Koyunbaba samples (Element oxide values are given as weight percent).

Oxides (%)	KB-1	KB-2	KB-6	KB-9	KB-12	KB-14
SiO_2	31.42	72.46	45.63	11.89	63.35	52.58
TiO_2	0.71	0.29	0.39	0.00	0.37	0.88
Al_2O_3	10.01	12.95	10.97	4.20	15.27	16.25
Fe_2O_3	3.67	2.26	4.49	5.59	3.05	5.53
MgO	5.52	0.17	2.87	15.07	0.46	1.51
CaO	21.75	1.16	12.14	23.81	4.31	4.34
Na_2O	1.61	2.85	1.84	0.81	2.23	2.26
K_2O	1.69	3.28	2.42	0.76	2.75	2.63
SO_3	0.22	0.20	0.18	0.13	0.21	0.31
LOI	23.32	3.87	18.62	37.43	7.56	13.40
Total	99.82	99.49	99.55	99.69	99.56	99.69

SiO2 values of the Koyunbaba Section ranges between 11,89 wt% and 72,46 wt%. The relative amount of SiO2 down to the section increases showing the moderate leaching conditions favoured in the region. This value is also from mineral compositions of quartz and clays which is consistent with the XRD findings (Figure 5.1).

Al_2O_3 like TiO_2 is assumed to be constant during weathering. While some other components are easily leached away from the section, Al retains its composition. It values range from 4.20 wt% to 16.25 wt%. Therefore, the values for Al_2O_3 through the section are almost constant except one level. The constant values of Al_2O_3 are also constant with the presence of the clay minerals all through the section (Figure 5.1).

The Fe_2O_3 composition through the section is between 2.26 wt% and 5.59 wt %, which means it is also almost constant implying almost no change in oxidation/reduction reactions in the region during the depositional period of this section (Figure 5.1).

MgO generally follow the same trends as iron, reaching their greatest concentration along with iron. However, the conditions sometimes may differ if dolomite is in the composition of the samples. The amount of MgO ranges between 0.17 wt % to 15.07 wt %. Its abundance fluctuates from level to level but as a general trend it increases up to the section which is consistent with the increasing amount of dolomite up to the section (Figure 5.1).

CaO like MgO shows a general increasing trend up to the section which is also consistent with the increasing carbonate content. Its values range from 1.16 wt % to 23.81 wt % (Figure 5.1).

Both Na and K are more readily mobilized elements released by weathering, therefore they would be expected to have lower values in the units which are not resistant to weathering. Both plots the same trend with respect to depth showing increasing and decreasing values depending on the characteristics of the lithologies through the section. Na_2O and K_2O values range from 0.81 wt % to 2.85 wt % and 0.76 wt % to 3.28 wt %, respectively (Figure 5.1).

Ti has a constant distibution from bottom to top of the section which shows its high resistance to mobilization. Its values is always less than 1% through the section, possibly implying the constant low sediment influx (Figure 5.1).

Ti-normalised values of major oxides versus depth plots clearly show that SiO_2, Al_2O_3, Na_2O and K_2O plot almost the sam trend but Ca and Mg show the same patterns. Ca and Mg values are directly related with the carbonate minerals in the section, while the other oxides except Fe_2O_3 shows the same increasing and decreasing trends when normalised to Ti most possibly implying that they are all representing the same chemical provenance (Figure 5.2).

Unfortunately due to low project budget, the samples of Koyunbaba Section analysed for their major oxides could not be evaluated in terms of their trace element compositions. Therefore, the ratios for the weathering behaviours and provenance conditions could not be employed for this section.
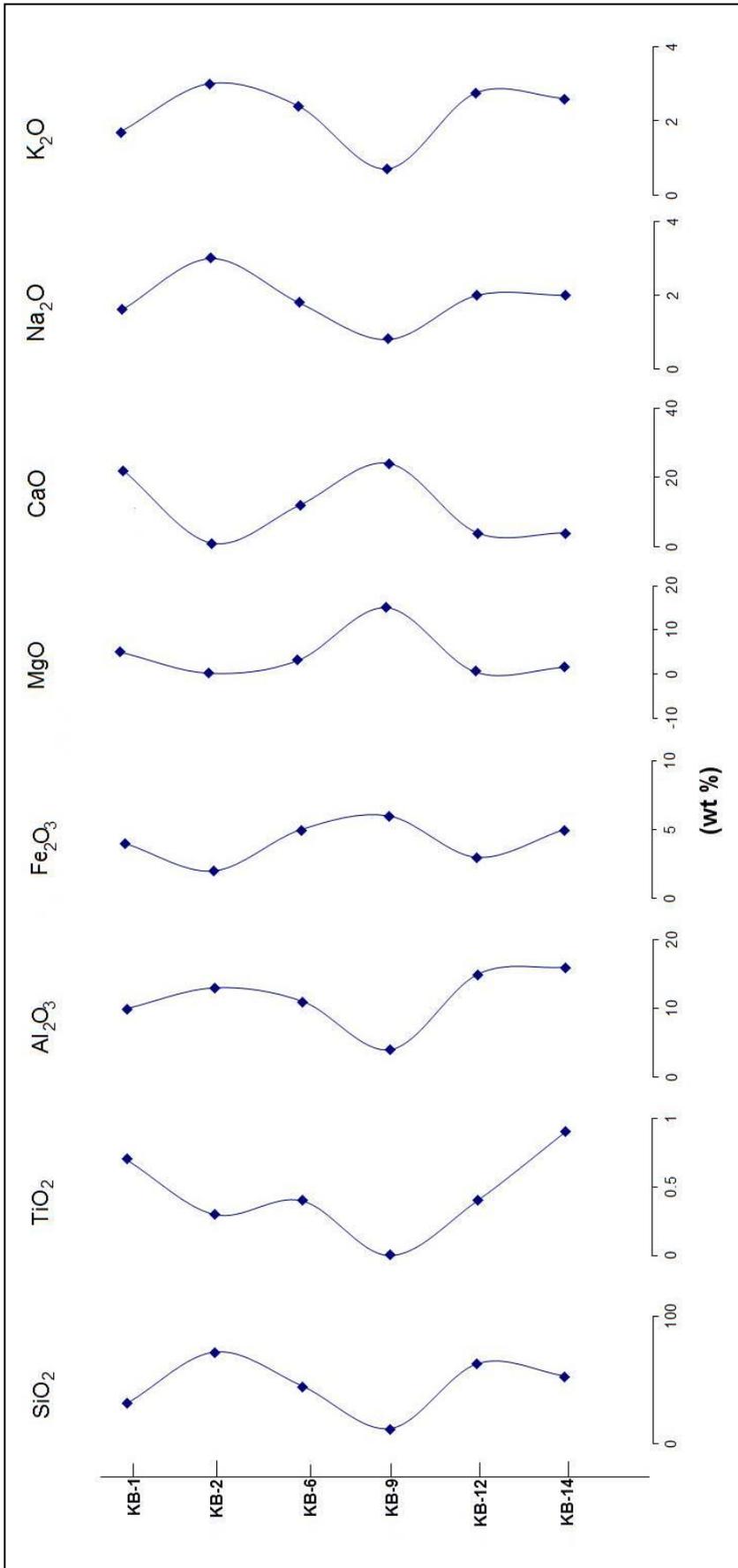
Figure 5.1. Major oxides (wt %) versus depth plot of Koyunbaba Section.
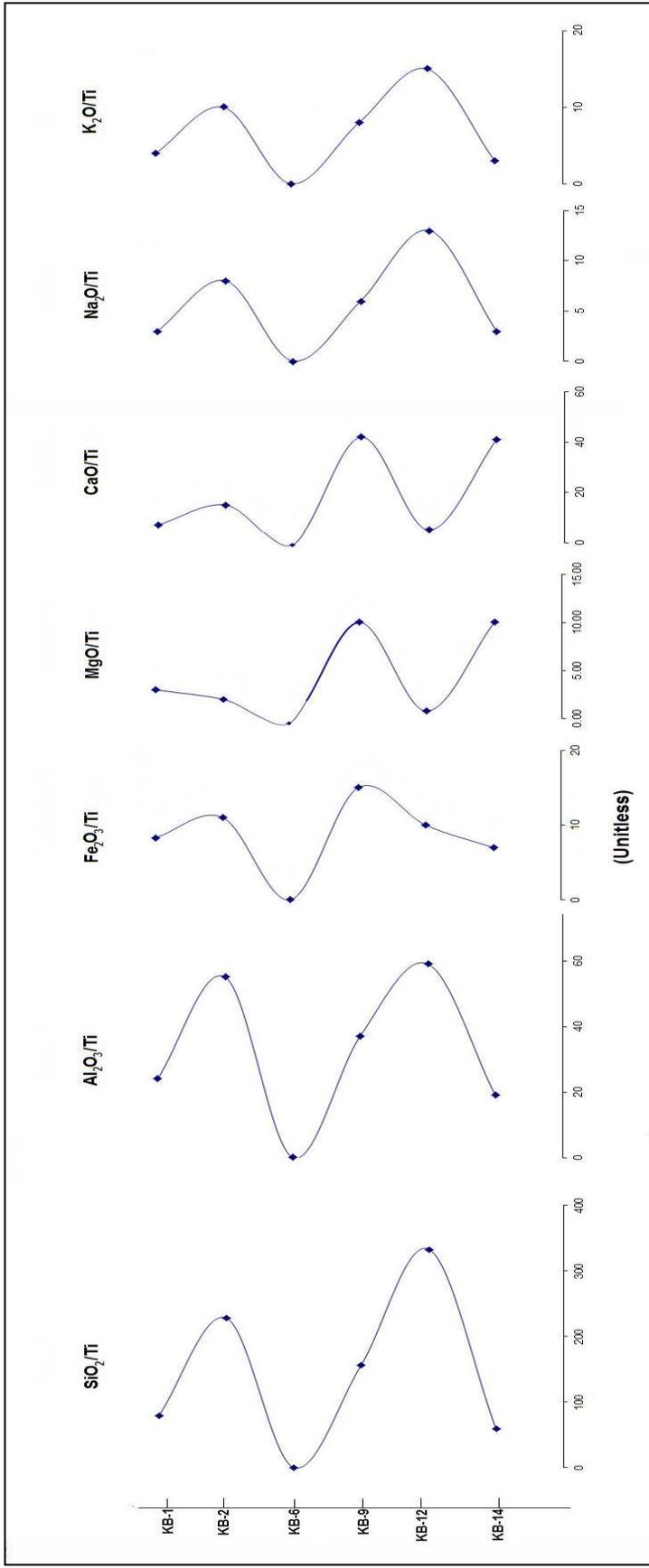
Figure 5.2. Major oxides (wt %) normalized to Ti versus depth plot of Koyunbaba Section.

According to the major oxide values of the Koyunbaba Section samples, molecular weathering values are calculated (Figure 5.3). Base saturation values which depends all the bases ratios, show fluctuations through the section, lower to the top. It is directly related with the solubility and mobility of the elements. Clayeyness values are almost constant through the section, getting a little higher at the top of the section. Hydration on the other hand plots lowering to the top pattern. Oxidation is also almost constant except KB–6 sample where oxidation gets higher while saturation and hydration get lower. Salinization is also constant for Koyunbaba Section, while calcification shows a little increasing upward trend except KB-6 sample where the value is highest. Salinization for the semi-arid conditions should be greater than 1, and Koyunbaba samples plots close to 1 or higher values. Hydration, naturally plots an opposite trend to the clayeyness, while the other weathering ratios are parallel to each other (Figure 5.3).

Chemical Index of Alteration (CIA) and Mg-Index (MgI) values are also calculated from the major oxides. CIA values for the samples are lower than 50%, meaning that alteration passed through this section was not so intense, it can be classfied as moderate to low. On the other hand, Mg-index of alteration values, where Ca, Na and K are omitted from the calculation, ranges around 70% to 90% except KB-6 sample which shows 21% Mg-I value (Figure 5.4).
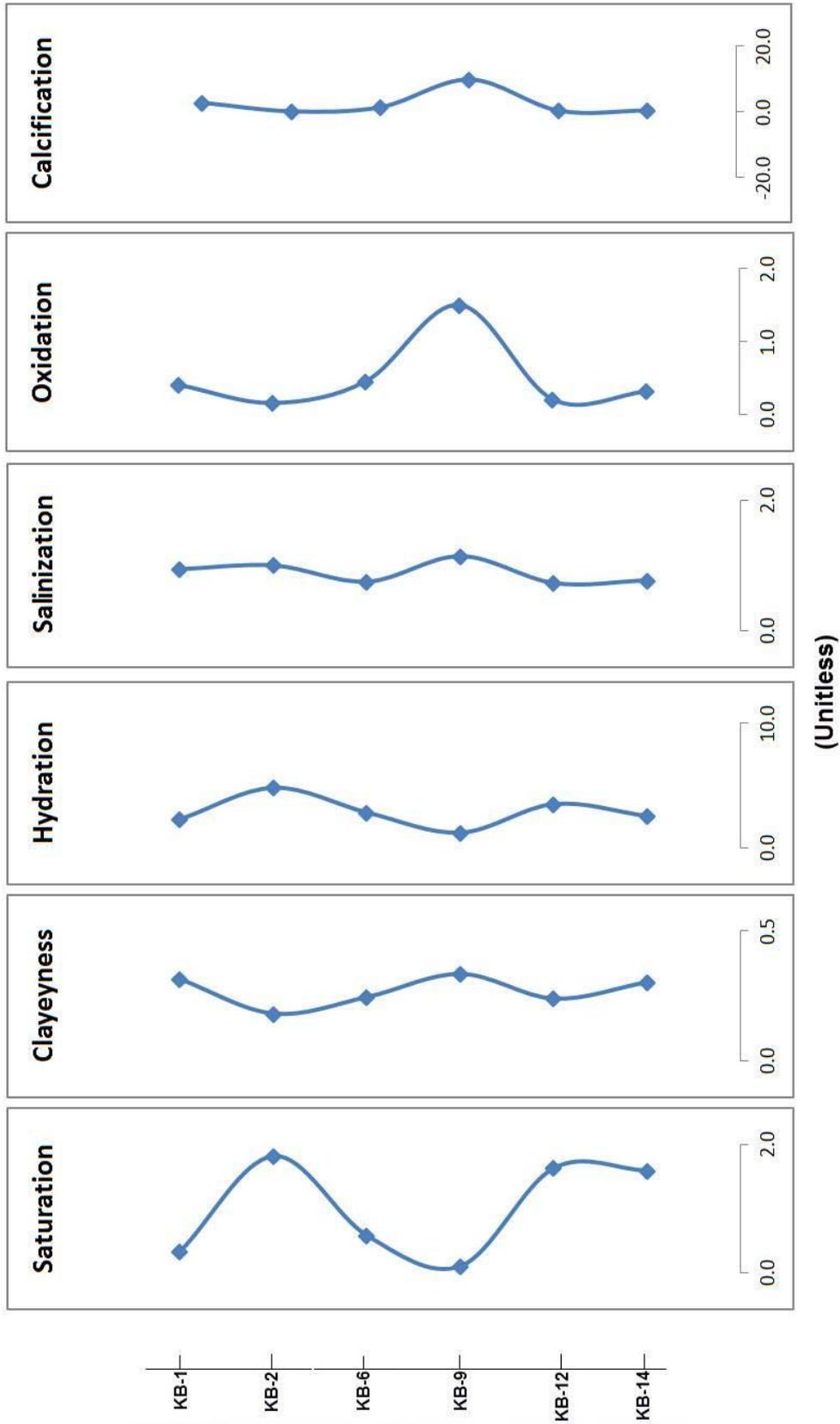
Figure 5.3. Molecular weathering ratios of Koyunbaba Section..
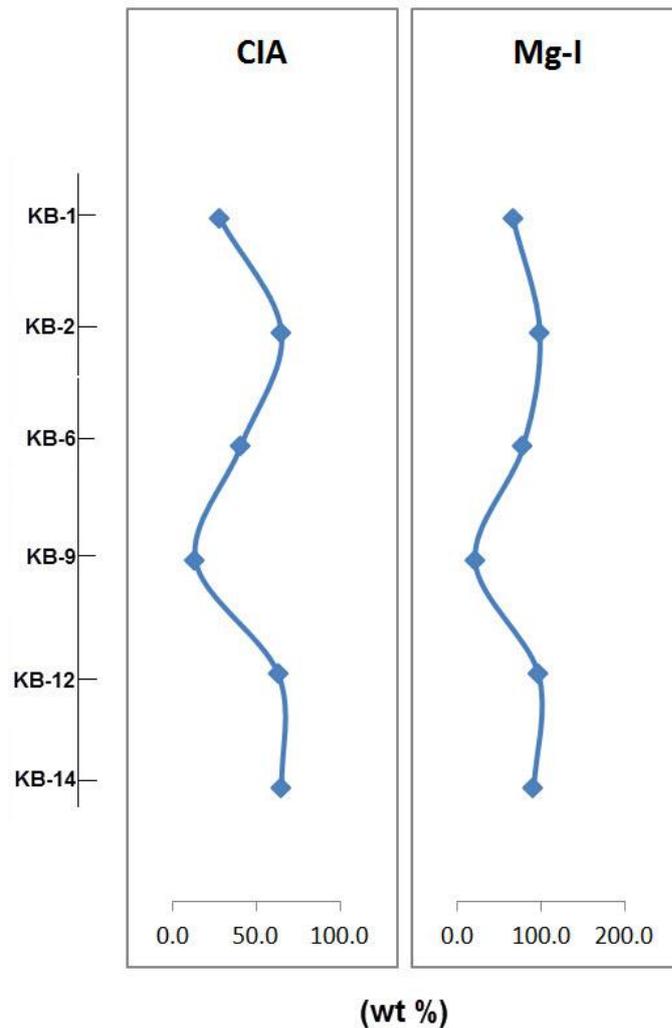
Figure 5.4. CIA and Mg-I values of Koyunbaba Section.

5.3. Killlik Section

The results of whole rock geochemical analysis of of the samples from Killik Section are listed in Table 5.3. Major and trace element concentrations are given in weight percentages (wt%) and in parts per million (ppm), respectively. The molecular weathering ratios and chemical index of alteration values are calculated according to the given formulas in part 5.1. Ti is also accepted as a normalizing element for major oxides and Al for trace element concentration for Killik Section. The values are plotted against depth to reveal the changes.

SiO_2 values of the Killik Section ranges between 57,01 wt% and 71,05 wt%. The amount of SiO_2 down to the section is almost constant. This value is from mineral compositions of quartz and clays which is consistent with the XRD findings (Figure 5.5).

Al2O3 and TiO2 are also constant during weathering, while some other components are easily leached away from the section. In Killik Section, Al2O3 is also constant through the section, providing a parallel trend to the SiO2 in depth to value diagram. Al2O3 values are between 11wt% and 17,19 wt%. TiO2 also display a very narrow range in between 0,13 wt% and 0,86 wt% (Figure 5.5).

56

The Fe2O3 composition through the section shows a little wider range between 0,58 wt% and 6,63 wt%, which implies some changes occurred in oxidation/reduction reactions in the region during the depositional period of this section (Figure 5.5).

MgO follows the same trends with iron, manganese and phosphorous reaching their greatest concentration up to the section but the uppermost unit has the lowest composition. The amount of MgO ranges between 0,86 wt% to 4,82 wt%. MnO, on the other hand, follows a narrow range from 0,01 wt% to 0,03 wt % (Figure 5.5).

CaO shows parallel trend with Na2O and K2O, almost constant up to the section, but the last unit shows increasing trend. Its values are from 0,3 wt% to 10,39 wt%. Na2O vlaues range from 1,73 wt% to 5,64 wt%, the range of which is very similar to the CaO. K2O is also thje same with CaO and Na2O, with the values between 0,22 wt% and 4,3 wt%. The last elemental composition is P2O5, whose values are less than 1wt%, showing the presence of very little amount of organic matter (Figure 5.5).

Like Koyunbaba Section, Ti has a constant distibution from bottom to top of the section which shows its high resistance to mobilization. Therefore, it also selected as a normalizing element for the major oxides (Figure 5.6).

Ti-normalised values of major oxides versus depth plots clearly show that SiO2, Al2O3, Na2O, Fe2O3 and MgO plot almost the same trend, most possibly implying the constant source for these elements through the deposition of the Killik Scetion. Ca plots constant values but a higher value at the top. The P2O5 values normalised to Ti are also constant all through the section, implying constant organic supply during the deposition (Figure 5.6). Trace element ratios are also drwan with respect to depth (Figure 5.7)

According to the major oxide values of the Killik Section samples, molecular weathering values are calculated (Figure 5.8). Base saturation values which depends all the bases ratios, show decreasing upward trend through the section. It is directly related with the solubility and mobility of the elements. Clayeyness values are almost constant through the section. Hydration is also almost constant upt ot he scetion but at the top shows increaing trend. Salinization increases towards the top of the section, implying the aridity increasing up to the surficial levels. Calcification plots also increaing trend towards the top, paralell to the salinization. Oxidation, on the other hand, plots an opposite trend to the hydration and salinization values. It decreases upward. Leaching, parallel to saturation, is low at the top, higher at the middle of the section(Figure 5.8).

Chemical Index of Alteration and Mg-Index values are also calculated from the major oxides. CIA values for the samples are mostly higher than 50%, reaching 86% meaning that alteration passed through this section was intense. Additionally, Mg-index of alteration values, where Ca, Na and K are omitted from the calculation, ranges around 70% to 90%, again showing intense alteration occured in this region (Figure 5.9).

Table 5.3. Major oxide (wt%) and trace element (ppm) contents of Killik samples.

Oxide	HB1	HB2	HB4	HB6	HB8	HB9	HB10
SiO_2	57,95	57,01	64,42	71,05	63,58	63,27	67,74
TiO_2	0,24	0,67	0,86	0,13	0,83	0,64	0,63
Al_2O_3	11,00	16,14	16,41	15,32	17,19	16,81	16,49
Fe_2O_3	0,58	6,63	5,09	2,28	4,70	5,53	2,36
MnO	0,01	0,03	0,01	0,01	0,02	0,01	0,01
MgO	0,86	4,82	3,40	3,13	2,14	2,88	1,63
CaO	10,39	0,88	0,41	0,30	2,09	0,91	2,09
Na_2O	5,64	2,19	1,73	1,96	3,23	2,47	3,44
K_2O	0,54	4,30	0,76	0,22	1,13	0,86	1,47
P_2O_3	0,11	0,03	0,13	0,03	0,12	0,07	0,09
LOI	12,60	7,00	6,50	5,30	4,50	6,00	3,40
Total	99,91	99,70	99,72	99,74	99,52	99,45	99,33
Trace El.	**HB1**	**HB2**	**HB4**	**HB6**	**HB8**	**HB9**	**HB10**
Sc	5	18	11	2	10	11	2
V	12	173	155	13	99	104	66
Cr	22	149	147	18	189	100	86
Co	4	30	25	11	17	26	13
Ni	12	89	58	15	70	88	44
Cu	11	31	21	1	27	29	16
Zn	27	82	78	39	59	84	44
Rb	17	153	41	11	58	99	60
Sr	791	99	137	52	292	150	358
Y	10	14	7	31	22	27	19
Zr	49	139	209	107	206	194	192
Nb	15	16	22	28	24	22	24
Ba	211	267	64	388	929	142	1132
Pb	26	18	23	47	24	27	27
Th	15	14	18	31	22	25	21
U	2	0	5	9	2	1	2
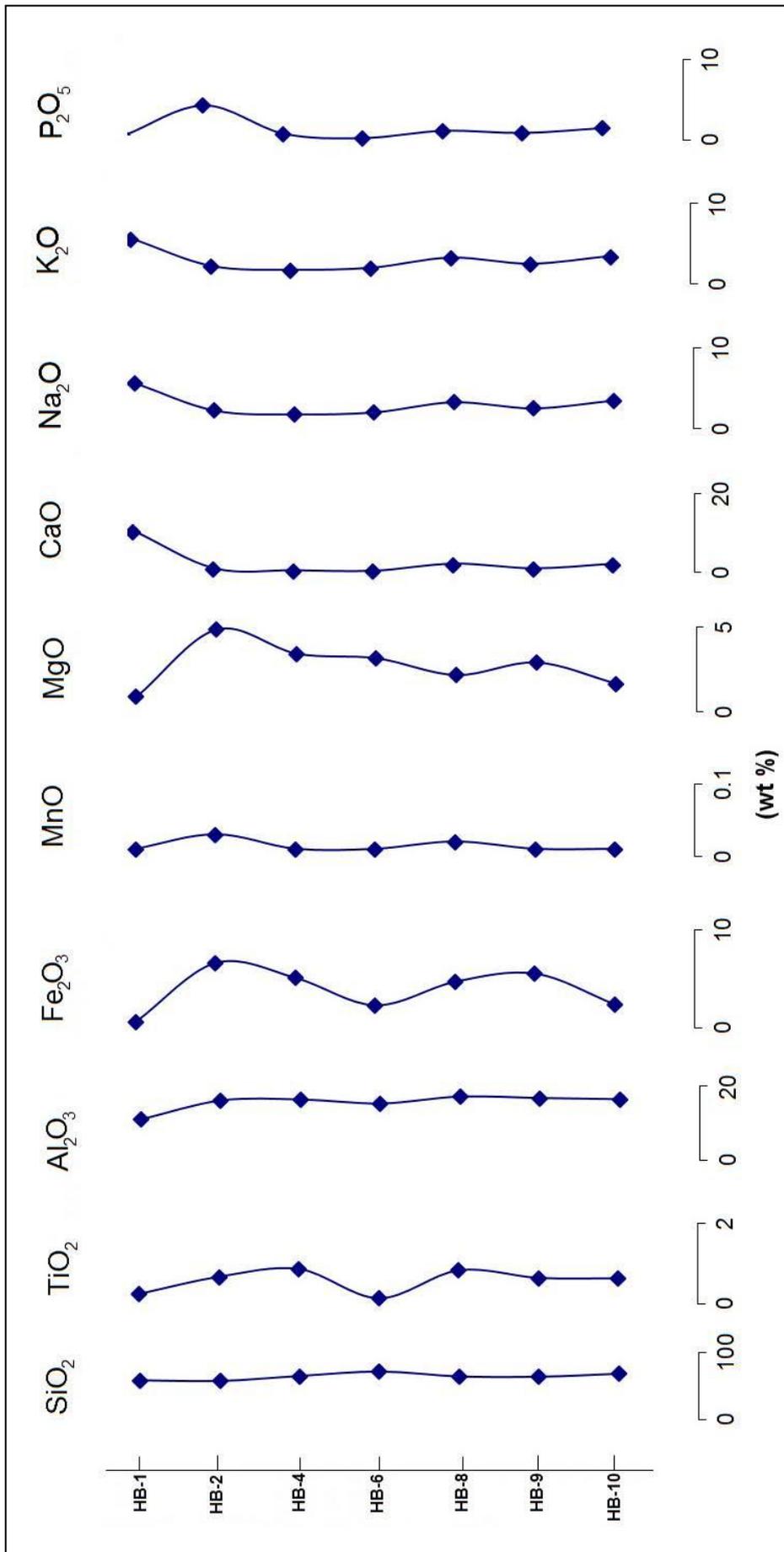
Figure 5.5. Major oxides versus depth plot of Killik Section..

59
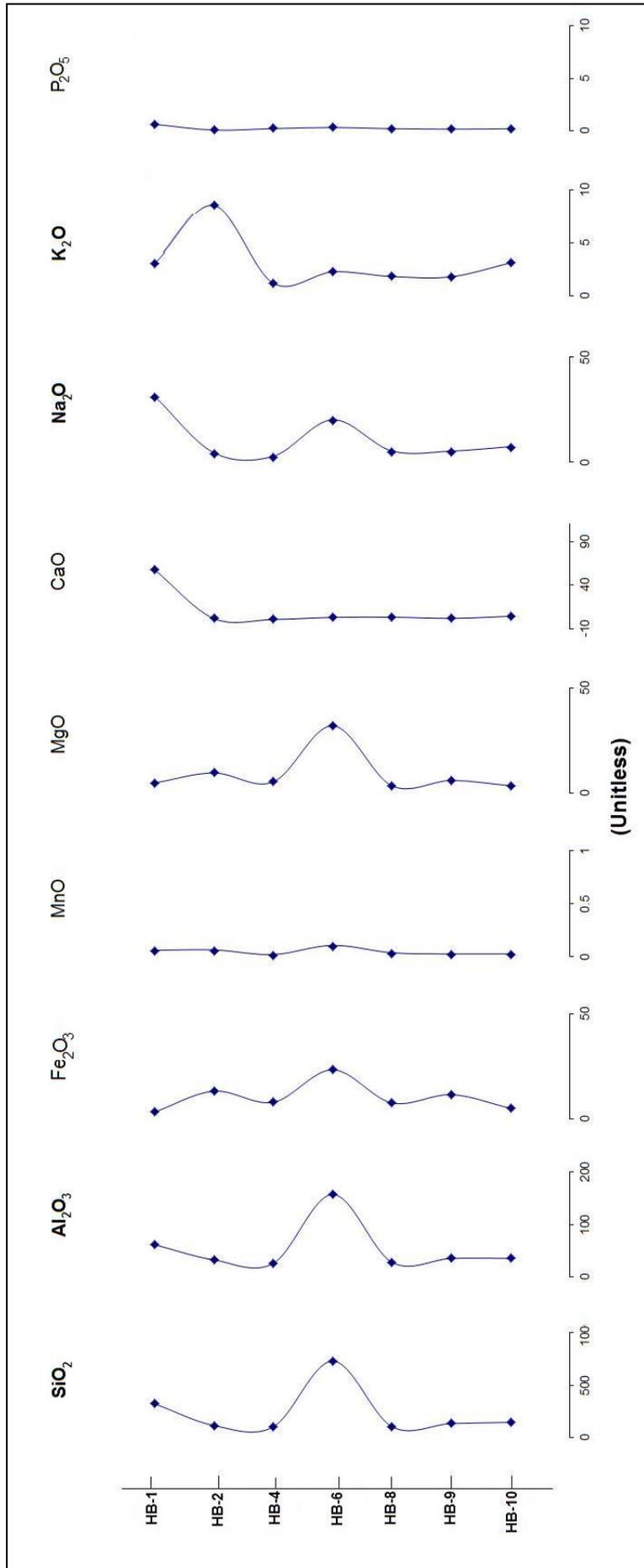
Figure 5.6. Ti-normalised major oxides versus depth plot of Kilik Section (wt%/wt...
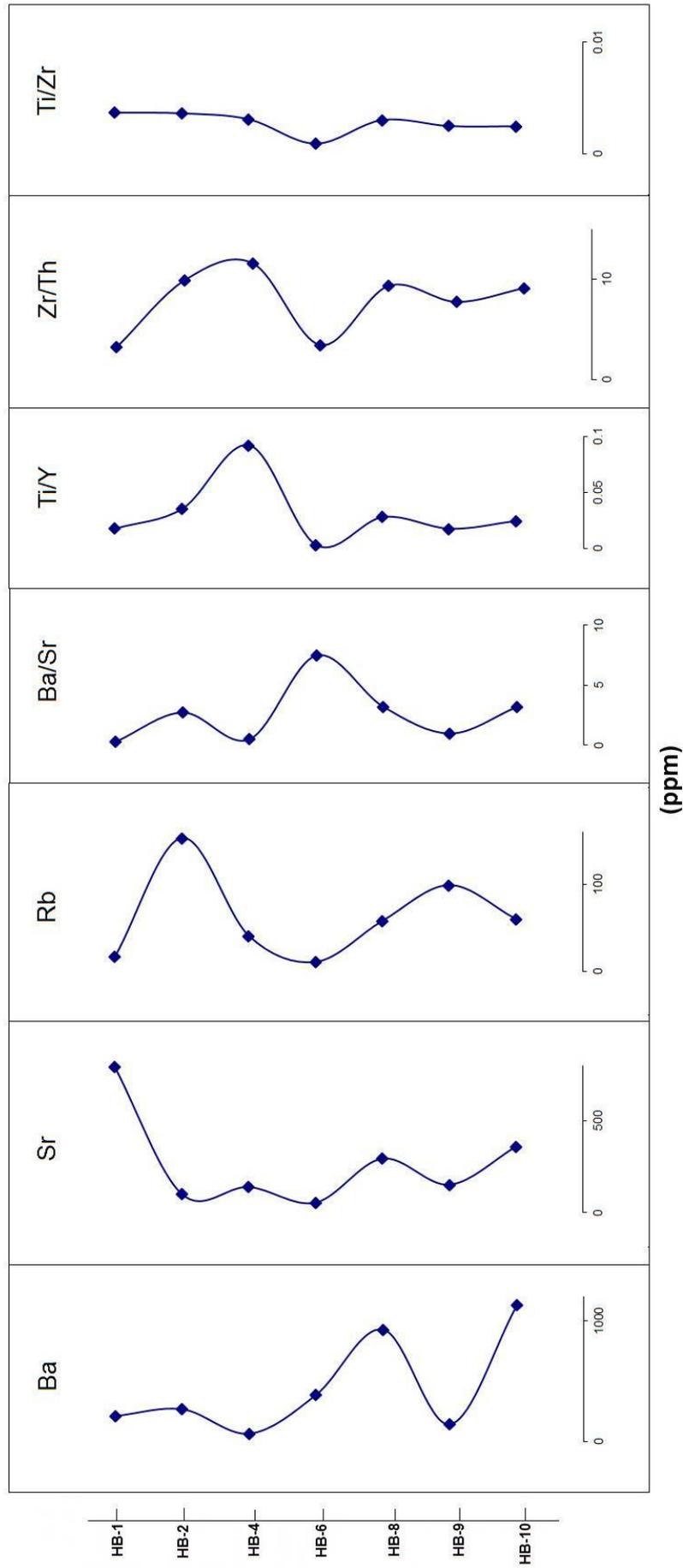
Figure 5.7. Trace element contents (ppm) and trace element ratios versus depth plot of Killik Section
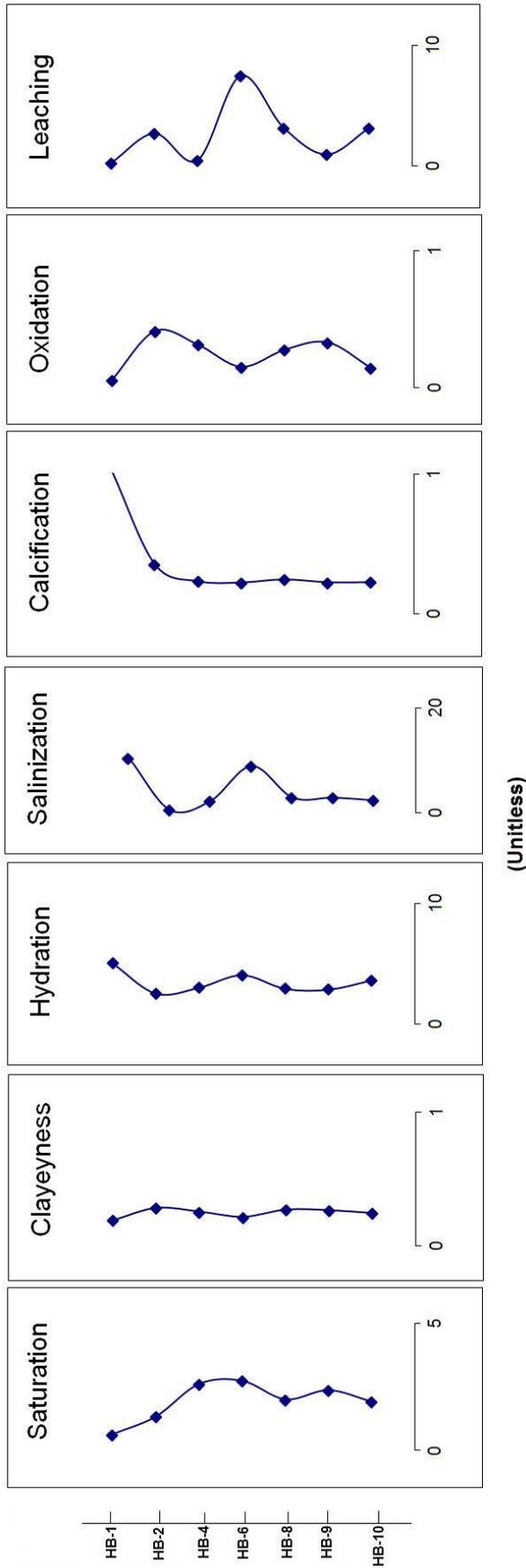
Figure 5.8. Molecular weathering ratios versus depth plot of Killik Section

.
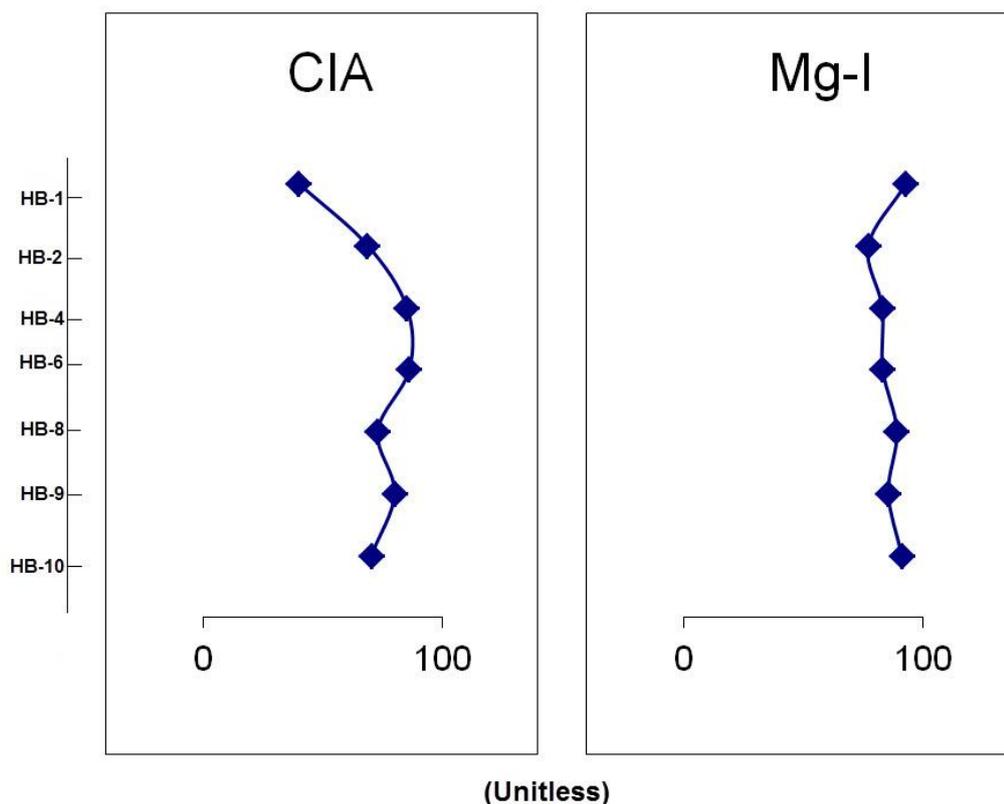
Figure 5.9. Alteration index versus depth plots of Killik Section.

5.4. SSK-1 Section

The results of the samples taken from the different levels of SSK-1 borehole location are given in Table 5.4. Major oxide compositions are given as weight precentages (wt%) and trace element compositions as ppm. 24 samples were analysed at ACME Laboratories, Canada for major and trace element analyses. The results are also plotted with respect to depth.

According to the results, HAN 2,HAN 3, HAN 7, HAN 9, HAN 10 have similar compositions. Low amounts of Al and Si and high amounts of Ca and Mg indicate that the sample is rich in dolomite. HAN 4 is taken from grayish green colored siltstone derived from silicic rocks and is rich in Al supporting the the transportation of smectite and the formation of analcime. HAN 14 is taken from light gray colored tuff. Here the presence of very high Sr value is very important finding, supporting the idea that the lake was saline and alkaline. HAN 16 sample is taken from clayey limestone. It has similar values with HAN 2 indicating that the presence of dolomite (Figure 5.10).

HAN 19 sample was taken from tuff, rich in SiO_2 and CaO. HAN 23 and HAN 26 samples were taken from mudstone and claystone. HAN 23 shows similarities with HAN 4 with a high amount of Al_2O_3 content whereas HAN 26 is also rich in MgO, supporting the presence of dolomite. HAN 33 sample is taken from tuff layer. This sample again is rich in Al_2O_3 (%11.63) indicating the presence of clay minerals. Bentonitic layer is represented by HAN 37 sample. It is rich in SiO2 and CaO. HAN 41 sample is taken from andesite. Its composition is very different than the other units, high Rb and Ce values are also recognized for this unit. HAN 43 and HAN 53 were taken from mudstone and they have similar chemical compositions. HAN 46, HAN 49, HAN 54, and HAN 57 samples were taken

63

from carbonate rich lithologies. All the samples are rich in Ca. HAN 53, HAN 62, HAN 63, HAN 64, and HAN 65 samples were taken from mudstone (Figure 5.10).

Major oxide and trace elements versus depth plots are shown in Figure 5.10 and 5.11, respectievly. SiO_2, Al_2O_3, K_2O, TiO_2 and Fe_2O_3 are all parallel to each other, implying that the changes in their values are affacted fom the same chemical environment and represented with the same clay and nonclay minerals. MgO and CaO, on the other hand are also parallel to each other and their fluctuations are consistent with the expected lake level changes. MnO values are important clues for the determination of wet and dry conditions. Therefore, the peak points correlate with the lake level highstands. Ba, like MnO is high when the lake level is high. Co, Cs, Ga, Hf, Nb, Rb are parallel to eah other and generally high at low stands. V, W, Zr, Dy, Ho, Ta, Th are also parallel to each other, implying that there is no additional sediment influx to the lake during the deposition. Sr is well-correlated with the lake level fluctutaions. Y, La, Ce, Pr, Nd, Sm, Eu, Gd, Tb, Er, Tm, Yb, and Lu are also parallel to each other, representing that there was no additional sediment influx from different chemical environment (Figure 5.11).

Table 5.4. Major oxide compositions (wt%) of the ssamples from SSK-1 borehole.

Element		SiO2	Al2O3	Fe2O3	MgO	CaO	Na2O	K2O	TiO2	P2O5	MnO	Cr2O3	LOI	TOT/C	TOT/S	SUM
Samples		%	%	%	%	%	%	%	%	%	%	%	%	%	%	%
HAN 2	Clayey Limestone	26,17	5,1	2,33	12,28	18,12	0,89	0,87	0,21	0,16	0,15	0,006	33,6	8,03	<,01	99,9
HAN 3	"	10,76	1,66	1,14	17,02	26	0,31	0,26	0,07	0,11	0,05	0,004	42,5	11,3	0,03	99,89
HAN 4	Siltstone	51,19	12,96	4,19	5,6	2,87	1,37	2,48	0,51	0,02	0,02	0,022	18,8	1,15	0,01	100,05
HAN 7	Marl	27,99	7,45	3,04	11,53	15,29	1,26	1,53	0,26	0,15	0,08	0,007	31,3	6,79	<,01	99,89
HAN 9	Mudstone	23,36	5,26	2,23	13,63	17,5	0,34	1,42	0,19	0,04	0,05	0,009	35,9	8,06	0,02	99,94
HAN 10	Clayey Limestone	14,91	3,45	1,54	16,26	22,03	0,19	0,77	0,13	0,05	0,03	0,005	40,6	9,73	<,01	99,97
HAN 14	Tuff	64,73	9,1	0,83	2,65	4,47	1,59	1,05	0,15	0,06	0,01	0,004	15,1	1,34	0,02	99,75
HAN 16	Clayey Limestone	22,43	4,84	2,08	14,01	18,98	0,33	1,17	0,21	0,04	0,07	0,006	35,8	8,63	<,01	99,97
HAN 19	Tuff	8,32	1,38	1,1	18,15	26,46	0,19	0,28	0,05	0,09	0,08	0,003	43,7	11,5	0,01	99,81
HAN 23	Mudstone	49,04	13,38	4,54	5,02	3,14	0,35	2,6	0,55	0,08	0,02	0,015	21,3	1,72	0,32	100,04
HAN 26	Claystone	23,08	4,77	2,22	12,37	20,3	0,52	0,73	0,18	0,35	0,31	0,005	35,1	8,56	0,05	99,94
HAN 33	Tuff	65,98	11,63	1,01	2,38	1,76	1,41	0,54	0,18	0,19	<,01	0,003	14,9	0,21	0,08	99,99
HAN 37	Bentonite	45,9	9,38	2,81	3,18	13,01	0,65	0,76	0,49	0,22	0,08	0,013	23,5	3,38	0,03	100
HAN 41	Andesite	65,13	9,99	3,22	2,67	4,3	2,44	2,23	0,4	0,1	0,06	0,009	9,5	1,57	0,02	100,04
HAN 43	Mudstone	48,07	12,45	5,38	3,9	7,3	1,2	2,5	0,72	0,21	0,09	0,019	18,2	2,24	0,01	100,05
HAN 46	Limestone	23,47	5,98	2,59	12,43	19,68	0,62	1,32	0,34	0,15	0,17	0,011	33,2	8,06	0,03	99,97
RE HAN 46		23,57	5,94	2,59	12,33	19,74	0,62	1,33	0,34	0,14	0,17	0,01	33,2	7,99	0,03	99,99
HAN 49	Marl	30,18	7,97	3,31	10,15	15,97	0,9	1,68	0,48	0,2	0,23	0,013	28,9	6,37	0,02	99,98
HAN 53	Mudstone	47,32	13,72	6,32	3,52	6,53	1,2	3,01	0,79	0,21	0,1	0,021	17,3	1,81	0,03	100,06
HAN 54	Marl	42,9	12,54	5,56	6,01	7,34	1,03	2,81	0,71	0,16	0,16	0,018	20,8	2,9	0,02	100,05
HAN 57	Limestone	24,36	7,13	2,77	1,96	29,77	0,63	1,57	0,4	0,14	0,33	0,011	30,9	7,22	0,07	99,97
HAN 62	Mudstone	48,29	15	7,11	3,96	3,71	1,02	3,45	0,81	0,2	0,08	0,022	16,4	1,19	0,03	100,07
HAN 63	Mudstone	41,99	12,46	6,4	5,03	8,01	0,94	2,75	0,75	0,2	0,22	0,021	20,2	3,01	0,25	98,98
HAN 64	Mudstone	51,01	16,3	7,63	3,17	1,61	1,05	3,47	0,9	0,15	0,04	0,025	14,7	0,48	0,03	100,06
HAN 65	Mudstone	48,51	15,74	6,42	3,71	3,46	1,09	3,33	0,84	0,16	0,07	0,024	16,6	1,16	0,03	99,97
STANDARD SO-18/CSC		58,15	14,16	7,64	3,33	6,37	3,67	2,15	0,69	0,82	0,39	0,549	1,9	3,27	4,18	99,82

Table 5.5. Trace element compositions (ppm) of the samples from SSK-1 borehole.

Element		Ba	Be	Co	Cs	Ga	Hf	Nb	Rb	Sn	Sr	Ta	Th	U	V	W	Zr
Samples		ppm	ppm	ppm	ppm	ppm	ppm	ppm	ppm	ppm	ppm	ppm	ppm	ppm	ppm	ppm	ppm
HAN 2	Clayey Limestone	194,6	1	8	3,3	5,8	1,6	5,6	35,2	1	1179	0,5	4	1,8	49	1,3	45,9
HAN 3	"	134,6	1	1,7	1	1,9	<,5	2,1	12,4	1	1292,9	0,3	1,3	1,4	17	0,7	14,9
HAN 4	Siltstone	189,2	1	13	9,2	16,8	3,5	14,6	123,9	2	241,7	1,1	11,1	1,2	85	1,5	102,1
HAN 7	Marl	188	1	11,1	5,9	10,2	2,4	10,5	68	1	1558,7	0,7	8,7	12,2	73	1,5	66,8
HAN 9	Mudstone	156	<1	7	3,1	6,4	1,4	6,4	66,9	1	1032,9	0,5	4,1	3,1	45	1,5	41,4
HAN 10	Clayey Limestone	88,3	1	3,2	1,9	4,6	1	5	36,9	1	706,5	0,3	2,9	1,2	22	0,9	27,3
HAN 14	Tuff	1220,6	2	3,9	1,5	10,9	2	16,4	27,5	2	1885,4	1,7	9,1	2,6	14	1	50,5
HAN 16	Clayey Limestone	146	<1	4,2	2,7	5,4	1,4	6,4	41,2	1	935,7	0,4	3,5	10,1	47	1	39,6
HAN 19	Tuff	146,1	1	0,6	0,6	1,5	<,5	1,8	10,2	<1	1214,3	0,1	1,4	4,3	15	0,4	12,3
HAN 23	Mudstone	169,3	2	16,3	8,9	16,6	3,4	15	117,3	2	270,2	1,1	11,2	4	156	3,3	113,3
HAN 26	Claystone	153,9	1	4,6	2,2	5,9	1,6	6,1	34,7	1	1023,2	0,5	6,4	1,9	25	1,8	54,3
HAN 33	Tuff	148,7	1	5,3	0,9	13,9	2,9	15,7	18,1	1	477,8	1,4	12,6	8,4	25	0,5	71,5
HAN 37	Bentonite	82,8	1	10,9	3,7	10,9	4,5	12,6	38,6	1	396	0,9	8,1	3,9	112	3,2	146,5
HAN 41	Andesite	281,3	1	9,4	3,8	11,1	3,7	12,8	73,7	1	284,8	1	8,9	2,3	59	0,9	127,2
HAN 43	Mudstone	189,6	1	19,5	7,6	14,5	4,3	16,2	106,2	2	263,8	1,1	10,5	2,6	115	1,8	138,1
HAN 46	Limestone	112,9	1	12,8	3,8	7	1,8	7,2	53,4	1	768,8	0,4	4,5	4,9	71	0,9	59,9
RE HAN 46		106,8	1	13,2	3,7	7	1,9	7,2	53,5	1	769,8	0,4	4,1	4,9	70	0,7	61,1
HAN 49	Marl	198	2	16,2	4,8	9,4	2,6	9,9	68,6	1	628,6	0,7	6,2	2,9	85	1	92,5
HAN 53	Mudstone	221,2	1	20,4	8,9	17,2	4,1	17,3	125,2	2	234,1	1,5	10,9	2,4	127	1,4	136,7
HAN 54	Marl	212,8	2	22,7	8,7	15,7	3,9	16,5	115,2	2	294,7	1,1	10,3	2,2	123	1,6	126,7
HAN 57	Limestone	672,1	1	9,6	4,4	8,8	2,1	8,7	61,3	1	199,8	0,4	6,1	1,6	66	1	74,7
HAN 62	Mudstone	284,4	2	22,9	11,3	19,1	4,5	19	146,8	2	217,6	1,2	13,1	2,5	146	1,5	150,5
HAN 63	Mudstone	10571	2	22,3	8,6	15,2	3,4	16,6	122,6	2	306,8	1	9,8	3,4	127	1,4	130,2
HAN 64	Mudstone	254,2	2	19,8	11,7	20,5	4,6	19,5	155,6	3	171,1	1,3	12,6	2,4	169	1,8	154,3
HAN 65	Mudstone	962,8	2	14,9	11,1	19,4	4,6	19,1	138,8	2	196,7	1,2	11,3	3,5	148	1,5	146,4
STANDARD SO-18/CSC		527,6	1	26,9	7	17,7	10,8	20,5	27,8	16	416,2	7,1	9,8	16,3	203	15,1	292,4

Table 5.5. cont'd.

Element		Y	La	Ce	Pr	Nd	Sm	Eu	Gd	Tb	Dy	Ho	Er	Tm	Yb	Lu
Samples		ppm	ppm	ppm	ppm	ppm	ppm	ppm	ppm	ppm	ppm	ppm	ppm	ppm	ppm	ppm
HAN 2	Clayey Limestone	10,8	9,7	17,8	2,07	7,9	1,45	0,39	1,58	0,27	1,6	0,33	0,88	0,14	0,86	0,14
HAN 3	"	2,9	2,1	4,7	0,56	2,1	0,43	0,1	0,42	0,07	0,4	0,08	0,3	0,05	0,26	0,04
HAN 4	Siltstone	6,8	17,8	36	3,87	14,3	2,26	0,51	1,58	0,25	1,3	0,23	0,68	0,1	0,65	0,11
HAN 7	Marl	13,9	11,5	23,2	2,53	9,7	1,92	0,41	1,8	0,35	2,03	0,42	1,35	0,19	1,24	0,2
HAN 9	Mudstone	10,4	8,2	16,7	1,9	7	1,62	0,37	1,5	0,29	1,55	0,31	0,9	0,14	0,84	0,13
HAN 10	Clayey Limestone	4,3	4,8	8,8	1,05	3,7	0,76	0,17	0,66	0,13	0,67	0,13	0,4	0,07	0,41	0,06
HAN 14	Tuff	12,1	9,2	20,2	2,3	7,9	1,89	0,25	1,59	0,35	1,92	0,37	1,06	0,17	0,97	0,15
HAN 16	Clayey Limestone	6	7,4	15,6	1,78	6,3	1,15	0,27	1	0,19	1,08	0,21	0,61	0,09	0,56	0,09
HAN 19	Tuff	3,8	3	6,6	0,77	3	0,55	0,12	0,56	0,1	0,61	0,12	0,39	0,05	0,36	0,05
HAN 23	Mudstone	15,2	21,7	45,8	4,84	17,2	3,2	0,72	2,71	0,49	2,51	0,51	1,43	0,23	1,41	0,22
HAN 26	Claystone	8,5	12,6	26,8	2,61	10	1,76	0,4	1,35	0,25	1,34	0,28	0,76	0,13	0,72	0,12
HAN 33	Tuff	13,2	19,2	37,9	3,93	13	2,35	0,51	1,73	0,34	1,87	0,37	1,22	0,19	1,14	0,19
HAN 37	Bentonite	9,6	16,2	31,6	3,18	11,6	1,89	0,43	1,57	0,28	1,43	0,31	0,86	0,15	0,91	0,15
HAN 41	Andesite	15	29,4	48,9	5,73	21,1	3,43	0,78	2,72	0,5	2,28	0,49	1,41	0,24	1,4	0,22
HAN 43	Mudstone	19,3	25,9	52,9	6,1	24	4,16	0,99	3,61	0,61	3,26	0,69	1,8	0,29	1,66	0,29
HAN 46	Limestone	11,4	14,9	27,7	3,16	12,4	2,03	0,53	1,9	0,34	1,71	0,36	1,04	0,2	0,99	0,17
RE HAN46		11,6	15,5	27,9	3,09	10,6	2,18	0,5	1,88	0,34	1,83	0,37	1,05	0,18	1,04	0,16
HAN 49	Marl	15,6	20	38	4,4	16,9	3,13	0,74	2,78	0,5	2,45	0,48	1,44	0,22	1,25	0,21
HAN 53	Mudstone	22,9	28,6	59	6,46	24,4	4,44	1,06	4,02	0,73	3,69	0,8	2,14	0,35	2	0,34
HAN 54	Marl	23	26,9	55,8	6,19	24,2	4,43	1,05	3,82	0,71	3,83	0,79	2,11	0,36	1,95	0,34
HAN 57	Limestone	14,7	19,3	35,1	3,78	14,7	2,76	0,61	2,34	0,44	2,16	0,47	1,37	0,22	1,25	0,21
HAN 62	Mudstone	22,3	29,9	63,2	7,19	27,6	5,16	1,17	4,09	0,76	3,72	0,76	2,1	0,35	2,02	0,33
HAN 63	Mudstone	23,1	26,7	53,6	6,05	23,2	4,18	0,85	3,67	0,63	3,49	0,7	2,03	0,35	1,85	0,32
HAN 64	Mudstone	21,9	30,6	64,2	7,13	26,9	5,17	1,16	4,16	0,76	3,89	0,79	2,16	0,35	1,97	0,33
HAN 65	Mudstone	23,8	28,2	60	6,69	25	4,87	1,09	4,12	0,75	3,96	0,81	2,25	0,37	2,12	0,34
STANDARD SO-18/CSC		31,7	11,4	26,3	3,29	13,4	2,81	0,84	2,79	0,52	2,88	0,58	1,72	0,27	1,68	0,26

Table 5.5. cont'd.

Element Samples		Mo ppm	Cu ppm	Pb ppm	Zn ppm	Ni ppm	As ppm	Cd ppm	Sb ppm	Bi ppm	Ag ppm	Au ppb	Hg ppm	Tl ppm	Se ppm	Ni ppm	Sc ppm
HAN 2	Clayey Limestone	1,4	114,4	6,8	28	50	8,1	0,3	0,1	0,1	0,4	1,8	0,02	0,2	<,5	38	5
HAN 3	"	0,6	29,2	4	9	14,9	5,2	<,1	0,1	0,1	<,1	2,3	0,02	<,1	<,5	17	2
HAN 4	Siltstone	0,1	38,8	17,6	54	114,4	8	0,1	0,1	0,3	<,1	1,5	0,06	0,3	0,8	141	11
HAN 7	Marl	0,5	14,5	11,6	33	40,7	69,4	0,2	0,2	0,2	<,1	6,7	0,06	0,2	0,5	38	6
HAN 9	Mudstone	0,3	12,8	9	19	50,9	38,7	0,1	<,1	0,2	<,1	<,5	0,03	0,2	0,6	57	5
HAN 10	Clayey Limestone	0,5	7	4,9	12	26,1	27,7	0,1	0,1	0,1	<,1	1,1	0,02	0,1	<,5	28	3
HAN 14	Tuff	0,2	4,9	11,8	22	15,7	13,8	0,1	0,1	0,4	<,1	0,7	<,01	0,4	<,5	18	2
HAN 16	Clayey Limestone	1,8	12,5	7,7	17	24	132,3	0,1	0,1	0,1	<,1	0,6	0,01	0,1	<,5	20	5
HAN 19	Tuff	0,3	3,4	2,1	10	8,8	13,1	<,1	<,1	<,1	<,1	<,5	<,01	<,1	<,5	<5	1
HAN 23	Mudstone	1,1	31,9	13,2	27	50	77,2	0,1	0,2	0,3	<,1	0,6	0,03	0,4	<,5	64	12
HAN 26	Claystone	0,3	13,4	14,3	13	11,9	50,5	0,1	0,1	0,2	<,1	0,6	0,03	0,2	<,5	17	3
HAN 33	Tuff	9,8	6	20	30	12,9	20,8	0,1	0,4	0,6	<,1	1,3	0,16	0,2	<,5	11	3
HAN 37	Bentonite	1,3	11,8	17	13	16,1	5,8	0,2	<,1	0,3	<,1	2,2	0,15	0,1	<,5	33	6
HAN 41	Andesite	0,4	21,1	9,4	29	29,7	6,2	<,1	0,2	0,1	<,1	0,9	0,01	0,2	<,5	34	5
HAN 43	Mudstone	0,4	15,2	15,6	41	55,4	3,7	0,1	<,1	0,2	<,1	<,5	0,02	0,2	<,5	77	12
HAN 46	Limestone	0,3	12,9	14,2	29	32,3	3	0,1	<,1	0,1	<,1	<,5	0,01	0,1	<,5	36	8
RE HAN 46		0,3	12,6	14,1	30	31,2	2,8	0,2	<,1	0,1	<,1	0,6	<,01	0,1	<,5	32	8
HAN 49	Marl	0,3	13,6	14,4	33	40	9,7	0,1	0,1	0,1	<,1	0,5	0,01	0,2	<,5	48	8
HAN 53	Mudstone	0,2	10,7	15,8	51	69	4,8	0,1	<,1	0,2	<,1	1,4	0,01	0,2	<,5	73	14
HAN 54	Marl	0,2	12	17,6	49	66,3	8,1	0,1	<,1	0,2	<,1	<,5	<,01	0,2	<,5	84	13
HAN 57	Limestone	0,1	11,7	14,7	23	28,6	1,7	0,4	<,1	0,2	<,1	1,6	<,01	0,1	<,5	37	9
HAN 62	Mudstone	0,2	9,8	14,3	61	85,5	4,1	0,1	<,1	0,2	<,1	1,1	<,01	0,2	<,5	92	16
HAN 63	Mudstone	0,3	14,6	27,5	59	73,4	1,6	0,3	<,1	0,2	<,1	0,5	<,01	0,2	<,5	74	13
HAN 64	Mudstone	0,1	22,7	11,1	58	72,5	1,1	0,1	<,1	0,2	<,1	1,9	<,01	0,2	<,5	86	17
HAN 65	Mudstone	0,1	129,8	14,4	50	52	0,7	0,1	<,1	0,1	<,1	1	0,02	0,2	0,5	67	18
STANDARD DS7		20,3	112,9	69,6	412	56,3	47,7	6,6	5,7	4,6	0,9	68	0,2	4,1	3,6	24	25
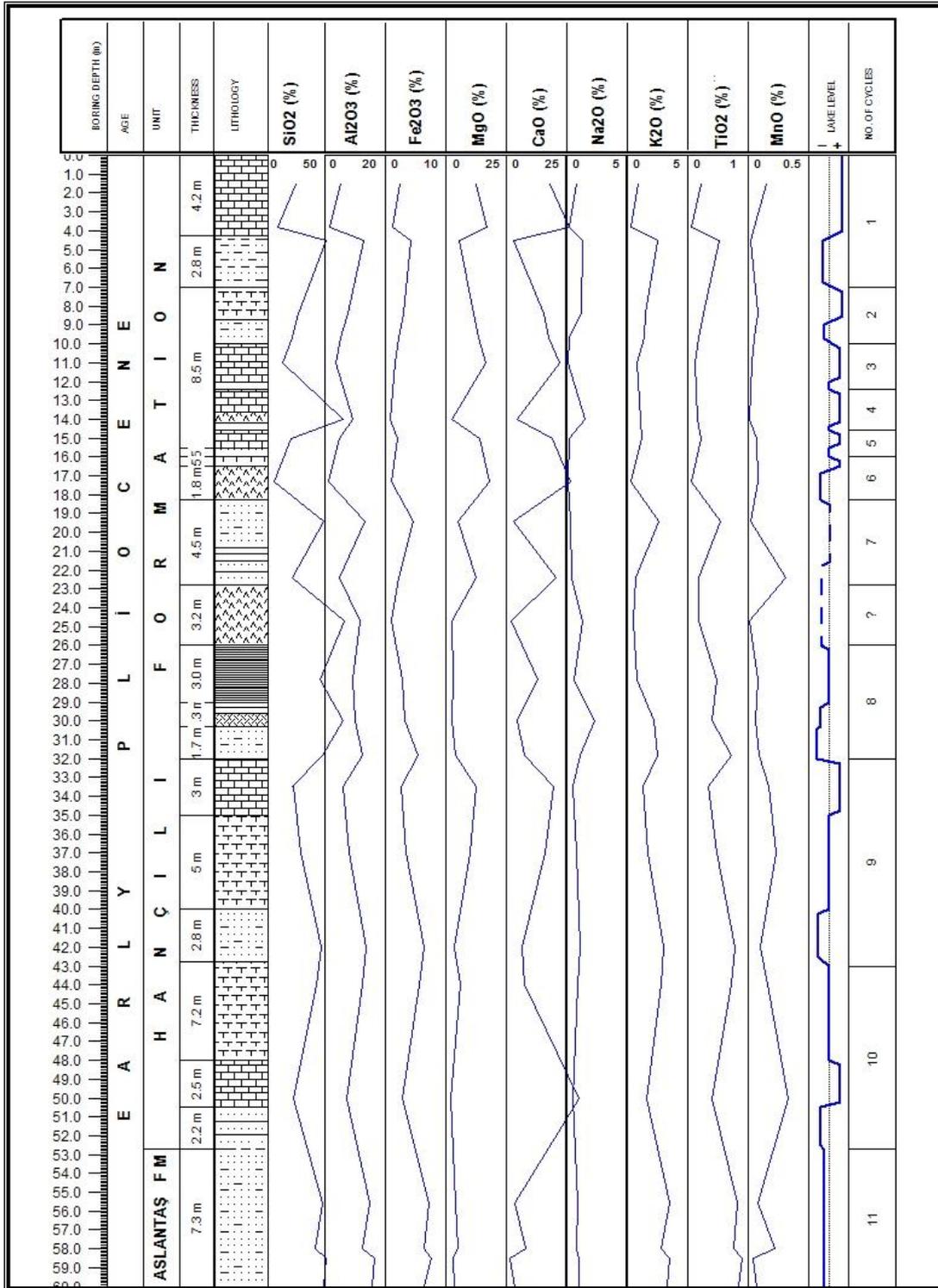
Figure 5.10. Major oxides (wt%) versus depth plot of SSK-1 Section.

69
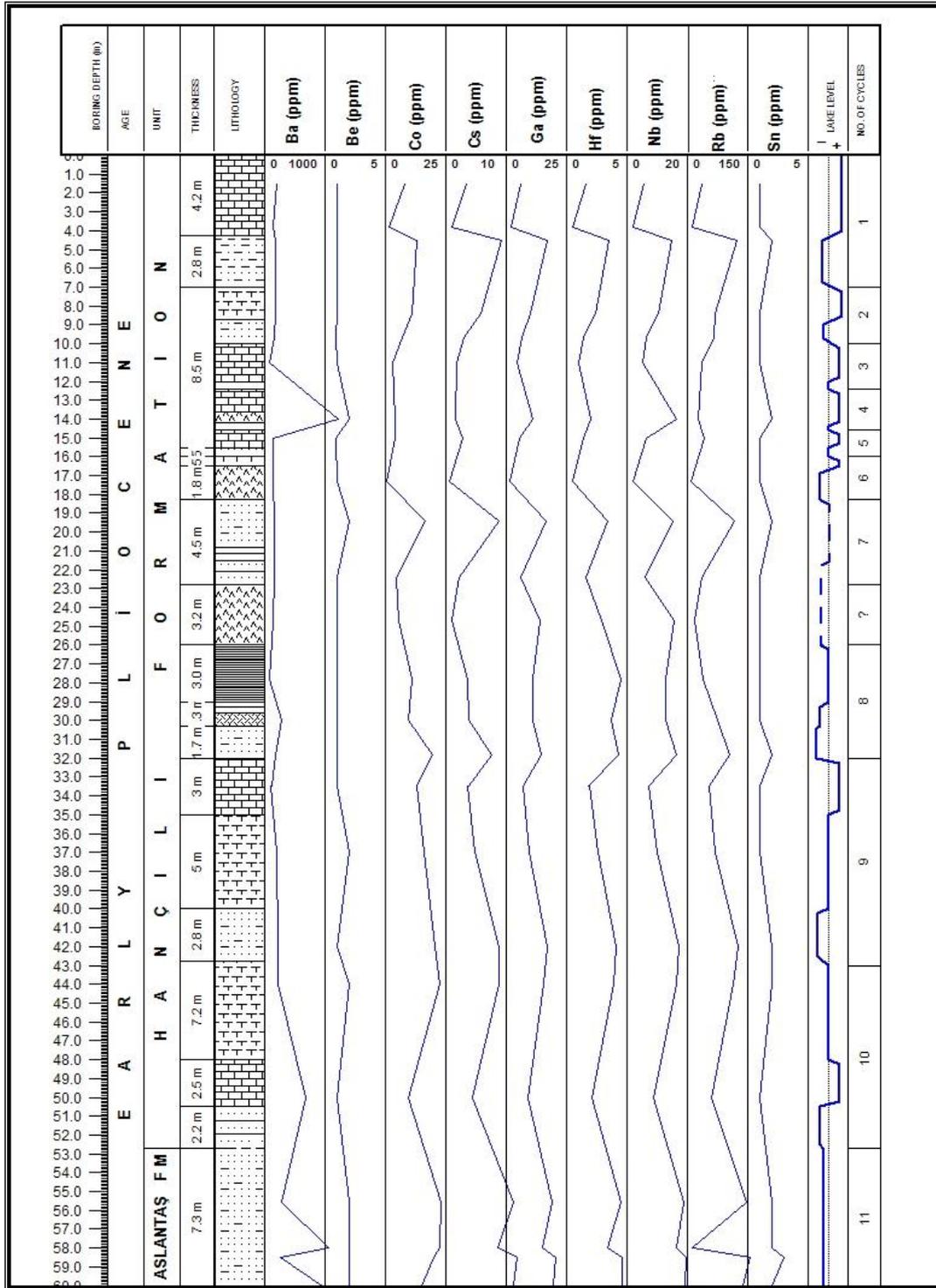
Figure 5.11. Trace elements (ppm) versus depth plot of SSK-1 Section.

70

Figure 5.11 cont'd.

71

Figure 5.11 cont'd.

72

Figure 5.11 cont'd.

73
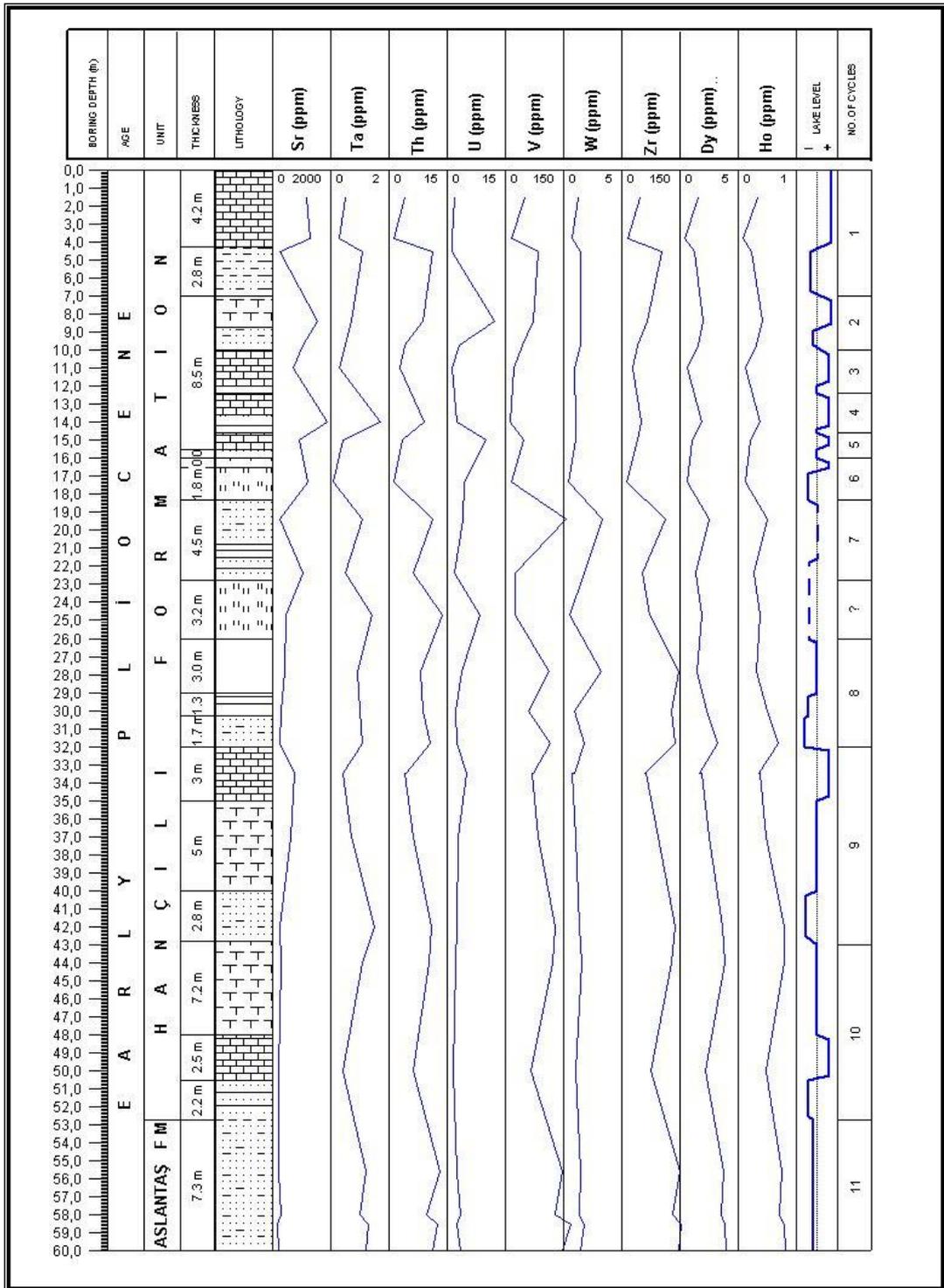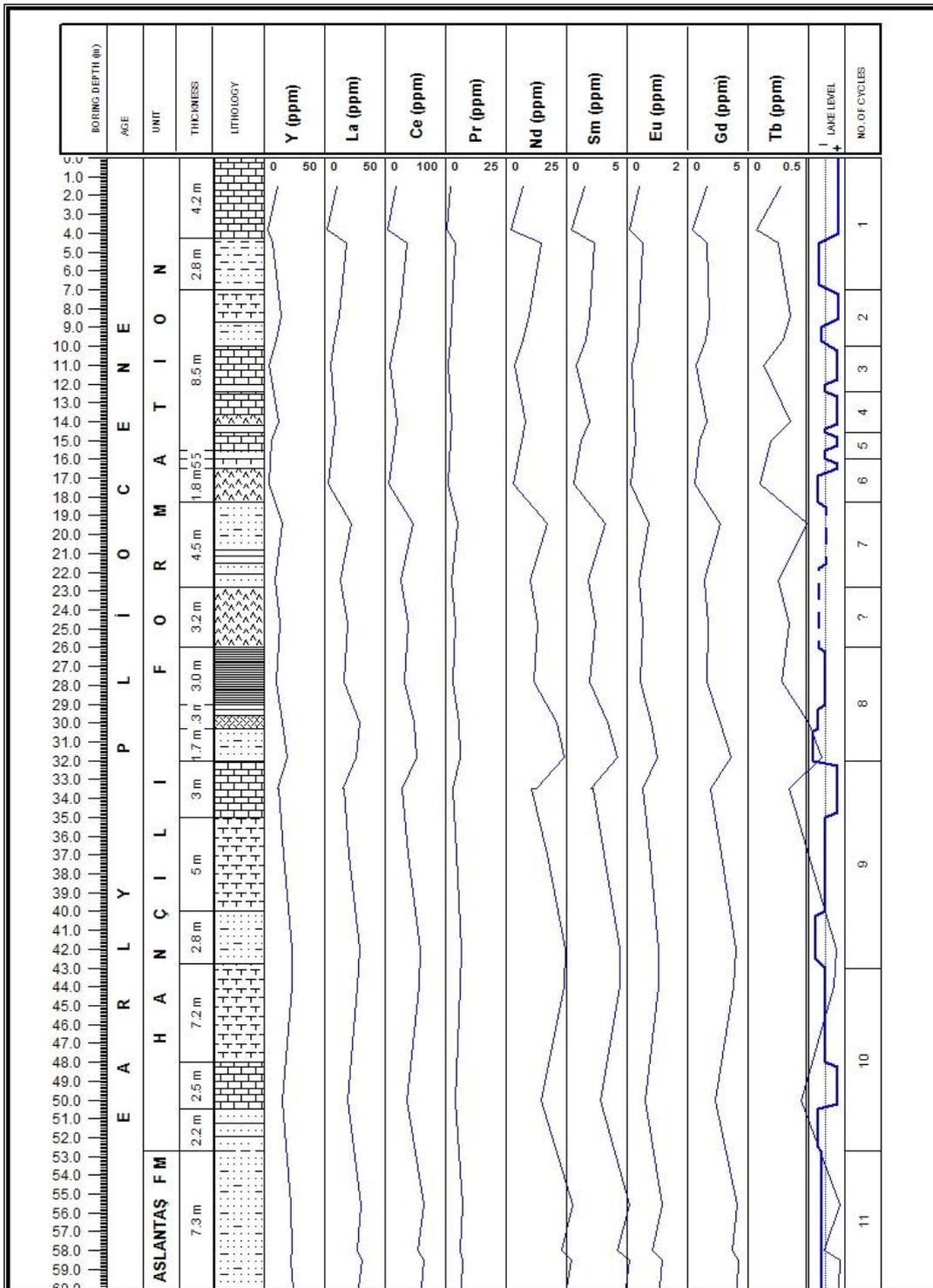
To check the provenance characteristics, Ti/Al, U/Th, Zr/Th, Ba/Sr and Ti/Y ratios were employed (Figure 5.12). Ti/Al, as expectively, is constant all through the section. U/Th ratio is constant but gets higher to the top. Zr/Th plots also decreasing upwar trend. They point that U and Zr concentrations are increasng relative to Th towards the top of the secton. All of these ratios and the trace lement concentrations versus depth plots suggest that there is almost constant sediment influx from the same chemical environment.

The major oxide values are employed to calculate the molecular weathering ratios (Figure 5.13). Saturation all through the section is almost constant. Clayeyness shows a decreasing upward trend. Leaching is almost constant, but highest at the bottom.

Hydration increases upward but generally constant like salinization. It increases upward and is highest at the middle, greater than 2.

Calcification is almost constant up to the middle units, then increases towards the top. Oxidation from bottom to middle is constant, but then fluctutaes within a narrow range.

Chemical index of alteration values are calculated, they are between 5% and 80%, implying low to high alteration affected the region. CIA values decrease to the top. Mg-index is also calculated. The values are higher but consistent with the CIA values. They also decrease upward (Figure 5.14).
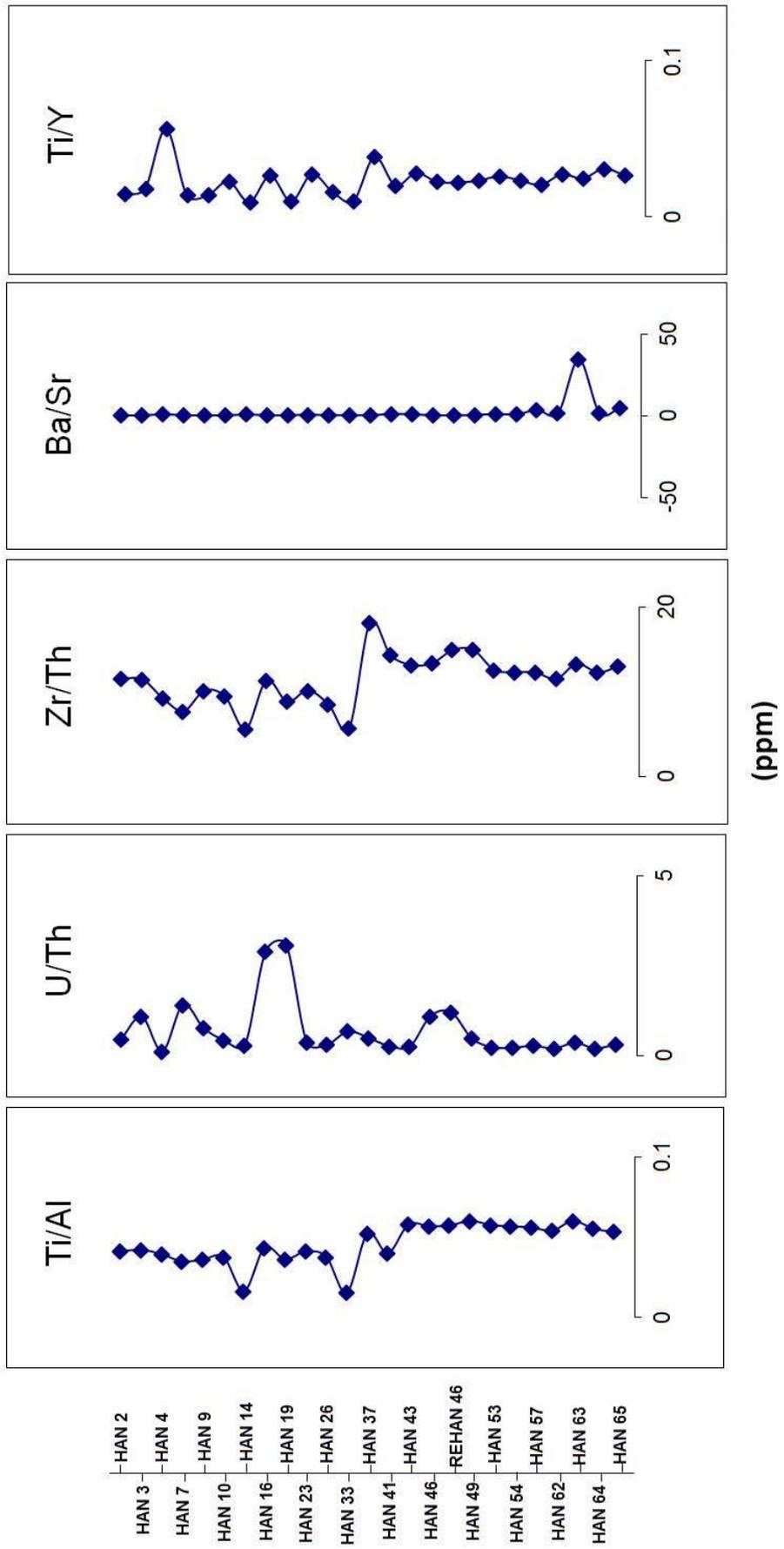
Figure 5.12. Trace element ratios of the samples from SSK-1 Section.
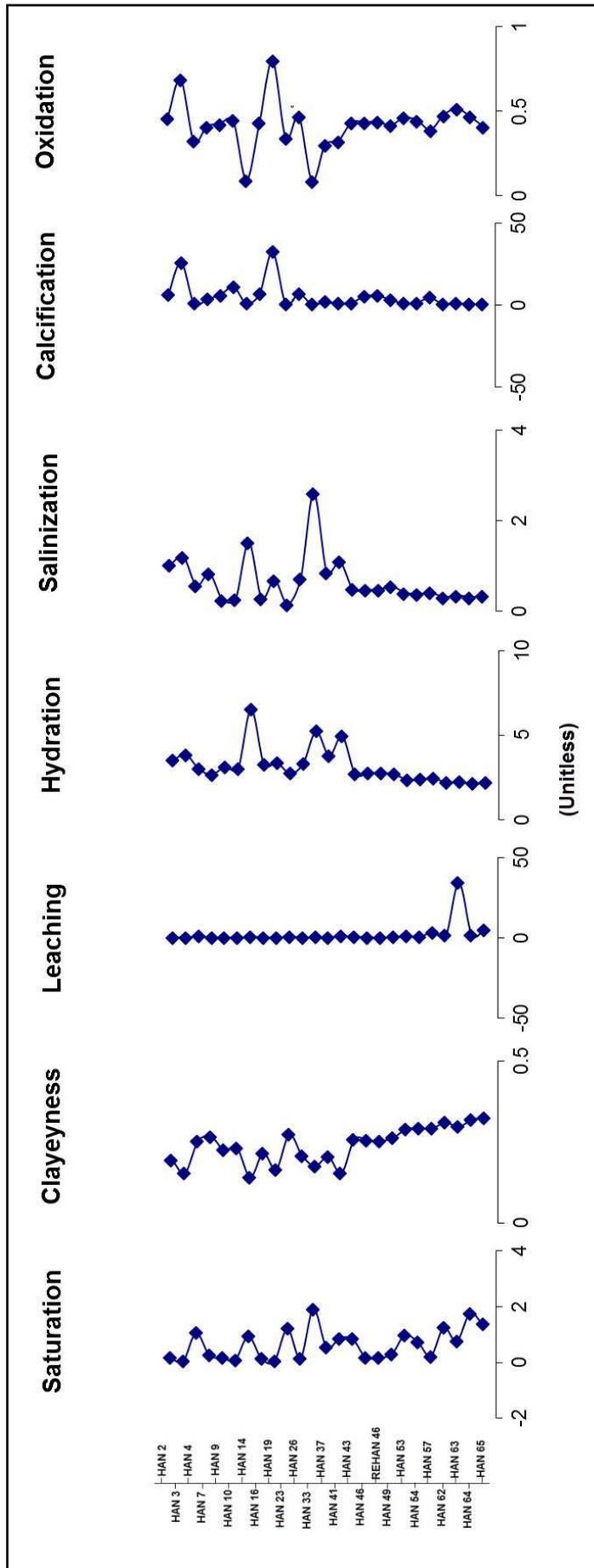
Figure 5.13. Molecular weathering ratios of the samples from SSK-1 Section
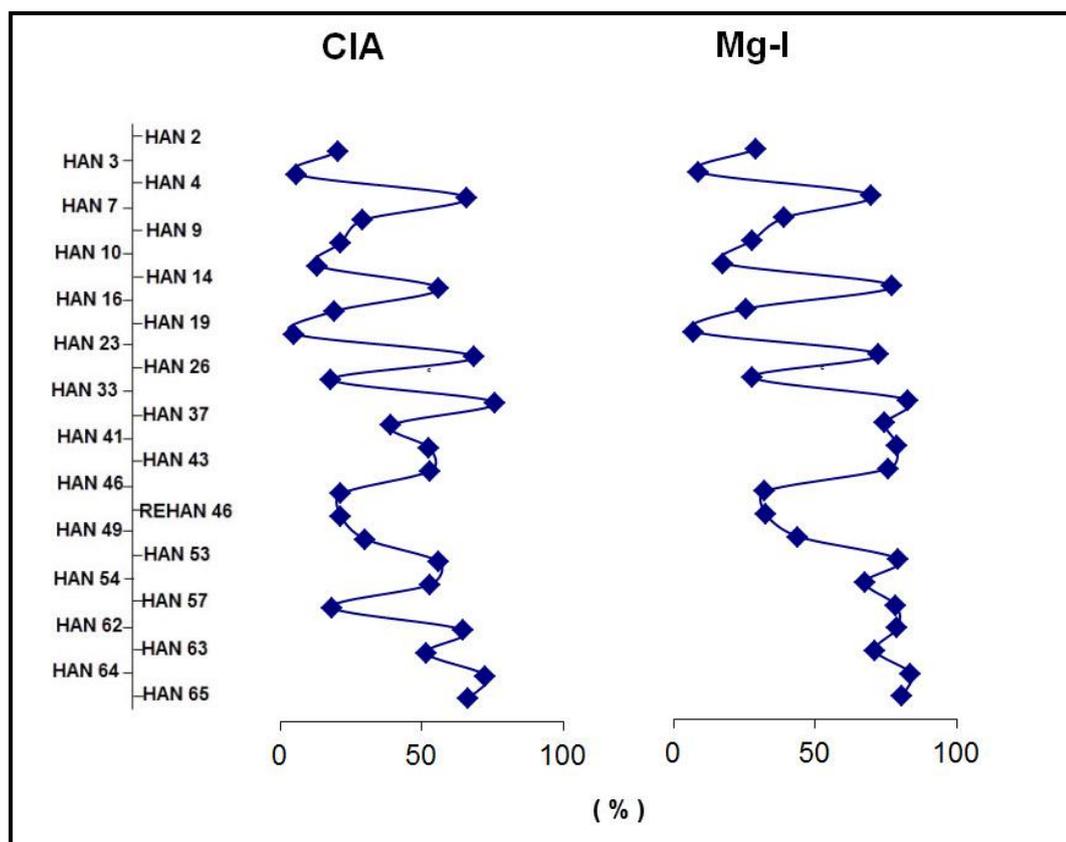
Figure 5.14. CIA and Mg-I values versus depth plots of SSK-1 Section.

5.5. Stable Isotope Geochemistry

Stable isotope data are accepted as good proxies reflecting the changes in environmental conditions. Stable isotopes ratios are measured relative to a standard, SMOW or VPDB. They are expressed with delta notation (δ) in parts per thousand (‰ or per mil). Delta notation is calculated as follows:

$$\delta^{18}O\ ‰ = \{ [^{18}O/^{16}O\ (sample) - ^{18}O/^{16}O\ (standard)] / ^{18}O/^{16}O\ (standard) \} \times 1000$$

Isotope fractionation, according to Rollinson (1993), takes place in three ways: the first one is isotopic exchange reactions. Secondly, kinetic processes affect the fractionation. Third one is physico-chemical processes like evaporation and condensation, melting, crystallization and diffusion can led the fractionation.

The stable carbon and oxygen isotopic composition of fluvial and lacustrine deposits are very important and sensitive paleoclimate indicators (Mack et al., 1991).

Wright and Tucker, (1991) stated that negative ^{13}C values as low as -10 indicate high input of ^{12}C from soil respiration and typically correlate with the vegatation cover dominated by C3 plants. Positive values, on the other hand, show mixing of soil respiration CO_2 and atmospheric CO_2 which reflect the seasonal nature of plant activity. C4 plants are more enriched in $\delta^{13}C$ than are C3 plants. They have $\delta^{13}C$ values between -6 and -19‰ (Deines, 1980) with an average of -13‰. C4 plants include warm season grasses, sedges, and a few halophytic shrubs and are better adapted to moisture and heat stress than C3 plants. Evaporation causes co-variation in C and O in soil carbonate, both becoming enriched in the

77

heavier isotope up the profile (Salomons et al., 1978). Evapotranspiration, however, does not cause any fractionation.

The stable isotope values of the selected samples from SSK-1 borehole are summarized in Table 5.6 in VPDB standard. The $\delta^{18}O$ values range from -2,32‰ to -8,77‰ VPDB reflecting the formation under the infuence of meteoric water. $\delta^{13}C$ values are between -3,85‰ and -7,63‰ VPDB which shows wider range. Therefore, the 13C isotope values are consistent wth the presence of C4 plants which are mostly dominated by warm season vegetations. There is a good covariance between $\delta^{13}C$ and $\delta^{18}O$ values which show that they were both affected from the same chemical environment during fractionation and therefore can be used as good proxy for the climatic reconstruction (Figure 5.15). The isotope values are plotted against depth, and the diagrams show that there is general increasing trend towards the top of the section, which suggest there is an increase in the temperatue as time passed.

$\delta^{18}O$ versus $\delta^{13}C$ plot is also drawn (Figure 5.16). It clearly shows that there is a linear increasing trend suggesting an increase in temperature up to the section. It is accepted as evaportaion in this study which is consistent with the other findings.

Table 5.6. $\delta^{13}C$ and $\delta^{18}O$ isotope ratios of the Hançılı Formation.

Depth (m)	Sample	CO3-content	$\delta^{13}C$	$\delta^{18}O$
		(%CaCO3)	(‰ VPDB)	(‰ VPDB)
-1,80	HAN-2	55,54	-4,91	-3,50
-3,80	HAN-3	86,97	-5,06	-2,97
-8,30	HAN-7	17,88	-4,77	-4,08
-11,00	HAN-10	70,84	-4,57	-2,32
-15,00	HAN-16	86,07	-3,85	-2,98
-27,80	HAN-37	46,23	-6,24	-5,73
-26,50	HAN-38	27,10	-5,91	-4,92
-32,70	HAN-45	54,09	-6,40	-5,27
-33,40	HAN-46	71,14	-6,35	-2,84
-37,00	HAN-49	12,79	-6,35	-3,37
-44,20	HAN-54	30,46	-5,86	-3,68
-50,00	HAN-57	67,28	-6,14	-6,45
-56,80	HAN-62	1,82	-5,66	-5,21
-58,10	HAN-63	0,34	-7,63	-8,77
-58,70	HAN-64	0,61	-6,26	-7,36
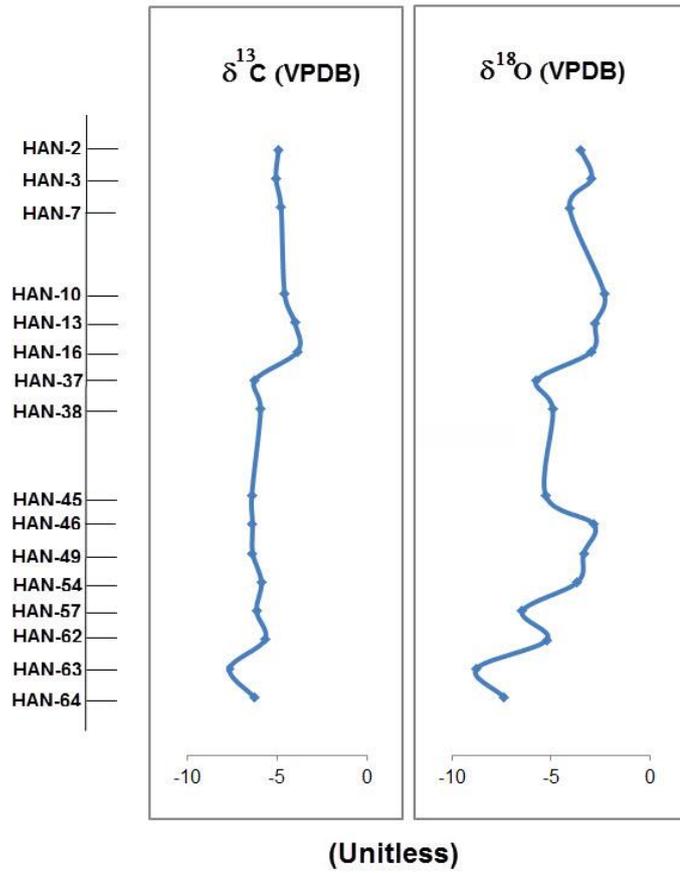
Figure 5.15. Stable isotope values versus depth plots of SSK-1 Section
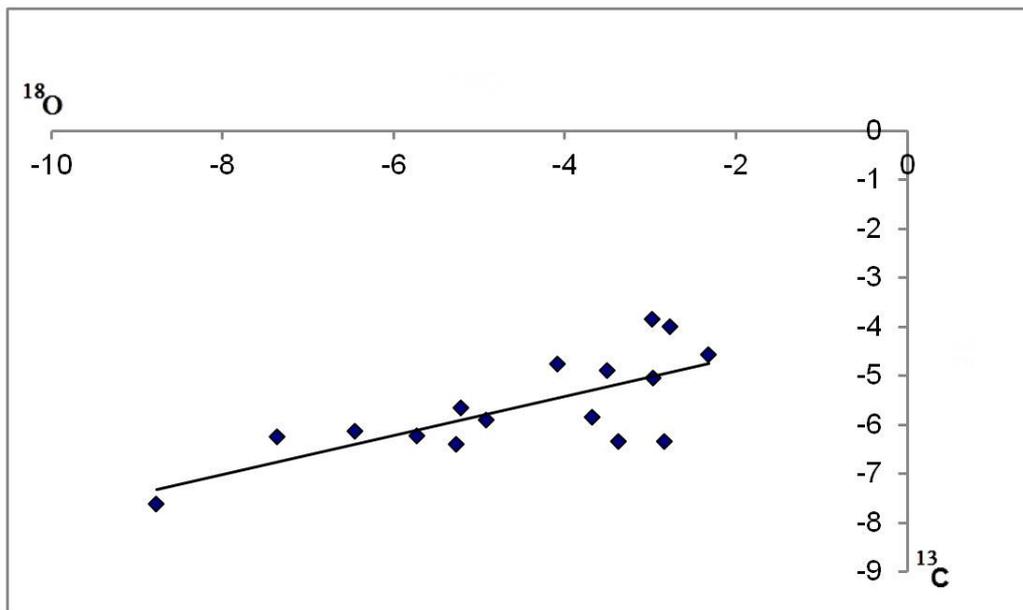
Figure 5.16. δ18O versus δ13C plot.

CHAPTER 6

DISCUSSION

Although the region has been studied widely by many scientists, the age of the Hançılı Formation has become a subject of debate. Some of the studies pointed out fossil records, some accept the stratigraphical position of the formation as a guide to suggest an age (Figure 6.1). The Figure below shows the literature survey modified from Kaymakçı (2000). Ayan (1969) and Birgili (1974) studied in the region, but did not give any age for the Hançılı Formation. Then, Dellaloğlu et al. (1992) studied and gave an age of Late Miocene. Özçelik (1994) did not mention the age of the formation but studied in the region. Türkmenoğlu et al. (1994) and Koçyiğit el al. ,(1995) studied in the region and gave an age of Early Pliocene because of some fossil records pointing the age of the Aslantaş Formation reached to the Late Miocene. Kaymakçı (2000) studied in the region and due to presence of some gastrapods of Middle Miocene age, gave an age of Burdigalian-Langhian.

With the help of field observations and the literature reviewed for this study, the age of the Hançılı Formation is suggested to be Middle Miocene-Early Pliocene. However, it is highly recommended to have radiometric age data to reconstruct the age of the Hançılı Formation.
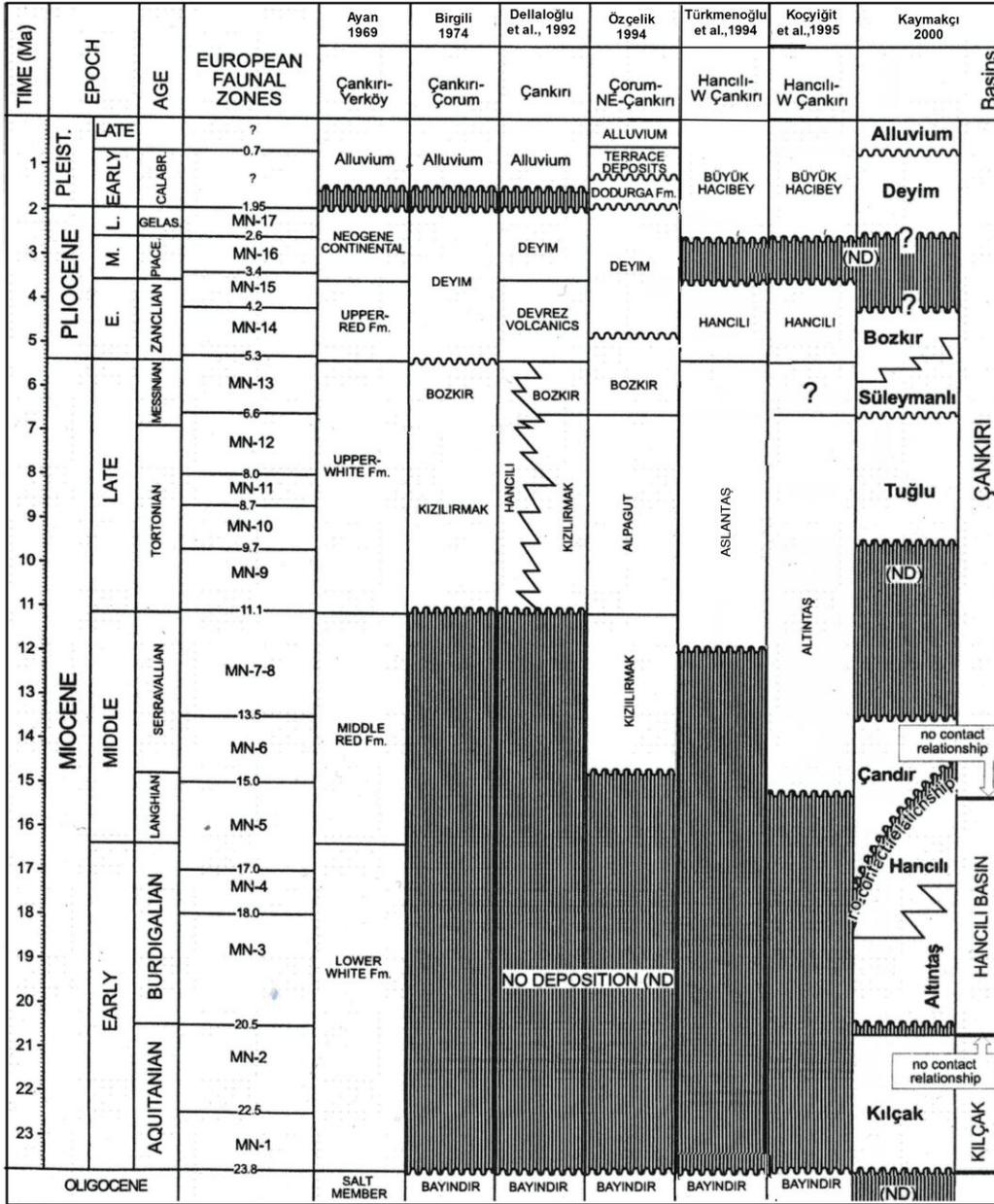
Figure 6.1. References used in age estimation (modified from Kaymakçı, 2000).

The mineral compositions of the Koyunbaba section are correlated with the molecular weathering ratios (Figure 6.2). The presence of dolomite generally has an opposite trend with the presence of calcite. Calcite is relatively rare than dolomite providing the dolomite as the dominant carbonate phase in the region. On the basis of the bulk mineral compositions, it is clear that the enrichments and depletions of the minerals relative to depth and each other are in pace with the lithologies and the alteration indexes. During the wet periods, CIA values are higher and amounts of dolomite and smectite; the values of calcification and saturation are lower due to low sediment influx. During arid and dry periods, the CIA values are lower, on the other hand, dolomite and smectite are enriched. When compared with each other, dolomite and smectite amounts are oppositely correlated. When smectite is relatively lower, dolomite becomes enriched, possibly suggesting the smectite weathering as one of the sources of Mg for the dolomite formation.

The mineral compositions of the Killik Section are also correlated with the geochemical data to reveal climatic conditions (Figure 6.3). The presence of smectite is well correlated with the increase in salinity and calcification and oppositely correlated with the CIA values implying the dry conditions favouring the formation of smectite in the region. On the other hand, the low content of smectite is also correlated with the high CIA value, piointing the high lake level and open environment for the chemical alteration.

For the SSK-1 section, mineralogical and geochemical proxies are correlated with the isotope data and compared with the $\delta^{18}O$ global stack curve from Feakins et al. (2012) to show how our data from SSK-1 possibly match with the global curve on Miocene Climatic Optimum (Figure 6.4). It is obviously seen the increase in salinization and calcification periods match with the positive trends on stable isotope curve while CIA values are negatively correlated. This means there is a strong covariance among the paleoclimate proxies for Hançılı Formation. The periods of dry and arid seasons correlate with high $\delta^{18}O$ and $\delta^{13}C$ values where the lake level was low stands. The wet seasons which are well correlated with the high CIA, low salinization, calcification and high MnO values can be represented by the lake level high stands.
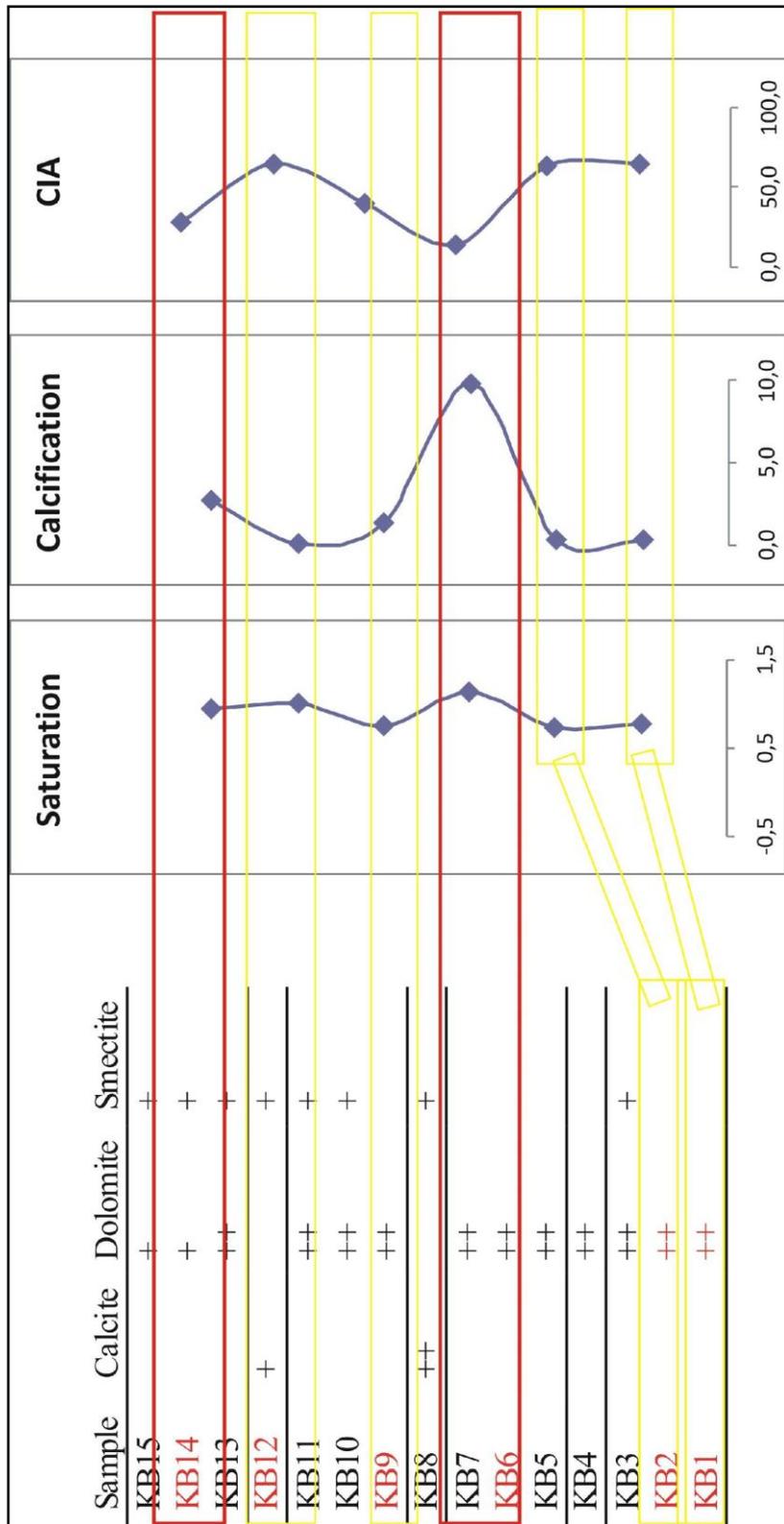
Figure 6.2. Interpretation of all proxies for Koyunbaba Section (red rectangles represent the dry and arid seasons; yellow ones point the wet periods).
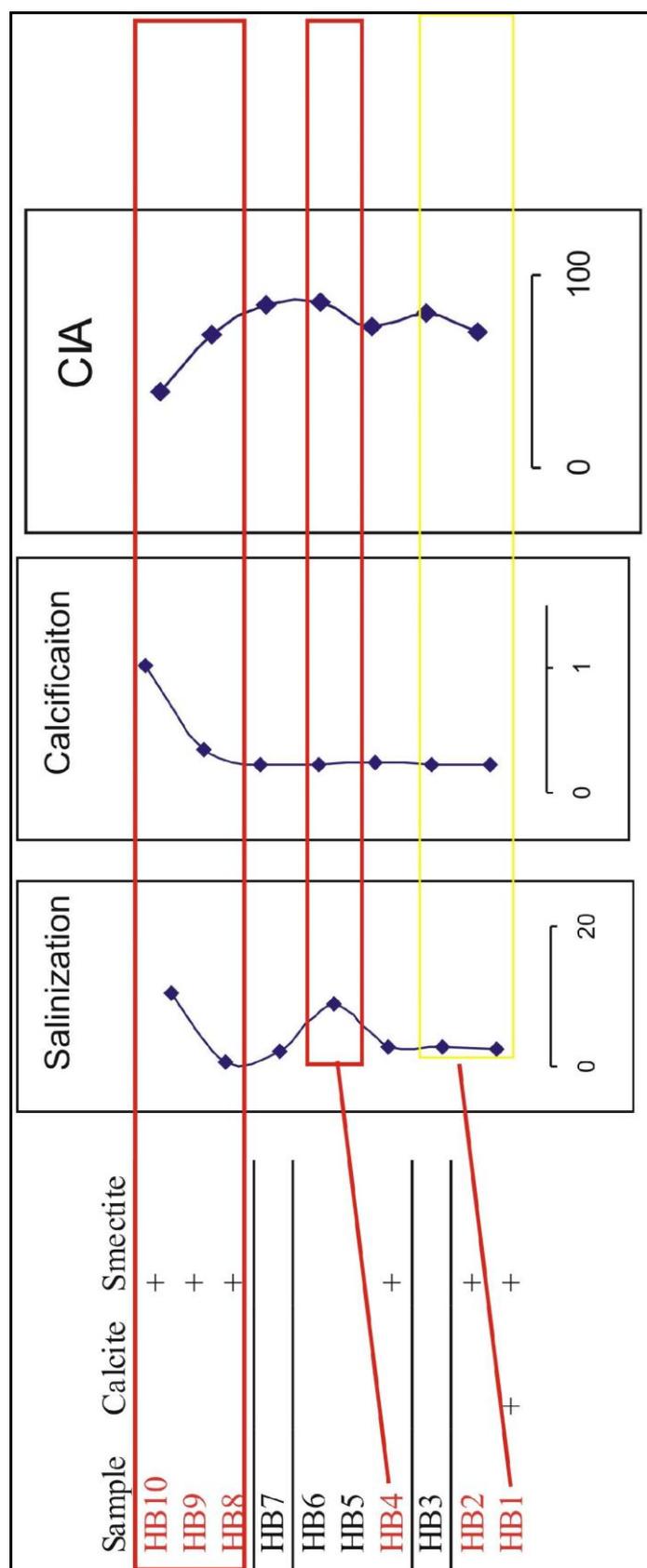
Figure 6.3. Interpretation of all proxies for Killik Section (red rectangles represent the dry and arid seasons; yellow ones point the wet periods).

85
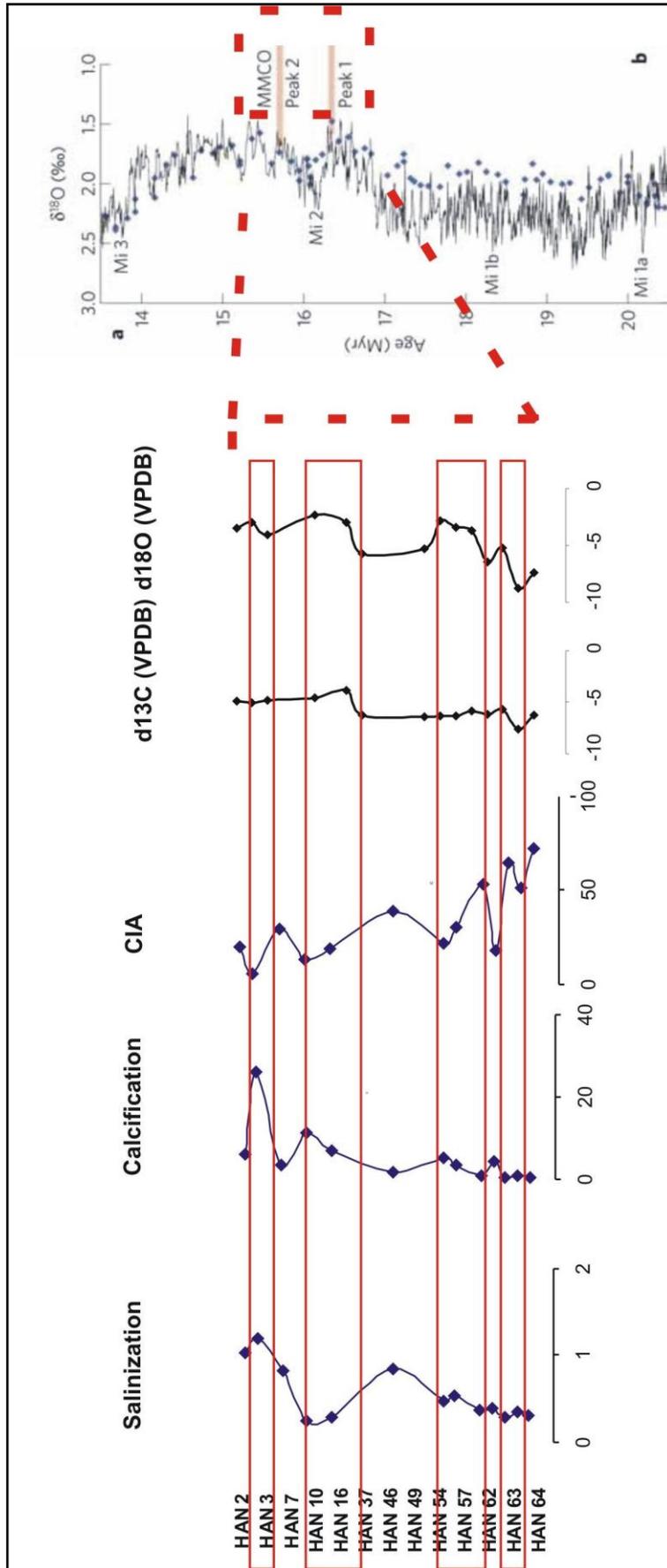
Figure 6.4. Interpretation of all proxies for SSK-1 Section and comparison with the δ18O global stack curve from Feakins et al. (2012) (red rectangles represent the dry and arid seasons;).

CHAPTER 7

CONCLUSION

The following conclusions can be figured out.

1) By the field observations and the literature reviewed for this study, the age of the Hançılı Formation is suggested to be Middle Miocene-Early Pliocene. However, it is highly recommended to have radiometric age data to reconstruct the age of the Hançılı Formation.

2) Quartz, plagioclase, analcime are the non-clay components of most of the samples, while smectite, illite and chlorite form the clay fractions.

3) The dolomite and smectite as mineral proxies, salinization, calcificaiton and CIA values as geochemical proxies are employed for Koyunbaba and Killik Sections. Together with these proxies, stable isotope values are also used to interpret SSK-1 Section.

4) All the proxies employed for this study show that there is strong warm periods occurred during the deposition of Hançılı Formation which are interrupped wet cycles. Especially the proxies for the SSK-1 section plot the warm periods which are very well correlated with each other.

5) The $\delta^{13}C$ values suggest that the dominant vegetation during the deposition of Hançılı Formation was C4 plants which represent warm seasons. Therefore, it is highly recommended for the future studies that palinological analyses should be carried out in the Basin.

6) The dolomite is thought to be authigenic in origin, therefore used as paleoclimate proxy in this study. Illite and chlorite, on the other hand, are the detrital components in the clay fractions.

7) The Aslantaş Formation represents fluvial environments, while it changed into lacustrine when Hançılı Formation started to be deposited in the basin.

8) The lake level fluctuations recorded with the lithologies are consistent with the other proxies, showing the wet seasons as high stands and dry periods as low stands.

9) The Middle Miocene to Early Pliocene was a period where there was a warm Middle Miocene and then cold Early Pliocene. The isotope values are consistent with the warm periods of Middle Miocene Climatic Optimum. Therefore, the studied portion of the Hançılı Formation was suggested to be deposited in a saline-alkaline environment during the warm Middle Miocene.

REFERENCES

Akyürek, B., Bilginer, E., Çatal, E., Dağer, Z., Soysal, Y. and Sunu, O., Eldivan – Şabanözü (Çankırı) dolayında ofiyolit yerleşimine ilişkin bulgular, 1979, Jeoloji Müh. Odası Yayınları, No. 9.

Akyürek, B., Bilginer, E., Çatal,E., Dağer,Z.,Soysal,Y.,Sunu,O.,1980, Şabanözü (Çankırı) , Hasayaz-Çandır (Kalecik-Ankara) dolayının jeolojisi, MTA Rapor no. 6741.

Akyürek,B., Bilginer,E., Akbaş,B., Hepşen,N., Pehlivan,Ş., Sunu,O., Soysal,Y., Dağer,Z., Çatal,E., Sözeri,B., Yıldırım,H. and Hakyemez,Y.,   1984,   Ankara-Elmadağ-Kalecik dolayının temel jeolojik özellikleri, Jeoloji Mühendisliği, C20,31-46.

Akyürek, B., Akbaş, B. and Dağer, Z., 1988, 1:100 000 Ölçekli açınsama nitelikli Türkiye Jeoloji Haritaları serisi – Çankırı E-16 paftası: MTA, Ankara, 21s.

Akyürek, B., 1981. İç Anadolu'nun jeolojisi simpozyumu, Ankara melanjının kuzey bölümünün temel jeolojik özellikleri: TJK Yayını, 41-45, 56-58.

Akyürek, B., Bilginer, E., Çatal, E., Dağer, Z., Soysal, Y. and Sunu, O., 1979b. Eldivan Şabanözü (Çankırı) dolayında ofiyolit yerleşimine ilişkin bulgular, JMO, 9.

Akyürek, B., Bilginer, E., Çatal, E., Dağer, Z., Soysal, Y. And Sunu, O., 1980. Eldivan-Şabanözü (Çankırı) Hasayaz-Çandır (Kalecik-Ankara) dolayının jeolojisi, MTA Derleme No: 6741 (unpublished).

Akyürek, B., Bilginer, E., Akbaş, B., Hepşen, N., Pehlivan, Ş., Sunu, O., Soysal, Y., Dağer, Z., Çatal, E., Sözeri, B., Yıldırım, H. and Hakyemez, Y., 1982. Ankara-Elmadağ-Kalecik dolayının jeolojisİ, MTA Derleme No: 7298 (unpublished).

Akyürek, B., Bilginer, E., Akbaş, B., Hepşen, N., Pehlivan, Ş., Sunu, O., Soysal, Y., Dağer, Z., Çatal, E., Sözeri, B., Yıldırım, H. and Hakyemez, Y., 1984. Ankara-Elmadağ-Kalecik dolayının temel jeolojik özellikleri, Jeoloji Mühendisliğ,, 20, 31-46.

Akyürek, B., Duru, M., Sütçü, Y.F., Papak, İ., Şaroğlu, F., Pehlivan, N., Gönenç, O., Granit, S., Yaşar, T., 1997. MTA Genel Müdürlüğü Ankara F-15 Paftası, 1:100 000 ölçekli açınsama nitelikli Türkiye Jeoloji Haritaları, No.55.

Asikainen, C. A., Brigham-Grette, J. 2001. Sedimentological Studies of the Paleoclimate record from core PG1351, El'gygytgyn Crater Lake, NE Russia. Artic Workshop, University of Massachusetts.

Bradley, R.S., 1999. Paleoclimatology: Reconstructing Climates of the Quaternary. Academic Press, San Diego, p 610.

Bektimuroğlu, O.,1978, Ankara ili- Kalecik ilçesi Hancılı Köyü Bentonit sahası Hakkında Ön Rapor, MTA, Rapor No.1978.

Böhme, M., 2003. The Miocene Climatic Optimum: evidence from ectothermic vertebrates of Central Europe. Palaeogeography, Palaeoclimatology, Palaeoecology. 195 (3–4), 389–401.

Brindley, G.W., 1980. Quantitative X-ray analyses of clays. In: Brindley, G.W. and Brown, G. (eds), Crystal Structures of Clay Minerals and Their X-ray Identification. Mineralogical Society Monograph 5, 411–438.

Bruch,A.A., Utescher, T., Mosbrugger, V., NECLIME members, 2011. Precipitation patterns in the Miocene of Central Europe and the development of continentality. Palaeogeography, Palaeoclimatology, Palaeoecology, 304, 202–211.

Buol, S.W., Hole, F.D., McCracken, R.J. and Southard, R.J., 1997. Soil Genesis and Classification, Iowa State University Pres, Mes, IA, p 527.

Chamley, H., 1989. Clay Sedimentology, Springer, New York, p 623.

Chen, P.Y., 1977. Table of key lines in X-ray powder diffraction patterns of minerals in clays and associated rocks. Department of Natural Resources, Geological Survey Occasional Paper 21. Bloomington, Indiana, USA.

Dönmez, M., and Akçay, A.E., 2010. 1/100 000 Ölçekli Açınsama Nitelikli Türkiye Jeoloji Haritaları Serisi, Çankırı H-30 Paftası, MTA Yayınları.

Eder-Kovar, J., Jechorek, H., Kvaček, Z., Parashiv, V., 2008. The integrated plant record: an essential tool for reconstructing Neogene zonal vegetation in Europe. Palaios, 23, 97–111.

Eroğlu,Ş. and Farsakoğlu, K.,1982, Ankara ili Kalecik ilçesi-Hançılı, Demirtaşlı köyleri bentonit yatağı etüd raporu, MTA Rapor No. 7440.

Eronen, J.T., Mirzaie, M., Karme, A., Micheels, A., Bernor, R.L., Fortelius, M., 2009. Distribution history and climatic controls of the Late Miocene Pikermian chronofauna. Proceedings of the National Academy of Science 106, 11867–11871.

Fagel, N., Boski, T., Likhoshway, L., Oberhaensli, H., 2003. Late Quaternary clay mineral record in Central Lake Baikal (Academician Ridge, Siberia). Palaeogeography Palaeoclimatology Palaeoecology, 193, 159-179.

Feakins, S.J., Sophie, W., Jung-Eun, L., 2012. Hydrologic cycling over Antarctica during the middle Miocene warming. Nature Geoscience, 5, 557-560.

Güngör, P.,1992, Mineralogical and Chemical Properties of Bentonites from Southwest Çankırı Basin, M.S. Thesis, METU, Ankara, 95p.

Hakyemez, y., Barkurt, M. Y., Bilginer, E., Pehlivan, Ş., Can, B., Dağer, Z. And Sözeri, B., 1986. Yapraklı-Ilgaz-Çankırı, Çandır dolayının jeolojisi, MTA Rapor No 7966.

Harzhauser, M., Piller, W.E., 2007. Benchmark data of a changing sea—palaeogeography, palaeobiogeography and events in the Central Paratethys during the Miocene. Palaeogeography, Palaeoclimatology, Palaeoecology, 253, 8–31.

Harzhauser, M., Latal, C., Piller, W.E., 2007. The stable isotope archive of Lake Pannon as a mirror of Late Miocene climate change. Palaeogeography, Palaeoclimatology, Palaeoecology 249, 335–350.

Harzhauser, M., Mandic, O., 2008a. Neogene Dreissenids in Central Europe — exploring the limits. In: Van der Velde, G., Rajagopal, S., Bij de Vaat, A. (Eds.), Zebra Mussels in Europe.

Harzhauser, M., Mandic, O., 2008b. Neogene lake systems of Central and South-Eastern Europe: faunal diversity, gradients and interrelations. Palaeogeogr. Palaeoclimatol. Palaeoecol.

Ilyina, L.B., Shcherba, I.G., Khondkarian, S., 2004a. Map 8: Middle Late Miocene (LateTortonian–Early Messinian–Early Maeotian–Late Pannonian). Cour. Forsch.-Inst. Senckenberg 250, 31–33.

Ilyina, L.B., Shcherba, I.G., Khondkarian, S.O., Goncharova, I.A., 2004b. Map 6: Mid Middle Miocene (Middle Seravalian, Late Badenian, Konkian). Cour. Forsch.-Inst.Senckenberg 250, 23–25.

Ivanov, D., Utescher, T., Mosbrugger, V., Syabryaj, S., Djordjević-Milutinović, D., Molchanoff, S., 2011. Miocene vegetation and climate dynamics in Eastern and Central Paratethys (Southeastern Europe). Palaeogeography, Palaeoclimatology, Palaeoecology, 304, 262–275.

Karadenizli, L., 2011. Oligocene to Pliocene palaeogeographic evolution of the Çankırı-Çorum Basin, central Anatolia, Turkey. Sedimentary Geology, 237, 1–29.

Karadenizli, L., Saraç, G., Sen, S., Seyitoğlu, G., Antoine, P.O., Kazancı, N., Varol, B., Alçiçek, M.C., Gül, A., Erten, H., Esat, K., Ozcan, F., Savasci, D., Antoine, A., Filoreau, X., Hervet, S., Bouvrain, G., de Bonis, L., Hakyemez, H.Y., 2004. Oligo-Miocene Mammalian Biostratigraphy an Depositional Evolution of the Western and Southern parts of Çankiri-Çorum Basin, Central Anatolia. TUBITAK Project no: 101Y108: MTA report, No:10706.

Kaymakçı, N., 2000. Tectono-stratigraphical evolution of the Çankırı Basin (Central Anatolia Turkey). Geologia Ultraiectina 190, 1–247.

Koçyiğit,A., Türkmenoğlu,A., Beyhan,A., Kaymakcı, N. and Akyol, E., 1995, Post-collisional tectonics of Eskişehir-Ankara-Çankırı segment of İzmir-Ankara-Erzincan suture zone (IAESZ) , Ankara orogenic phase, TPJD Bülteni,C.6/1, 69-86.

Kojumdgieva, E., Popov, N., 1989. Paléogéographic et evolution géodinamique de la Bulgarie Septentrionale au Néogène. Geologica Balcanica 19, 73–92.

Lewis, A.R., Marchant, D.R., Ashworth, A.C., Hemming, S.R., Machlus, M.L., 2007. Major middle Miocene global climate change: evidence from East Antarctica and the Transantarctic Mountains. Geological Society of America Bulletin 119, 1449–1461.

Mack, G.H., Cole, D.R., Giordano, T.H., Schaal, W.C., and Barcelos, J.H., 1991. Paleoclimatic controls on stable oxygen and carbon isotopes in caliche of the Abo Formation (Permian), south-central New Mexico, U.S.A. Journal of Sedimentary Petrology 61, 458–472.

Meulenkamp, J.E., Sissingh, W., 2003. Tertiary palaeogeography and tectonostratigraphic evolution of the Northern and Southern Peri-Tethys platforms and the intermediate domains of the African-Eurasian convergent plate boundary zone. Palaeogeography, Palaeoclimatology, Palaeoecology 196 (1–2), 209–228.

Meulenkamp, J.E., Kovac, M., Cicha, I., 1996. On Late Oligocene to Pliocene depocentre migrations and the evolution of the Carpathian–Pannonian system. Tectonophysics, 266, 301–317.

Nesbitt, H.W. and Young, G.M., 1982. Early Proterozoic climates and plate motions inferred from major element lutites. Nature, 299, 715-717.

Nesbitt, H.W. and Young, G.M., 1984. Prediction of some weathering trends of plutonic and volcanic rocks based thermodynamic and kinetic considerations. Geochimica et Cosmochimica Acta, 48, 1523-1534.

Nesbitt, H.W. and Young, G.M., 1989, Formation and diagenesis of weathering profiles, Journal of Geology, 97, 129-147.

Özalp,T., 1991, Geology, Mineralogy, Petrography and Chemical Composition of Hancılı Bentonites and Associated Rocks,Northwest of Kalecik, Ankara, M.S. Thesis,METU, Ankara, 87 p.

Özalp,T., Türkmenoğlu,A.G. and Akıman,O., 1991, Occurrence of analcime and bentonite in the Late Miocene hançılı formation at Hançılı area (Kalecik-Ankara), V. UlusalKil Sempozyumu, Bildiriler, 100-111.

Özoğul, İ. 1976, Ankara ili Kalecik ilçesi Hançılı köyü bentonit sahası detay etüd raporuMTA Rapor no. 3203.

Özalp,T., 1998, Geological System Analysis for Mineral Exploration in Sedimentary Basins by Using Spaceborn Imaging Systems;An Imaging Radar Case Stdy for theKalecik-Hasayaz Basin, Ankara, Turkey, Ph.D. Thesis, METU, Ankara, 375p.

Retallack, G.J., 2001. Soils of the past. Blackwell, Oxford. 600 p.

Rögl, F., 1998. Palaeogeographic considerations for Mediterranean and Paratethys seaways (Oligocene to Miocene). Ann. Naturhist. Mus. Wien 99 A, 279–310.

Rögl, F., 1999. Mediterranean and Paratethys. Facts and hypotheses of an Oligocene to Miocene paleogeography (short overview). Geologica Carpathica 50, 339–349.

Rögl, F., 2001. Mid-Miocene Circum-Mediterranean palaeogeography. Ber. Inst. Geol. Paläont., K.-F.-Univ. Graz 4, 49–59.

Salomons, W.,Goudie, A. and Mook, W.G., 1978. Isotopic composition of calcrete deposits from Europe, Africa and India, Earth Surf. Proc., 3, 43-57.

Sheldon, N.D. and Tabor, N.J., 2009. Quantitative paleoenvironmental and paleoclimatic reconstruction using paleosols. Earth-Science Reviews, 95, 1-52.

Shevenell, A.E., Kennett, J.P., Lea, D.W., 2004. Middle Miocene Southern Ocean Cooling and Antarctic Cryosphere Expansion. Science 305, 1766–1770.

Sun, J., Zhang, Z., 2008. Palynological evidence for the Mid-Miocene Climatic Optimum recorded in Cenozoic sediments of the Tian Shan Range, northwestern China. Global and Planetary Change, 64, 53–68.

Şen, Ş., Seyitoğlu G., Karadenizli,L.,Kazancı N., Varol, B. and Araz,H., 1998, Mammalian biochrnology of Neogene deposits and its evolution with the ithostratigraphy in the Çankırı-Çorum basin, central Anatolia, Turkey, Eclogae Geol. Helv., 91, 307-320.

Tabor, N.J., 2002. Paleoclimate Isotopic Proxies Derived from Paleozoic, Mesozoic, Cenozoic Paleosols and Modern Soils. University of California, PhD Thesis, p 213.

Tekkaya, İ., Atalay,Z., Gürbüz,M. Ünay,E. and Ermumcu,M.,1975, Çankırı-Kalecik bölgesi karasal Neojeninin biyostratigrafi araştırması, Türkiye Jeoloji Kurumu Bülteni, 18, 77-80.

Thorez, J., 1976. Practical Identification of Clay Minerals, 89 p.

Türkecan, A., Hepşen, N., Papak, İ., Akbaş, B.,Dinçel, A., Karataş, S.,Özgür, İ.B., Akay, E., Bedi, Y., Sevin, M., Mutlu, G., Sevin, D., Ünay, E., Saraç, G., 1991. Seben-Gerede (Bolu)- Güdül-Beypazarı (Ankara) ve Çerkeş-Orta-Kurşunlu (Çankırı) yörelerinin (Köroğlu Dağları) jeolojisi ve volkanik kayaçların petrolojisi. MTA Report, No: 9193.

Türkmenoğlu, A.G., Aker, S., Göğüş, G. and Turan, C.,1987. Ankara-Çankırı bölgesi bentonitlerinin mineralojisi, petrografisi ve oluşumu, II. Ulusal Kil Sempozyumu, Bildiriler, 101-112.

Türkmenoğlu, A.G., Göktürk, E.H., Güngör, P., and Özalp, T., 1991. Chemical characterization of Hançılı Bentonites, Kalecik,Turkey,Proc. 7th Euroclay Conf. Dresden'91, Griefswald,1107-1110.

Türkmenoğlu, A.G., Koçyiğit,A. and Özalp, T., 1994, Anadolu'da bazı Üst Tersiyer havzalarının evrimi ve ekonomik poatansiyeli için tip alan çalışması: Güneybatı çankırı havzası, TÜBİTAK Proje no. YBAG-0058, 317p.

Türkmenoğlu,A.G., Koçyiğit,A. and Özalp, T., 1995, Kalecik-Hasayaz havzasındaki göl sedimanlarının jeolojisi ve kil mineralojisi, VII. Ulusal Kil Sempozyumu, Bildiriler, 55-63.

Wright, V.P., Tucker, M.E., 1991. Calcretes. Blackwell Scientific Publications, Oxford, p. 351.

Yao, Y.-F., Bruch, A.A., Mosbrugger, V., Li,, C.S., 2011. Quantitative reconstruction of Miocene climate patterns and evolution in Southern China based on plant fossils. Paleogeography, Palaeoclimatology, Palaeoecology, 304, 291–307.

Zachos, J., Pagani, M., Sloan, L., Thomas, E., Billups, K., 2001. Trends, rythms, and abberations in global climate 65 Ma to the present. Science, 292, 386–392.

CURRICULUM VITAE

PERSONAL INFORMATION

Surname, Name   : Aker, Serdar
Nationality   : Turkish (TC)

Date and place of Birth **:** 01 April 1955, Iğdır
Marital Status   : Single
Phone   : +90 312 472 39 80
Fax: : +90 312 472 39 19
e-mail   : srdrkr@gmail.com

EDUCATION

Degree	Institution	Year of Graduation
MS	METU Geological Engineering	1985
BS	METU Geological Engineering	1980
High School	Mustafa Kemal High School / Ankara	1974

WORK EXPERIENCE

Year	Place	Enrollment
1983 – 1991	METU Geological Engineering Department	Teaching Assistant
1991 – 1992	DAR Müh. Müş.A.Ş.	Geotechnical Engineer
1992 – 1994 Geotechnical	NUROL İnşaat A.Ş.	Site Manager–
1994 – 1995 Geotechnical	Yüksel Domaniç Müh. Ltd. Şti.	Site Manager–
1995 – 1999 June Head	Saudi Strategic Storage Programme	Rock Works Branch
1999 June- Present	PETRA Müh. Müş. ve İnş. Ltd. Şti.	Partner

FOREIGN LANGUAGES

Fluent English, Intermediate French

Petra Müh.Müş.ve İnş.Ltd.Şti.
SONDAJ LOGU / BORING LOG

SONDAJ / NO / Borehole No	SSK-1
SAYFA / Page	1 / 1

PROJE ADI/Project Name	PALEO-CLIMATE AND PALEO-ENV. MODELLING(E),İk ÇAPI/Hole Diameter	4 3/4 "
SONDAJ YERI/Boring Location	ÇANKIRI — YERALTI SUYU/Groundwater	
	ÇANDIR (HANÇILI KÖYÜ) — MUH.BOR.DER./Casing Depth	12.00 MHW
SONDAJ.DER/Boring Depth	60 m. — BAŞ.-BİT. TARİHİ/Start-Finish Date	01/02/200 *** 01/05/2006
SONDAJ KOTU/Elevation	100 m. — KOORDINAT/Coordinate(Northing)	4470125
SON. MAK.&YONT./D Rig & Met.	CRAELIUS D-900 — KOORDINAT/Coordinate(Easting)	534250

GEOLOGICAL DESCRIPTION

Columns: BORING DEPTH/m · AGE · UNIT · THICKNESS · GEOLOGICAL DESCRIPTION · LAKE LEVEL · NO. OF CYCLE · SAMPLE NO · SAMPLE TYPE

Depth	Thickness	Geological description
0.0–4.2	4.2 m	Clayey LIMESTONE; Dirty white-cream colored, hard, fine grained.
	2.8 m	SILTSTONE; Grayish green colored, hard, fine grained, occasionally carbonaceous, open joints.
~7.0	8.5 m	MARL; Dirty white-cream colored, hard, fine grained, micritic, occasionally C banded, 9,23-9,43; C content around %80.
		MUDSTONE; Light greenish gray colored, dispersible.
		CLAYEY LIMESTONE; (Lake environment) Cream colored, fine grained.
		MUDSTONE; (Carbonaceous) Light green colored.
		LIMESTONE; Dirty white-cream colored, hard, micritic.
		TUFF-TUFFIT; Açık gray-green colored.
		ORGANIC MUDSTONE; Dark gray-black colored, fine grained, fossil grained.
		CLAYEY LIMESTONE; Dirty white colored, occasionally oxidised.
	0.5 m	MUDSTONE (Bentonite); Grayish green colored.
	0.5 m	MARL; Light green colored, fine grained.
	1.8 m	TUFF; Greenish gray-cream colored, fine-medium grained.
	4.5 m	MUDSTONE; Dark greenish gray colored, occasionally carbonaceous (19,35-19,60 carbonate rich).
		CLAYSTONE; Light greenish gray-cream colored, silty, carbonaceous.
		MUDSTONE; Greenish gray colored, occasionally limonitized.
		MUDSTONE-CLAYSTONE; Cream colored.
	3.2 m	TUFF-TUFFIT; Açık gray-green colored.
	3.0 m	BENTONITE, BENTONITIC CLAYSTONE; Grayish green colored, fine grained.
	1.3 m	MUDSTONE; Grayish green-cream multi colored, fine-coarse grained, (Flow property observed).
		CONGLOMERATE
		ANDESITE
	1.7 m	MUDSTONE; Dark gray, occasionally reddish brown colored, (flow property observed).
	3 m	LIMESTONE; Grayish green colored, micritic.
	5 m	MARL; Reddish brown-grayish green colored, clayey silty.
	2.8 m	MUDSTONE; reddish brown colored.
	7.2 m	MARL; Reddish brown-grayish green colored, clayey silty.
	2.5 m	LIMESTONE; Grayish green colored, contains sparry calcite.
	2.2 m	SANDSTONE; Reddish brown colored, fine-coarse grained, clayey.
	7.3 m	MUDSTONE; Gray -occasionally red colored.

AGE: E · O · S · E · N · transition · F · O · R · M · A · T · I · O · N · ... HANÇILI · ... · ASLANTAŞ FM (?)

Sample numbers: HAN-1 through HAN-65

SONDOR / Driller	İsmail AYTEKIN
SONDAJ MÜHENDISI / Drilling Engineer	Serdar AKER
TARİH / Date	15/06/2006
IMZA / Sign	